Tina Katharina Herbst
Matrikelnr.: 0411943

Polyakov-Loops and the QCD Phase Structure

Dissertation

zur Erlangung des akademischen Grades einer
Doktorin der Naturwissenschaften

verfasst am Institut für Physik - FB Theoretische Physik
der Karl-Franzens-Universität Graz

Erstgutachter: Priv.-Doz. Dr. Bernd-Jochen Schaefer
Institut für Theoretische Physik, Karl-Franzens-Universität Graz

Zweitgutachter: Prof. Dr. Daniel Litim
Department of Physics and Astronomy, University of Sussex

Graz, August 2012

Präambel

Ich bestätige hiermit, dass es sich bei der vorliegenden Dissertation um eine Originalarbeit handelt, die von mir selbstständig und unter Zuhilfenahme ausschließlich der angegebenen Hilfsmittel verfasst wurde.

Ort, Datum

Tina Katharina Herbst

Für meine Familie

Contents

1. Aspects of Quantum Chromodynamics

Quantum Chromodynamics (QCD) is the theory that is strongly believed to properly describe the dynamics of the strong interactions. This theory is a successor of the *quark model*, introduced by Gell-Mann and Nishijima in the 1960s. It was designed as an ordering scheme for the plethora of hadrons that were being discovered in experiment during the 1950s and 1960s. While the so-called *Eightfold Way* of Gell-Mann and Ne'eman [1, 2] was very successful - for the prediction of the Ω^- baryon and its properties, Gell-Mann actually received the Nobel price in 1969 - it had problems explaining for example the spin-3/2 baryon Δ^{++}. This particle required the combination of three up quarks with parallel spins and therefore seemed to violate Pauli's exclusion principle. This apparent shortcoming was remedied in the 1970s by the introduction of an additional charge of the quarks. In order to solve the Δ^{++} mystery, there should be three different values of this so-called *colour charge*, as has been verified since.

In modern-day language, QCD is formulated as a gauge theory, similar to quantum electrodynamics (QED). The local gauge group in this case is $SU(N_c)$ with $N_c = 3$ the number of colours. The requirement of local gauge invariance leads to the introduction of an octet of gauge bosons mediating the strong interactions, called *gluons*. While the quark fields transform under the fundamental representation of the gauge group, the gluon fields live in the adjoint representation. Due to the non-Abelian nature of the gauge group, three- and four-gluon interactions occur in addition to quark-gluon interactions, which distinguishes the strong interaction from, e.g. QED.

The experimentally detected hadrons appear in QCD as colour-neutral bound states of three quarks (baryons) or quark-antiquark (mesons). In particular, it is an experimental fact that no single coloured particle has ever been measured. This circumstance is one of the long-standing problems of theoretical physics: *What is the physical mechanism behind the confinement of coloured quarks and gluons into colour singlet states?*

While confinement is easily characterised in terms of experimental observation, its theoretical derivation from the QCD Lagrangian is intricate. To date, various different characterisations of confining theories are on the market. For example, a linearly rising, static interquark potential at large distances or a temporal Wilson loop developing an area law. For a discussion of different ideas see e.g. [3]. Moreover, thus far we still lack a proof that QCD indeed is confining, and actually according to some of the proposed criteria, it is not. The mechanism underlying confinement hence is still not fully understood.

In order to comprehend hadron masses within QCD, confinement alone is not enough. Especially, the mass difference between the lightest mesons, the three pseudoscalar pions $\pi^{\pm}, \pi^0$ with $m_\pi \approx 140$ MeV and the other hadrons needs to be explained. In QCD this is ascribed to the *dynamical breaking of chiral symmetry*. The pions occur as the pseudo Goldstone bosons of this spontaneous symmetry breaking. Their non-vanishing mass is understood as the impact of the explicit breaking of chiral symmetry by finite quark masses.

The theoretical treatment of QCD is exacerbated by the running of the gauge coupling. Contrary to QED, where the coupling is small at large distances, due to an antiscreening effect of gluons the strong coupling is large in the infrared. At small distances, on the other hand, the coupling is small and QCD is characterised by *asymptotic freedom*. This was first demonstrated in 1973 in the Nobel price winning works of D. Gross, F. Wilczek and D. Politzer [4, 5]. This circumstance allows perturbative calculations in the high-energy region, which show remarkable agreement with experiment. At low energies, a perturbative treatment, however, is bound to break down, which is signaled by a divergence in the (perturbatively calculated) strong coupling constant - the so-called *Landau pole* Λ_{QCD}.

In this thesis, we will pose the question whether there is a relation between chiral symmetry breaking and confinement, and especially between the related finite temperature phase transitions. Both, chiral symmetry breaking and confinement are related to the intermediate and low momentum region, where due to the increase of the gauge coupling, the use of non-perturbative tools is mandatory.

In the following, we will first give a brief review of the symmetries and symmetry breaking patterns of QCD, in order to set the stage and clarify notation. Furthermore, order parameters for the two transitions will be discussed. Especially, we generalise a well-known quantity related to confinement to arbitrary gauge groups and discuss its properties in detail. Subsequently, the expected phase structure of QCD at finite temperature and quark chemical potential will be reviewed, followed by a short introduction to some non-perturbative techniques. Special emphasis is put on the non-perturbative functional renormalisation group (FRG), which is well-suited for the study of phase transitions and will be used throughout this thesis.

1.1. Symmetries and Symmetry Breaking Pattern

Let us start by recalling the QCD symmetry structure. The Lagrangian density of this non-Abelian gauge theory can be written as

$$\mathcal{L}_{\mathrm{QCD}} = \bar{\psi}_{i,f}\left(i\gamma^{\mu}D_{\mu}^{ij} - \hat{m}_{f,f'}\delta^{ij}\right)\psi_{j,f'} - \frac{1}{4}F_{\mu\nu}^{a}F_{a}^{\mu\nu}\,, \tag{1.1}$$

where $(\bar{\psi}_{i,f})\ \psi_{j,f'}$ label the (anti-)quark fields that transform under the (anti-)fundamental representation of the global flavour group $SU(N_f)$, labelled by the indices $f, f' = 1, \ldots, N_f$. Quarks transform furthermore under the fundamental representation of colour gauge group $SU(N_c)_{\mathrm{loc}}$ with colour indices $i, j, \cdots = 1, \ldots, N_c$. Moreover, the matrix $\hat{m}$ denotes the quark mass matrix generated by the Higgs-sector of the standard model. In this work we will not concern ourselves with the origin of the quark masses and rather treat them as external parameters of the theory.

In analogy to QED, the QCD Lagrangian is constructed such that it is invariant under local gauge transformations with a space-time dependent parameter $\theta_a(x)$

$$U = e^{-i\theta_a(x)t^a} \in SU(N_c)\,, \tag{1.2}$$

where $t^a = \lambda^a/2$, $a = 1, \ldots, N_c^2 - 1$ are the Hermitean generators of the Lie algebra $su(N_c)$. The λ^a denote the Gell-Mann matrices, which are traceless and obey the relation $\mathrm{tr}(\lambda^a\lambda^b) = 2\delta^{ab}$. In order to achieve this invariance, the ordinary derivative has to be

replaced by the covariant one

$$D^{\mu}_{ij} = \partial^{\mu}\delta_{ij} - i\bar{g}A^{\mu}_{ij}\,. \tag{1.3}$$

In this manner, gauge fields $A^{\mu}_{ij}(x)$ are introduced that couple in a minimal fashion, with gauge coupling $\bar{g}$, to the quark fields. The gauge fields by construction transform according to the adjoint representation of the gauge group and can be written componentwise via the generators $A^{\mu}_{ij} = A^{\mu}_{a}t^{a}_{ij}$.

While a mass term for the gauge field would spoil the gauge invariance of the theory, a kinetic term is perfectly allowed and hence included. It can be constructed as the trace of the field strength tensor

$$F^{a}_{\mu\nu} = \partial_{\mu}A^{a}_{\nu} - \partial_{\nu}A^{a}_{\mu} - \bar{g}f^{abc}A^{b}_{\mu}A^{c}_{\nu}\,, \tag{1.4}$$

where f^{abc} denotes the structure constants of $SU(N_c)$. The inclusion of this term $\sim\ F^{a}_{\mu\nu}F^{\mu\nu}_{a}$ gives rise to gluon self-interactions that result in the formation of flux tubes between colour charged objects and in this manner are related to confinement. In particular, the formation of a colour string limits the range of strong interactions to $\sim 10^{-15}$ m, despite the fact that the mediators of this interaction are massless.

Note also that the invariance of Eq. (1.1) completely determines the interactions between quarks and gluons by the colour and flavour independent gauge coupling $\bar{g}$.

1.1.1. Chiral Symmetry

Let us now briefly discuss the global symmetry structure of the theory. In the so-called *chiral limit*, i.e. for vanishing quark masses, the apparent symmetry of the Lagrangian, apart from the colour gauge group, is given by

$$\mathcal{G} \quad = \quad U(N_f)_R \otimes U(N_f)_L\,. \tag{1.5}$$

The unitary groups can be decomposed into $U(N_f) = U(1)/Z_{N_f} \otimes\ SU(N_f)$. One of these $U(1)$ groups is referred to as axial $U(1)$. On the level of the Lagrangian, this symmetry seems to be present, however, this invariance is broken due to quantum effects. This is referred to as the *axial anomaly* [6–9] and relates, for example, to the mass of the η' meson.

The second $U(1)$ symmetry, on the other hand, is unbroken and results in the conservation of *baryon number*

$$B = \frac{1}{3}\int d^3x\ \psi^{\dagger}\psi\,. \tag{1.6}$$

While the QCD Lagrangian possesses the symmetry

$$\mathcal{G}' = U(1)/Z_{N_f} \otimes SU(N_f)_R \otimes SU(N_f)_L\,, \tag{1.7}$$

it is generally believed that the vacuum is not invariant under the full symmetry group - part of the symmetry is *broken spontaneously*. To understand this in more detail, consider the $SU(N_f)_R \times SU(N_f)_L$ part of $\mathcal{G}'$, which corresponds to an invariance under separate $SU(N_f)_{R,L}$ transformations of the left- and right-handed quark fields defined via

$$\psi_{R,L} = \frac{1}{2}(1 \pm \gamma_5)\psi\,, \tag{1.8}$$

with $\gamma_5 = i\gamma_0\gamma_1\gamma_2\gamma_3$ the product of the Dirac matrices. Due to its relation to the "handedness" of (massless) quarks, this invariance is called *chiral symmetry*. While the Lagrangian allows separate transformations

$$\psi_R \to V_R\,\psi_R\,, \quad \psi_L \to V_L\,\psi_L\,, \tag{1.9}$$

in the vacuum $|\Omega\rangle$ only simultaneous rotations $V_R = V_L$, corresponding to $SU(N_f)_{L+R}$ are possible. Chiral symmetry is hence broken spontaneously

$$SU(N_f)_R \otimes SU(N_f)_L \to SU(N_f)_{L+R}\,. \tag{1.10}$$

The spontaneous breaking of chiral symmetry is accompanied by the condensation of quark-antiquark pairs forming the quark condensate

$$\langle\bar{\psi}\psi\rangle = \langle\Omega|\bar{\psi}\psi|\Omega\rangle \neq 0\,, \tag{1.11}$$

which acts as an order parameter. Lattice simulations with dynamical u, d, s quarks confirm the above claim and give a chiral condensate $\frac{1}{2}\langle\bar{u}u+\bar{d}d\rangle \simeq -\,(234(04)(17)\text{ MeV})^3$ [10]. By the formation of the condensate in the vacuum, a quark mass is generated dynamically, which contributes to the mass of the observed hadrons.

Note that the chiral symmetry is actually only well-defined for vanishing bare quark masses. A mass term, $\bar{\psi}\hat{m}\psi$, mixes quark fields of opposite chirality and hence breaks chiral symmetry explicitly. In Nature, the u and d quark masses, $m_{u,d} \approx 2-5$ MeV, are rather small compared to the relevant scale $\Lambda_{\text{QCD}}\sin 200$ MeV, making $SU(2)_R \otimes SU(2)_L$ a good approximate symmetry. The mass difference of the next heavier strange quark to the lightest ones is also relatively small, $m_s \approx 100$ MeV, and experiment suggests that also $SU(3)$ is a good approximate symmetry.

The *Goldstone theorem* relates the spontaneous breaking of chiral symmetry Eq. (1.10) to the appearance of $N_f^2 - 1$ massless Nambu-Goldstone bosons. For the case of $N_f = 2$, these are associated with the three pions. Their non-vanishing masses can be attributed to the explicit breaking of chiral symmetry.

In this thesis we are especially interested in the behaviour of QCD under the influence of external parameters such as temperature T and quark chemical potential μ. Owing to thermal fluctuations, the chiral condensate melts at high temperatures and vanishing chemical potential and chiral symmetry is restored. A complete restoration of chiral symmetry is, however, only possible in the chiral limit. The related phase transition temperature, T_χ, can be computed in, e.g. lattice, functional and model approaches, see also the following chapters of this thesis. By now, different methods agree on the fact that the transition at the physical mass point is a crossover as a result of the explicit breaking of chiral symmetry, and occurs in the range $T_\chi \simeq 150 - 200$ MeV.

1.1.2. Center Symmetry

Next, we consider the limit of infinitely heavy quarks, in which QCD exhibits a global Z_{N_c}*-center symmetry*. To study this symmetry we consider QCD in Euclidean space-time. Using the imaginary-time formalism, space-time is compactified to a torus $S^1 \times \mathbb{R}^3$ with Euclidean time direction $x_0 \in (0, \beta = 1/T]$. One easily finds that in addition to the

standard, periodic gauge transformations

$$U(\vec{x}, x_0 + \beta) = U(\vec{x}, x_0)\,, \tag{1.12}$$

also topologically non-trivial transformations

$$U(\vec{x}, x_0 + \beta) = h\, U(\vec{x}, x_0)\,, \quad h \in SU(N_c) \tag{1.13}$$

are permissible [11, 12]. Periodicity of the gauge field $A_\mu(\vec{x}, x_0 + \beta) = A_\mu(\vec{x}, x_0)$, however, provides a restriction for the prefactor h, namely $h \in Z_{N_c}$, or in more detail

$$h = z\mathbb{I}\,, \quad z = e^{2\pi i n/N_c}\,, \quad n \in \{0, \ldots, N_c - 1\}\,, \tag{1.14}$$

where $\mathbb{I}$ is the N_c-dimensional unit matrix. In the presence of dynamical quarks with finite mass, the invariance of the action under these *twisted transformations* is explicitly broken. Applying a center transformation Eq. (1.13) to the fermion field yields

$$^U\psi(\vec{x}, x_0 + \beta) \;=\; -z\, {}^U\psi(\vec{x}, x_0)\,. \tag{1.15}$$

Thus, the transformed fermion field respects the antiperiodic boundary conditions only if we restrict $z = 1$.

We would like to emphasis that this global center symmetry is defined in Euclidean space-time. It should not be considered as a subgroup of the local gauge group $SU(N_c)$, that is a symmetry group of the Lagrangian also in Minkowski space-time. In particular, the center symmetry - in contradistinction to the local gauge symmetry - can also be broken spontaneously, cf. [13]. This effect is of relevance, since it provides a link to the confinement transition. This connection will be studied in more detail in the following.

1.1.3. Properties of the Polyakov-Loop

It is well-known that the renormalised *Polyakov-loop*[1] acts as an indicator for the spontaneous breaking of center symmetry in the pure gauge sector of QCD. For later convenience, we will, however, extend its definition to general gauge groups with non-trivial center and matter in arbitrary representations R thereof. The properties of this quantity discussed here will play an important role in our classification of gauge theories in Chap. 4.

For matter transforming in the representation R of the gauge group, the definition of the Polyakov-loop variable reads

$$L_{\mathrm{R}}[A_0] = \frac{1}{d_{\mathrm{R}}}\, \mathcal{P}\, \mathrm{e}^{\mathrm{i}\bar{g} \int_0^\beta dx_0\, A_0(x_0, \vec{x})}\,, \tag{1.16}$$

where d_{R} is the dimension of the representation R, A_0 is the temporal component of the gauge field and $\mathcal{P}$ denotes path ordering of the exponential. Note, that we implicitly assume the use of Polyakov-Landau-DeWitt gauge in the following. Then, the ground state $\langle A_0 \rangle$ is an element of the Cartan subalgebra of the gauge group and is defined as

[1] Note that in lattice studies the Polyakov-loop need not be appropriately renormalised a priori. The unrenormalised quantity suffers from a UV divergence due to a divergent self-energy contribution. Hence, in the continuum limit the Polyakov-loop vanishes also in the deconfined phase. This problem can be solved by proper renormalisation, cf. [14].

the minimum of the associated order parameter potential. Under an arbitrary center transformation of the ground state $\langle A_0 \rangle$,

$$\langle A_0 \rangle \longrightarrow {}^{U}\langle A_0 \rangle \,, \tag{1.17}$$

the Polyakov-loop transforms according to

$$\mathrm{tr}_{\mathrm{R}} L_{\mathrm{R}}[\langle A_0 \rangle] \xrightarrow{U} z^{\mathcal{N}_{\mathrm{R}}} \mathrm{tr}_{\mathrm{R}} L_{\mathrm{R}}[\langle A_0 \rangle] \,. \tag{1.18}$$

Here, $\mathcal{N}_{\mathrm{R}}$ denotes the so-called N-ality of the representation R and $z \in Z_{N_c}$ is a center element as defined in Eq. (1.14).

To discuss some more properties of the generalised Polyakov-loop Eq. (1.16), we expand $\langle A_0 \rangle$, which by construction is an element of the Cartan subalgebra of the gauge group, in terms of the generators of this subalgebra

$$\beta \bar{g} \langle A_0 \rangle = 2\pi \sum_{a=1}^{d_{\mathrm{C}}} T^{(a)} \phi^{(a)} = 2\pi \sum_{a=1}^{d_{\mathrm{C}}} T^{(a)} v^{(a)} |\phi| \,, \tag{1.19}$$

where $v^{(a)}$ denotes a unit vector and the $T^{(a)}$'s are the generators of the gauge group in the representation R. Furthermore, d_{C} denotes the dimension of the Cartan subalgebra. For $SU(N_c)$, for example, this value is $d_{\mathrm{C}} = N_c - 1$. The set $\{\phi^{(a)}\}$ will be called the coordinates of $\langle A_0 \rangle$ in the following.

Fundamental Representation

The fundamental representation (R=F) has N-ality $\mathcal{N}_{\mathrm{R}} = 1$ and we obtain the transformation property

$$\mathrm{tr}_{\mathrm{F}} L_{\mathrm{F}}[\langle A_0 \rangle] \xrightarrow{U} z \, \mathrm{tr}_{\mathrm{F}} L_{\mathrm{F}}[\langle A_0 \rangle] \,. \tag{1.20}$$

Similarly it can be seen that $\langle \mathrm{tr}_{\mathrm{F}} L_{\mathrm{F}}[A_0] \rangle$ transforms in the same manner under center transformations of the gauge field A_0. Hence we conclude that both $\mathrm{tr}_{\mathrm{F}} L_{\mathrm{F}}[\langle A_0 \rangle]$ and $\langle \mathrm{tr}_{\mathrm{F}} L_{\mathrm{F}}[A_0] \rangle$ represent order parameters for center-symmetry breaking.

Let us now explore the relation of $\Phi = \langle \mathrm{tr}_{\mathrm{F}} L_{\mathrm{F}}[A_0] \rangle$ to the deconfinement transition. It can be shown, see e.g. [15], that Φ is related to the free energy F_q of a static test quark

$$\Phi \sim e^{-\beta F_q} \,. \tag{1.21}$$

We have seen above that the Polyakov-loop vanishes in the center-symmetric phase. This implies that the free energy of a static fundamental charge (fundamental color source) is infinite, i.e. this is the confined phase. In particular, the related quark-antiquark potential is linearly rising at large distances in this phase and no string breaking occurs. On the other hand, in the deconfined phase the free energy F_q is finite and so is the Polyakov-loop. Hence, center symmetry is spontaneously broken in this regime. In this way the Polyakov-loop distinguishes the confined from the deconfined phase for static test charges in the fundamental representation.

Remark 1.1:
As already pointed out, in full QCD the presence of dynamical quarks breaks center symmetry explicitly. Hence, the Polyakov-loop is only an approximate order parameter, similar to the chiral condensate. Note, however, that both, the chiral condensate and the Polyakov-loop can be used as order parameters for the related crossover transitions at finite m_q. This has been confirmed by lattice studies and will be exploited in the following.

Remark 1.2:
At finite chemical potential the Polyakov-loop Φ and its conjugate $\bar{\Phi}$ are not simply related by complex conjugation. Actually, both of them are real valued and positive in the definition used in, e.g., Chap. 3. In fact, the Polyakov-loop is related to the free energy of quarks and while its conjugate is related to that of antiquarks

$$\Phi \sim e^{-\beta F_q}\,, \quad \bar{\Phi} \sim e^{-\beta F_{\bar{q}}}\,. \tag{1.22}$$

Since the quark chemical potential μ measures the excess of quarks over antiquarks in our setup, at finite chemical potential the Polyakov-loop and its conjugate do not agree, but we have $\bar{\Phi} \geq \Phi$.

We have seen above that the center-symmetric, low temperature phase is signaled by

$$\langle \mathrm{tr_F} L_\mathrm{F}[A_0] \rangle = \mathrm{tr_F} L_\mathrm{F}[\langle A_0 \rangle] = 0\,. \tag{1.23}$$

From this expression it follows - in the class of Polyakov-Landau-DeWitt gauges - that the position $\langle A_0 \rangle$ of the center-symmetric ground state is uniquely determined by, cf. [16]

$$\mathrm{tr_F}(L_\mathrm{F}[\langle A_0 \rangle]^n) = 0\,, \tag{1.24}$$

where $n = 1, \ldots, d_\mathrm{C}$. Actually, this equation holds only for the center-symmetric ground-state for $n \mod N_c \neq 0$. For $n \mod N_c = 0$ and N_c even, we find

$$\mathrm{tr_F}(L_\mathrm{F}[\langle A_0 \rangle]^n) = (-1)^{\frac{n}{N_c}} \frac{1}{N_c^{n-1}}\,, \tag{1.25}$$

while odd N_c result in

$$\mathrm{tr_F}(L_\mathrm{F}[\langle A_0 \rangle]^n) = \frac{1}{N_c^{n-1}}\,. \tag{1.26}$$

Let us now consider the opposite regime of asymptotically high temperatures. Then we are in the perturbative regime where $\langle A_0 \rangle \to 0$ and accordingly $\mathrm{tr_F} L_\mathrm{F}[\langle A_0 \rangle] \to 1$, see e. g. Refs. [16–20]. Since $\mathrm{tr_F} L_\mathrm{F}[\cdot]$ is a monotonic function of temperature in the domain defined by the trajectory of $\langle A_0 \rangle(T)$, $\mathrm{tr_F} L_\mathrm{F}[\langle A_0 \rangle]$ is monotonic and $\mathrm{tr_F} L_\mathrm{F}[\langle A_0 \rangle] > 0$ in the phase with broken center symmetry, see also the discussion below.

From the above we can determine the coordinates $\{\phi^{(a)}\}$ of the center-symmetric ground state for some specific gauge groups. For the example of $SU(2)$ we have $\{1/2\}$ and for $SU(3)$ the coordinates are given by $\{2/3, 0\}$.

Moreover, the order-parameter potential in the adjoint algebra is periodic. It is invariant under discrete rotations about the origin, with rotation angles determined by the

gauge group under consideration. The periods in the different directions depend on the eigenvalues of the corresponding generators $T^{(a)}$. Center transformations of the ground state $\langle A_0 \rangle$ can then be viewed as discrete rotations of the coordinates $\{\phi^{(a)}\}$ around the center symmetric point.

Let us consider $SU(2)$ first, where we have a reflection symmetry with respect to $\phi = 1/2$. The associated center transformation can then be written as

$$\phi \longrightarrow {}^{U}\phi = 1 - \phi \tag{1.27}$$

with $\phi \in [0, 1/2]$. Under such a center transformation, the order parameter

$$\mathrm{tr_F} L_\mathrm{F}[\langle A_0 \rangle] \equiv \mathrm{tr_F} L_\mathrm{F}[\phi] = \cos(\pi\phi) \tag{1.28}$$

transforms according to

$$\mathrm{tr_F} L_\mathrm{F}[\langle A_0 \rangle] \quad \longrightarrow \quad \mathrm{tr_F} L_\mathrm{F}[{}^{U}\langle A_0 \rangle] = -\mathrm{tr_F} L_\mathrm{F}[\langle A_0 \rangle] \,, \tag{1.29}$$

as expected from Eq. (1.20).

For $SU(3)$, center transformations of the ground state $\langle A_0 \rangle$ can be written as rotations by angles of $2\pi n/3$, $n = 0, 1, 2$ around the center-symmetric point $\{2/3, 0\}$. The behaviour of the order parameter under such transformations is indeed as in Eq. (1.20).

Adjoint Representation

Considering Eq. (1.18), we observe that there may exist representations R, for which $\mathrm{tr_R} L_\mathrm{R}[\langle A_0 \rangle]$ does *not* represent an order parameter for center-symmetry breaking, namely when $\mathcal{N}_\mathrm{R} = 0$ (zero N-ality). For example, consider the adjoint representation (R=A). In this case, we find the following transformation behaviour

$$\mathrm{tr_A} L_\mathrm{A}[\langle A_0 \rangle] \longrightarrow \mathrm{tr_A} L_\mathrm{A}[{}^{U}\langle A_0 \rangle] = \mathrm{tr_A} L_\mathrm{A}[\langle A_0 \rangle] \tag{1.30}$$

under a twisted transformation. For example for $SU(2)$, we have

$$\mathrm{tr_A} L_\mathrm{A}[\langle A_0 \rangle] \equiv \mathrm{tr_A} L_\mathrm{A}[\phi] = \frac{1}{3}\left[1 + 2\cos(2\pi\phi)\right], \tag{1.31}$$

which is insensitive to the center transformations defined in Eq. (1.27). Hence we conclude that $\mathrm{tr_A} L_\mathrm{A}[\langle A_0 \rangle]$ is not an order parameter for center-symmetry breaking, see also [21,22].

Also in the adjoint representation we find equivalent transformation properties for $\mathrm{tr_A} L_\mathrm{A}[\langle A_0 \rangle]$ and $\langle \mathrm{tr_A} L_\mathrm{A}[A_0] \rangle$: Both quantities are insensitive to center transformations. This is related to the fact that quarks in the adjoint representation do not break the underlying center symmetry of the gauge group, in contrast to quarks in the fundamental representation. From a phenomenological point of view, there is indeed no strict notion of confinement of quarks in the adjoint representation, even in the static limit. In this case, static quarks can be screened by the gluonic degrees of freedom and form a colour-singlet state, as can be seen from the decomposition of the tensor product of two adjoint multiplets. Therefore, a quark-antiquark pair at large distances can split up into two singlet states. The associated quark-antiquark potential thus flattens at large distances and does

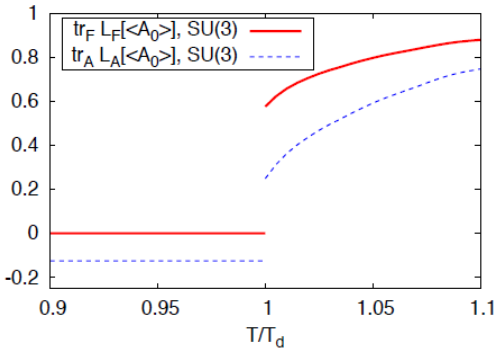

Figure 1.1.: The quantities $\mathrm{tr}_\mathrm{F} L_\mathrm{F}[\langle A_0 \rangle]$ and $\mathrm{tr}_\mathrm{A} L_\mathrm{A}[\langle A_0 \rangle]$ for $SU(3)$ Yang-Mills theory as a function of temperature. For $T < T_d$ we have $\mathrm{tr}_\mathrm{F} L_\mathrm{F}[\langle A_0 \rangle] = 0$ and $\mathrm{tr}_\mathrm{A} L_\mathrm{A}[\langle A_0 \rangle] = -1/8$, see Eqs. 1.24 and 1.36. Data for $\langle A_0 \rangle$ has been taken from [19, 20]

not rise linearly, as is the case for static quarks in the fundamental representation, see e. g. Refs. [21–25] for lattice studies. In particular, the Polyakov-loop $\langle \mathrm{tr}_\mathrm{A} L_\mathrm{A}[A_0] \rangle$ is non-vanishing for all temperatures [21, 22]. On the other hand, $\langle \mathrm{tr}_\mathrm{A} L_\mathrm{A}[A_0] \rangle$ is related to the free energy of a static adjoint quark, and it follows that the free energy is finite, even in the center-symmetric phase at low temperatures. However, note that the behaviour of the quantities $\langle \mathrm{tr}_\mathrm{A} L_\mathrm{A}[A_0] \rangle$ and $\mathrm{tr}_\mathrm{A} L_\mathrm{A}[\langle A_0 \rangle]$ changes qualitatively at $T = T_\mathrm{d}$, even though they *do not* represent order parameters for center-symmetry breaking. As we shall discuss below, this is due to the fact that $\langle \mathrm{tr}_\mathrm{A} L_\mathrm{A}[A_0] \rangle$ and $\mathrm{tr}_\mathrm{A} L_\mathrm{A}[\langle A_0 \rangle]$ can be related to the order parameters $\langle \mathrm{tr}_\mathrm{F} L_\mathrm{F}[A_0] \rangle$ and $\mathrm{tr}_\mathrm{F} L_\mathrm{F}[\langle A_0 \rangle]$, respectively. This behaviour is illustrated in Fig. 1.1, where we show the temperature dependence of $\mathrm{tr}_\mathrm{F} L_\mathrm{F}[\langle A_0 \rangle]$ and $\mathrm{tr}_\mathrm{A} L_\mathrm{A}[\langle A_0 \rangle]$ for $SU(3)$ Yang-Mills theory.

General Representations

Let us now summarise a few more useful relations for $\mathrm{tr}_\mathrm{R} L_\mathrm{R}[\langle A_0 \rangle]$. First, consider again the fundamental representation. It is useful to note that this quantity can be related to the standard Polyakov-loop via the *Jensen inequality*

$$f(\langle \cdot \rangle) \geq \langle f(\cdot) \rangle \,, \tag{1.32}$$

which holds for *concave* functions f. For the Polyakov-loop, this yields

$$\mathrm{tr}_\mathrm{F} L_\mathrm{F}[\langle A_0 \rangle] \geq \langle \mathrm{tr}_\mathrm{F} L_\mathrm{F}[A_0] \rangle \,, \tag{1.33}$$

which is known to hold for $SU(2)$ and $SU(3)$ gauge theories in the deconfined phase [16, 19, 20]. For general gauge groups and representations R this inequality does not necessarily hold, since it relies on $\mathrm{tr}_\mathrm{R} L_\mathrm{R}[\cdot]$ being a concave function in the relevant domain. Provided that $\langle A_0 \rangle(T)$ lies sufficiently close to the origin, which is true, e.g., for sufficiently large temperatures T, the inequality may, however, hold for any gauge group and representation. For a more detailed discussion of the relation Eq. (1.33) the reader is referred to Ref. [26].

We want to state two more simple, but useful inequalities that hold for arbitrary representations. The first one:

$$0 \leq \frac{1}{d_{\mathrm{R}}} \left|\mathrm{tr}_{\mathrm{R}}(L_{\mathrm{R}}[\langle A_0 \rangle]^n)\right| \leq \frac{1}{(d_{\mathrm{R}})^n}\,, \tag{1.34}$$

follows from the generalised triangle inequality. Furthermore

$$-\frac{1}{(d_{\mathrm{R}})^n} \leq \frac{1}{d_{\mathrm{R}}} \mathfrak{Re}\left[\mathrm{tr}_{\mathrm{R}}(L_{\mathrm{R}}[\langle A_0 \rangle]^n)\right] \leq \frac{1}{(d_{\mathrm{R}})^n} \tag{1.35}$$

holds for $n \in \mathbb{N}$.

For later reference, we now evaluate the quantity $\mathrm{tr}_{\mathrm{R}} L_{\mathrm{R}}[\langle A_0 \rangle]$ for specific values of $\langle A_0 \rangle$. At very high temperatures $T \gg T_{\mathrm{d}}$, we have $\langle A_0 \rangle \to 0$ and $\mathrm{tr}_{\mathrm{R}} L_{\mathrm{R}}[\langle A_0 \rangle] \to 1$, independent of the gauge group and the representation. At low-temperature ($T < T_{\mathrm{d}}$), on the other hand, the value of $\mathrm{tr}_{\mathrm{R}} L_{\mathrm{R}}[\langle A_0 \rangle]$ does depend on both, the gauge group and the representation. For example, we have $\mathrm{tr}_{\mathrm{F}} L_{\mathrm{F}}[\langle A_0 \rangle] = 0$ for $T < T_{\mathrm{d}}$. For the adjoint representation, on the other hand, we find

$$\mathrm{tr}_{\mathrm{A}}(L_{\mathrm{A}}[\langle A_0 \rangle]^n) = -\frac{1}{(d_{\mathrm{A}})^n} = -\frac{1}{(N_c^2-1)^n} \tag{1.36}$$

with $n \mod N_c \neq 0$ and

$$\mathrm{tr}_{\mathrm{A}}(L_{\mathrm{A}}[\langle A_0 \rangle]^n) = \frac{1}{(d_{\mathrm{A}})^{n-1}} \tag{1.37}$$

for $n \mod N_c = 0$. Note especially the sign in Eq. (1.36): The quantity $\mathrm{tr}_{\mathrm{A}}(L_{\mathrm{A}}[\langle A_0 \rangle])$ is negative in the confined phase, in contrast to its counterpart in the fundamental representation.

In $SU(N_c)$ gauge theories, relation (1.36) can be proven straightforwardly by the tensor product decomposition of the triplet and the anti-triplet into the adjoint multiplet and a singlet

$$N_c \otimes \overline{N_c} = (N_c^2 - 1) \oplus 1\,. \tag{1.38}$$

Recall furthermore that the character of the product representation is given by the product of the characters of the representations. Using this relation, we immediately find

$$d_{\mathrm{A}}\, \mathrm{tr}_{\mathrm{A}}(L_{\mathrm{A}}[\langle A_0 \rangle]) = \left|d_{\mathrm{F}}\, \mathrm{tr}_{\mathrm{F}}(L_{\mathrm{F}}[\langle A_0 \rangle])\right|^2 - 1\,, \tag{1.39}$$

and similar relations for $\mathrm{tr}_{\mathrm{A}}(L_{\mathrm{A}}[\langle A_0 \rangle]^n)$ with $n > 1$ ($n \in \mathbb{N}$).

In addition to representations for which $\mathrm{tr}_{\mathrm{R}}(L_{\mathrm{R}}[\langle A_0 \rangle])$ vanishes (e.g. R=F) or is negative (e.g. R=A) in the low temperature phase $T < T_d$, this quantity can also assume positive values in the center-symmetric phase. One example for this is the ten-dimensional representation (R = **10**) of $SU(3)$. Using again the tensor product decomposition

$$3 \otimes 3 \otimes 3 = 10 \oplus 8 \oplus 8 \oplus 1\,, \tag{1.40}$$

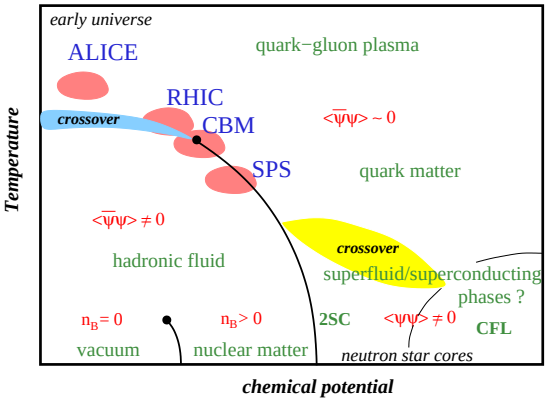

Figure 1.2.: Sketch of the expected QCD phase structure in the (μ, T) plane. See text for a detailed discussion. Picture taken from [27].

together with Eq. (1.38) for $N_c = 3$ we find

$$\begin{aligned} d(\mathbf{10})\,\mathrm{tr}_{\mathbf{10}}(L_{\mathbf{10}}[\langle A_0\rangle]) &= [d_{\mathrm{F}}\,\mathrm{tr}_{\mathrm{F}}(L_{\mathrm{F}}[\langle A_0\rangle])]^3 - 2\,|d_{\mathrm{F}}\,\mathrm{tr}_{\mathrm{F}}(L_{\mathrm{F}}[\langle A_0\rangle])|^2 + 1 \\ &= 1 \end{aligned} \tag{1.41}$$

for $T < T_{\mathrm{d}}$. Similar relations hold for $\mathrm{tr}_{10}(L_{10}[\langle A_0\rangle]^n)$ with $n > 1$ ($n \in \mathbb{N}$). As for the adjoint representation, the N-ality of the ten-dimensional representation of $SU(3)$ is zero, $\mathcal{N}_{\mathbf{10}} = 0$.

Summarising, we have found that the quantity $\mathrm{tr}_{\mathrm{R}} L_{\mathrm{R}}[\langle A_0\rangle]$ can vanish as well as assume positive or negative values in the center symmetric phase $T < T_{\mathrm{d}}$, depending on the representation R. This allows us to classify gauge theories. In Sec. 4.2, we shall see that this classification is to some extent related to the question whether the chiral phase transition temperature is smaller or larger than the deconfinement phase transition in a given gauge theory.

1.2. Phase Structure of QCD

This thesis focuses on achieving a more profound understanding of the QCD phase structure, especially in the plane spanned by temperature and quark chemical potential. Present experiments are able to probe the phase structure. By variation of the collision energy $\sqrt{s}$, different regions in the phase diagram with $\mu = \mu(\sqrt{s})$ can be probed. The experimental data points can be interpreted with the help of the hadron resonance gas (HRG) model, see [28] for a review, resulting in the so-called *chemical freeze-out curve* $T_{\mathrm{fr}}(\mu)$. A direct comparison of experimental outcomes and theoretical predictions is aggravated by the fact that the freeze-out points measured in experiment do not necessarily agree with the chiral and/or deconfinement transitions. The resulting freeze-out curve should, however, lie close to the QCD phase transition line, as proposed in [29]. Lattice simulations actually suggest that the two lines differ more and more as the chemical potential is increased [30, 31].

Let us now recapitulate some aspects of the QCD phase structure shown in Fig. 1.2: The low temperature and density region is home to our every-day world of hadrons, i.e.

confined, massive bound states of quarks and gluons prevail. Chiral symmetry is broken spontaneously in this regime. Going up in temperature, lattice and model calculations agree that a crossover transition occurs leading to the so-called quark-gluon plasma (QGP) phase. Contrary to previous expectations based on asymptotic freedom, however, the recent years have shown that the QGP created at the Relativistic Heavy-Ion Collider (RHIC) is not weakly interacting and this phase has since been renamed *strongly-coupled QGP*, see e.g. [32] for a review.

At very high temperatures chiral symmetry is restored, since thermal fluctuations lead to a melting of the chiral condensate, and furthermore deconfinement sets in. It has been found in various studies that the phase transitions associated with these two effects lie remarkably close to each other. To be precise, lattice groups report $T_\chi \approx 154 \pm 9$ MeV (HotQCD Collaboration) [33] and $T_\chi \approx 147 - 157$ MeV (Wuppertal-Budapest group) [34]. From a phenomenological point of view, this observation has important consequences for our understanding of the dynamics in heavy-ion collisions as well as of the generation of hadron masses in the early universe. In fact, a comprehensive picture of the dynamics close to the finite-temperature phase boundary of QCD is required for a reliable description of data from heavy-ion collision experiments [35].

Thus far it could, however, not be established whether the agreement of the chiral and deconfinement transition persists at finite chemical potential. In this connection, the notion of *quarkyonic matter* was put forward in the recent years. We will briefly repeat here the argument given in more detail in Ref. [36]: In the 't Hooft large-N_c limit, where $\bar{g}^2 N_c$ and N_f are kept fixed while $N_c \to \infty$, with $\bar{g}$ denoting the gauge coupling, one finds that the theory is still confining in the vacuum with a spectrum of mesons and glueballs. Baryon degrees of freedom are heavily suppressed in the confined phase due to their large mass $M_B \sim N_c$. At finite temperature, a first-order transition to a deconfined phase of quarks and gluons occurs, for which the pressure acts as an order parameter, as discussed below. The related transition temperature $T_d \sim \Lambda_{\mathrm{QCD}}$ is independent of the chemical potential $T_d(\mu) = T_d(0)$, since the coupling of quarks to gluons in large-N_c is of $\mathcal{O}(1/N_c)$. In the high temperature phase $T > T_d$, gluons prevail and accordingly the pressure behaves as $\mathcal{O}(N_c^2)$. Increasing chemical potential at $T = 0$, one finds that no Fermi surface is formed before the baryon chemical potential reaches the baryon mass. Hence, the low temperature, confined phase $T < T_d, \mu_B < m_B$ is populated by mesons and glueballs. This results in a pressure of $\mathcal{O}(1)$, since baryons are exponentially suppressed. For $\mu_B > m_B$, a dense phase of baryons forms in which the pressure is of order $\mathcal{O}(N_c)$. This phase is referred to as the quarkyonic phase. An illustration of the resulting phase structure is shown in Fig. 1.3. Furthermore, one can deduce by an analogy to a Skyrme crystal that chiral symmetry can in principle be broken or restored in the confined phase. The blue (curved) line in Fig. 1.3 denotes a possible chiral transition line, guided by the Skyrme crystal.

While the original arguments for quarkyonic matter are constructed in the large-N_c limit and without any reference to chiral symmetry, it was speculated subsequently that also at $N_c = 3$ a new phase could exist. This phase is also called quarkyonic phase, but is characterised by restored chiral symmetry while confinement persists, see e.g. [37–41]. In the present work we will demonstrate how fluctuations affect such a splitting of the two phase transitions. In particular, we find that by inclusion of the matter backcoupling to the gauge sector the quarkyonic phase shrinks, cf. Chap. 3.

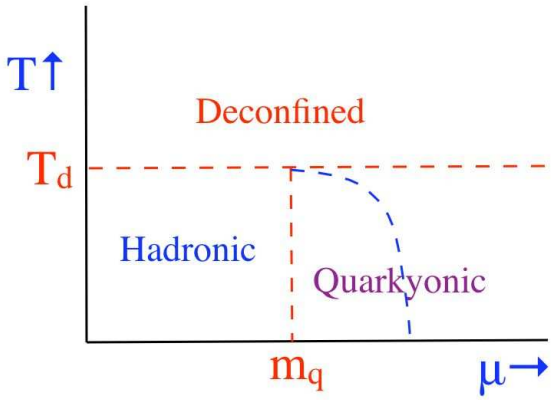

Figure 1.3.: QCD phase structure in the large-N_c limit. The blue (curved) line indicates a possible chiral phase transition in the quarkyonic region. See text for a more detailed discussion. Picture taken from [36].

At low temperatures and high chemical potentials, several model results, e.g. [42–49] point to the existence of a first-order transition in the QCD phase diagram. This suggests the existence of a QCD critical point of second order that marks the end of the first-order transition line. Such a critical endpoint (CEP) is related to long-range fluctuations in the form of a diverging correlation length ξ. The determination of its existence, location and properties are in the focus of present and future experiments such as the Nuclotron-Based Ion Collider Facility (NICA) at the Joint Institute for Nuclear Research (JINR), RHIC at Brookhaven National Laboratory (BNL) and the Compressed Baryonic Matter (CBM) experiment at the Facility for Antiproton and Ion Research (FAIR). From the theoretical side it is of utmost importance to provide a profound knowledge of the characteristics of the conjectured CEP. The experimental task of detecting the CEP is not as easy as it may naively seem, since the fireball created in a heavy-ion collision is a system of finite size, in which no second-order phase transition in the strict sense can occur. Subject to critical slowing down, the correlation length remains finite and is estimated to be of the order of $2-3$ fm [50, 51]. This is only slightly larger than the natural scale of $0.5-1$ fm away from the critical point. One task for experimentalists could be to detect a non-monotonic behaviour of, e.g. the number fluctuations. It has been suggested recently that it should be worthwhile to study higher moments of fluctuations, since these are related to higher powers of the correlation length, e.g. $\langle(\delta N)^2\rangle \sim \xi^{2-\eta}$ with $\eta \approx 0.12$, or $\langle(\delta N)^4\rangle \sim \xi^7$, cf. discussion in [52–54]. The behaviour of these observables and expected signals for experiment can also be conveniently studied within effective models.

Concerning the full phase diagram we want to add that at high chemical potential an abundance of phases might exist that are related to the phenomena of colour-flavour locking and colour superconductivity, see e.g. [55] for a review. Various pairing patterns of colour and/or flavour structures are possible that are relevant for, e.g. the physics of neutron stars [56–58]. Furthermore, additional external parameters such as an external magnetic field have been studied in the literature, see e.g. [59–61]. Especially, the response of strongly interacting matter to an external magnetic field is a highly relevant question in

heavy-ion collisions, where such large magnetic fields do occur, but have not been studied extensively thus far. The presence of an external magnetic field is furthermore related the phenomenon of magnetic catalysis.

Despite their interesting features, these aspects of the QCD phase structure will not be addressed further in this thesis. We will rather focus on the phase structure at moderate chemical potentials and study several thermodynamic observables.

1.3. Non-Perturbative Approaches to QCD

In order to address the above-mentioned aspects of QCD - and especially its phase structure - various techniques can be used. As pointed out above, perturbation theory, that has provided us with amazing results in, e.g. low-energy QED, is bound to fail in low-energy QCD due to the running of the strong coupling constant that is just opposite to the running of the electric charge. Moreover, the phenomena of spontaneous chiral symmetry breaking and confinement are inherently non-perturbative. It is thus clear that for a study of the phase structure at finite temperature and chemical potential, non-perturbative tools are indispensable.[2]

One such method has already been mentioned above, namely lattice gauge theory. In this approach, Euclidean space-time is discretised into a lattice with spacing a and volume V, see e.g. [62] for an introduction. Discretised versions of the gauge and fermion actions can then be used together with Monte-Carlo techniques to simulate QCD from first-principle, including non-perturbative contributions. In order to make contact with continuum QCD, in the end the continuum limit $a \to 0$ and the thermodynamic limit $V \to \infty$ have to be performed. This is only possible by extrapolation. The calculation at small pion mass is another obstacle of this method, since it requires a substantial amount of computer time to invert the Dirac operator at physical masses. Nevertheless, in the recent years it was possible to reach the physical mass point. Lattice gauge theory is hence well-suited to study the finite-temperature phase transitions. Its application at finite chemical potential is, however, hampered by the fact that the fermion determinant, which is used as a probability weight in lattice QCD, becomes complex in this regime. Sophisticated techniques such as re-weighting, Taylor expansion in μ/T or analytic continuation from imaginary chemical potential have been developed in the last years to overcome this problem, see e.g. [63–66]. However, lattice results for the QCD phase structure are still limited to small chemical potentials.

A complementary, non-perturbative approach is the use of so-called Dyson-Schwinger equations (DSEs), see [67–70] for reviews on this topic. The DSEs constitute the equations of motion for the n-point functions of the theory. If one could solve the whole (infinite) tower of them, the theory would be solved. However, the DSE for a given n-point function always contains higher $(n+m)$-point functions with $m > 0$, and in particular there exists no finite closed subset thereof. Hence, truncations are mandatory in practise. In contrast to the renormalisation group equations introduced below, regularisation and renormalisation have to be performed explicitly within this framework.

Recently, results for the $N_f = 2$ and $N_f = 2 + 1$ flavour QCD phase diagram calculated from DSEs have been put forward in [71–73]. As we will demonstrate, these results agree

[2] We want to point out that the list of functional methods given here is not exhaustive.

nicely with ours for $N_f = 2$, computed via the FRG. [3]

The method of choice for this thesis is yet another functional, non-perturbative technique: the functional renormalisation group (FRG) introduced below.

Owing to an increase in experience and computational resources in the last years, the application of these sophisticated methods to QCD starts to become feasible. However, first-principle studies of QCD still pose a formidable task and can only be accomplished one step at a time, see e.g. [75] for the current status of first principle studies of the QCD phase diagram. An additional, legitimate and very helpful tool is the use of effective models, that are designed to describe some aspects of the full theory, while being easier to handle. This approach is chosen in the present thesis in order to achieve insights into the phase structure at finite temperature and quark chemical potential. A detailed account on some effective models and their relation to QCD will be given in Chap. 2. We want to point out that, where applicable, good agreement between lattice simulations and functional studies of effective models is observed. This suggests that by now functional methods are in a position to provide competitive, and in particular reliable, results in the context of QCD.

1.3.1. Special Focus: Functional Renormalisation Group

It is well-known that physical processes may look different, when observed with different resolution. For the description of macroscopic phenomena, a detailed knowledge of the microscopic dynamics and degrees of freedom is often not necessary. QCD, for example, describes the interactions of quarks and gluons at high momenta, while its low energy sector is conveniently described by hadrons.

In fact, we would like to derive a macroscopic description from the underlying microscopic theory, in order to achieve an understanding of the mechanisms giving rise to the macroscopic phenomena. The functional renormalisation group (FRG) is especially well-suited to study this question. [4]

In quantum field theory, the quantities of interest defining the theory are a hierarchy the n-point Greens functions. They can be derived from the generating functional that is defined via the path integral.[5] However, in the evaluation of the path integral one usually encounters divergences that must be taken care of by regularisation and renormalisation.

The idea of the renormalisation group, as put forward by Wilson [77], is the following: In the description of a theory at a given RG scale k, the knowledge of higher scales is not necessary. One can rather describe the system at this scale effectively by a theory, where higher momenta have been integrated out. The integration over all momenta is hence not performed at once, but momentum-shell by momentum-shell from the ultraviolet (UV) down to the infrared (IR). In this manner it is possible to relate the different regimes of a theory - e.g. the weakly and strongly interacting ones.

Starting from a local initial action Γ_Λ in the UV[6], the RG flow describes the change

[3] Presently, also the case of $N_f = 2 + 1$ flavours is being studied within the FRG, see e.g. [74].

[4] Note that while the motivation given here relates to the momentum space version of the FRG it is also possible to formulate it in position space, where one can think of it in terms of Kadanoff's block-spin transformations [76].

[5] A proper mathematical definition of the measure needed in the path integral is an open problem for interacting quantum field theories, while the Wiener measure is applicable for non-interacting theories.

[6] In theory, the action should be defined in the UV, i.e. at the scale $\Lambda \to \infty$. In practise, however, one will always use a finite initial scale $\Lambda < \infty$. If this scale is chosen high enough, one can, for example,

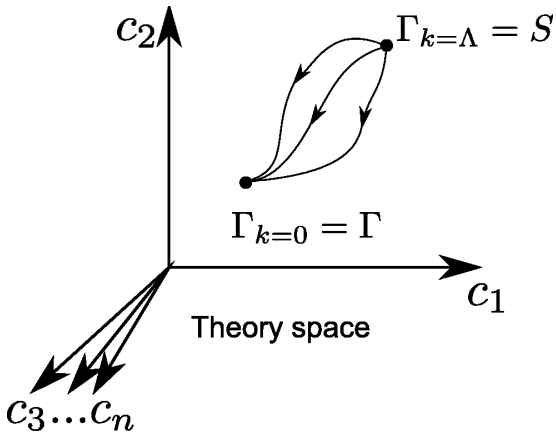

Figure 1.4.: Illustration of some RG trajectories in theory space that connect the initial action at the UV scale Λ to the full quantum effective action in the infrared. Picture taken from [78].

of the - now scale dependent - effective average action $\Gamma_k \to \Gamma_{k-\delta k}$. In fact, this flow can involve a change in degrees of freedom. The high-energy degrees of freedom may not show up in the low-energy description, but only indirectly influence the physics via their contribution to the scale dependent change in the arising couplings.

It is instructive to picture the RG flow in theory space, which is the space spanned by the couplings of all operators that are allowed by the symmetries and field content of the given system, see Fig. 1.4 for an illustration. In general, this space is infinite dimensional. The initial action Γ_Λ denotes one point in theory space, that corresponds to fixed values of a set of - usually renormalisable - couplings in Γ_Λ and all other couplings set to zero. The RG flow then maps out a trajectory in theory space, and in particular couplings that vanished initially are allowed to develop non-zero values dynamically. In the infrared, $k \to 0$, we are left with an action $\Gamma_{k\to 0}$ which includes all quantum fluctuations, as desired, but might contain entirely different operators than present in Γ_Λ. In practise, one distinguishes operators whose contribution increases towards the infrared (*relevant operators*) and those that vanish (*irrelevant operators*).[7]

In this setting, an intuitive understanding of *universality* can be achieved. Already before the RG was introduced it was known that entirely different physical systems show remarkably similar behaviour at second-order phase transitions. In particular, the critical exponents describing the systems at the critical point agree. This phenomenon can be understood with the help of the RG: Despite the fact that such systems are described by different microscopic actions, in the RG evolution the same operators turn out to be relevant. The IR behaviour of these systems is hence dictated by symmetry, field content and dimensionality only and agrees for systems which lie in the same universality class.

Let us furthermore add, that there exist different implementations of the above presented RG idea, for example Wilson RG [77], Polchinski RG [79], Wetterich RG [80], proper-time

use perturbative results to fix Γ_Λ.

[7] In fact there is also a third category of *marginal operators*, which do not belong to any of the aforementioned classes and require special analysis.

RG [81] etc. In this thesis, the exact renormalisation group equation (ERGE) will be used.

Remark 1.3:
Note that while the standard proper-time RG involves a RG-improvement by hand - i.e. is not exact - there exists an RG regulator function which yields the same flow equation as the Wetterich equation if the optimised regulator [82] is used in the latter. In general it is known that the standard proper-time RG can be made equivalent to the ERGE by adding a term $\sim \partial_t \Gamma_k^{(2)}$. *The resulting equation is referred to as generalised proper-time RG. Since there exists a derivation from first principles for Wetterich's equation, we choose to employ this variant in the present work.*

A brief derivation of Wetterich's equation is provided in App. A, where also some common truncation schemes are introduced.

2. QCD Effective Models

In the recent years, a lot of progress in our understanding of QCD and its phase structure has been achieved. In this connection one should be aware that these insights have, to a large extent, been gained by the use of effective models. For example, lattice simulations are hampered by the notorious sign problem at finite chemical potential. Also functional first-principle studies of full QCD still pose rather sophisticated tasks, due to the highly non-trivial nature of this non-Abelian gauge theory. Hence, effective models provide a very fruitful alternative approach. These are designed to describe some aspects of the underlying theory, but are easier to handle. Despite the fact that effective models by construction leave out some features of the full theory, valuable insights can be achieved in such an approach. For example, the spontaneous breaking of chiral symmetry can be very well described within Nambu–Jona-Lasinio type models and their partially or fully bosonised relatives, as demonstrated in this chapter.

Moreover, as will be discussed in more detail below, some of these models can be related to QCD in a systematic fashion within the RG framework. On the one hand, this allows improvements towards the full theory and on the other hand enables an understanding of the influence of different aspects of the theory on the given observables.

In the following, we start from the purely fermionic Nambu–Jona-Lasinio (NJL) model and discuss how chiral symmetry breaking can be studied on the basis of this model. Subsequently, a bosonisation technique will be introduced that allows to reformulate and extend this model to the well-known quark-meson model, whose advantages in comparison to the NJL model will be in the focus of the following section. Furthermore, to get a more accurate description of QCD, our aim is to include some aspects of confinement into our effective models. It has been proposed recently that this can be achieved by coupling the Polyakov-loop to chiral effective models. This procedure will be outlined in Sec. 2.2. This chapter will be closed by some remarks on the systematic connection of effective models to QCD.

2.1. Chiral Symmetry

It has been known since the 1960s that chiral symmetry and its spontaneous and explicit breaking can be conveniently described within a purely fermionic model [83]. For some applications it may, however, be useful to employ models with additional degrees of freedom, such as mesons. From the phenomenological point of view, this is very intuitive: We expect the low energy sector of QCD to be well described by a theory of quarks and light mesons. While such an interpretations can also be applied to the purely fermionic formulation, it might be preferable to have explicit bosonic degrees of freedom in the model. In practise, both formulations have their advantages and will be discussed in the following.

2.1.1. Nambu–Jona-Lasinio Model

We start by discussing a purely fermionic effective model that has a very wide range of applicability: the *Nambu–Jona-Lasinio* (NJL) model [83]. This theory was originally designed to describe the interaction of nucleons and mesons and is constructed in analogy to the description of Cooper pairs in superconductivity. The fermionic degrees of freedom were soon reinterpreted as quarks and the NJL model was henceforth also used as an effective model for the chiral symmetry breaking in QCD.

The foundation of the construction of effective models are symmetries. In the case of the NJL model we consider N_f flavours of massless Dirac fermions. These should obey chiral symmetry and interact via a four-fermion coupling $\bar{\lambda}_\psi$

$$\mathcal{L}_{\mathrm{NJL}} = \bar{\psi} i \partial\!\!\!/ \psi + \frac{\bar{\lambda}_\psi}{2} \left[\left(\bar{\psi}\psi\right)^2 - \left(\bar{\psi}\gamma_5 \vec{\tau}\psi\right)^2 \right] . \tag{2.1}$$

As one can easily check, the kinetic term as well as the combination of four-fermion operators in the brackets are invariant under chiral $SU(N_f)_V \times SU(N_f)_A$ transformations

$$\begin{aligned} \psi &\longrightarrow e^{i\theta_a \lambda^a/2}\psi \,, \\ \bar{\psi} &\longrightarrow \bar{\psi} e^{-i\theta_a \lambda^a/2} \,, \end{aligned} \tag{2.2}$$

$$\begin{aligned} \psi &\longrightarrow e^{i\gamma_5\theta_a \lambda^a/2}\psi \,, \\ \bar{\psi} &\longrightarrow \bar{\psi} e^{i\gamma_5\theta_a \lambda^a/2} \,. \end{aligned} \tag{2.3}$$

As in QCD, additional axial and vector $U(1)$ phase transformation are permissible. Note that in addition to the interaction term shown in Eq. (2.1), which is a scalar-pseudoscalar term, also a vector $(\bar{\psi}\gamma_\mu\psi)^2$ and an axial-vector channel $(\bar{\psi}\gamma_\mu\gamma_5\psi)^2$ are allowed by chiral symmetry. In the vacuum, this list of permissible combinations of four-fermion operators is exhaustive. However, only two of these chiral invariants are independent, since they are related via so-called Fierz-transformations [84]. In principle, one should use a Fierz-complete ansatz and include also the vector and axial-vector interactions in the Lagrangian Eq. (2.1). At finite temperature, however, due to broken Lorentz invariance by the heat-bath more terms arise, making it tedious to construct a complete set of operators. We will comment further on the justification of the present truncation when we perform our FRG study in Chap. 4.

At this point we explicitly specify the number of flavours choosing $N_f = 2$, which will be used in all calculations of this thesis. Then, the vector $\vec{\tau} = (\sigma_1, \sigma_2, \sigma_3)$ denotes the Pauli matrices that couple the quark spinors in flavour space. Despite the fact that a fermion mass term in the Lagrangian is forbidden by chiral symmetry, mass can be generated dynamically in the NJL model by the spontaneous breaking of chiral symmetry. It is well-known [83] that this symmetry breaking is triggered by strong quark self-interactions and results in the generation of a chiral condensate $\langle\bar{\psi}\psi\rangle \neq 0$, which acts as an order parameter. Furthermore the condensate contributes to the dynamical generation of mass for the fermions.

Remark 2.1:
Note that in NJL-type models, multi-fermion interactions appear explicitly in the Lagrangian. In full QCD, on the other hand, quark self-interactions are not free parameters, but are generated dynamically and driven to criticality by the gauge degrees of freedom. This can be understood in simple terms from a RG analysis of the fixed-point structure of four-fermion interactions in gauge theories, see e.g. [85–88].

In four space-time dimensions, the NJL model is perturbatively non-renormalisable.[1] Hence one needs to introduce an ultraviolet cutoff Λ that constitutes an additional parameter of the model. Moreover the regularisation scheme belongs to the definition of the model as well. The role of the UV cutoff will be discussed in more detail in Chap. 4, where we make use of a similar ansatz for the action in order to study gauged four-fermion interactions coupled to the Polyakov-loop in various gauge groups. This will allow to gain analytic insights into the interplay of chiral symmetry breaking and confinement at finite temperature. However, it will also be shown there that a study of low-energy observables is rather tedious in this formulation. This is related to the fact that e.g. meson masses correspond to poles in the four-fermion couplings. In the above-introduced action, however, the coupling is independent of momentum, which is referred to as the *point-like approximation*. Clearly, such a formulation does not allow the study of the chirally broken phase. Still, as we will demonstrate in Chap. 4, it is worthwhile to study this model since it allows to gain analytical insights into the mechanisms at work when the chiral symmetry breaking scale is approached from the symmetric phase. Moreover, this limitation can be overcome by deriving a partially bosonised version of the NJL-type model via a Hubbard-Stratonovic transformation [90, 91]. In such a formulation, the study of infrared observables is made possible. This is the task of the subsequent section.

2.1.2. Quark-Meson Model

In order to relate the two-flavour NJL model to another well-known effective theory - the linear σ-model coupled to quarks - we make use of a Hubbard-Stratonovic transformation. To this end, consider the generating functional

$$Z[\bar{\eta},\eta] = \mathcal{N}_1 \int \mathcal{D}[\bar{\psi},\psi] \exp\left\{-S_{\mathrm{NJL}} + \int_x \bar{\eta}\psi + \int_x \bar{\psi}\eta\right\}, \tag{2.4}$$

which contains the action S_{NJL} and also fermion sources $\eta, \bar{\eta}$ have been introduced.

As a first step, we insert unity via a Gaussian-type integral over the auxiliary meson fields $\bar{\phi}^T = (\sigma, \vec{\pi})$. These will subsequently be interpreted as composites of the fermionic fields $\sigma \sim (\bar{\psi}\psi)$ and $\vec{\pi} \sim (\bar{\psi} i\gamma_5 \vec{\tau}\psi)$ and carry no internal colour or flavour structure

$$1 = \mathcal{N}_2 \int \mathcal{D}\phi \exp\left\{-\int_x \frac{\bar{m}^2}{2}\bar{\phi}^2\right\}. \tag{2.5}$$

Assuming translational invariance of the path integral, we can perform a shift in these

[1] In two dimensions, however, the theory is renormalisable. It is then referred to as the Gross-Neveu model [89].

additional variables

$$\sigma \rightarrow \sigma + \frac{i\bar{h}}{\bar{m}^2}\bar{\psi}\psi \tag{2.6}$$

$$\vec{\pi} \rightarrow \vec{\pi} + \frac{i\bar{h}}{\bar{m}^2}\bar{\psi}i\gamma_5\vec{\tau}\psi\,, \tag{2.7}$$

and further demand that the arbitrary parameters $\bar{h}$, $\bar{m}^2$ obey

$$\bar{\lambda}_\psi = \frac{\bar{h}^2}{\bar{m}^2}\,. \tag{2.8}$$

With this prescription, the four-fermion operators cancel and we are left with a theory of quarks coupled to scalar and pseudoscalar meson fields

$$S = \int d^4x \left\{ \bar{\psi}i\partial\!\!\!/\psi + i\bar{h}\bar{\psi}(\sigma + i\vec{\tau}\cdot\vec{\pi}\gamma_5)\psi + \frac{1}{2}\bar{m}^2\bar{\phi}^2 \right\}. \tag{2.9}$$

Now it should be clear what we previously mean by the term "partially bosonised": By the above procedure we eliminated the four-fermion interaction term while retaining the fermion kinetic term. Furthermore, a fermion-boson interaction term via the Yukawa coupling $\bar{h}\bar{\psi}(\sigma + i\vec{\tau}\gamma_5)\psi$ was generated. We hence have achieved a "mixed" quark-meson formulation. Note that it is also possible to fully bosonise the system, resulting in a purely bosonic description, cf. Sec. 4.3.1.

After the above described manipulation, a chiral transformation of the fermion field, as discussed in the previous section, acts on the meson fields $(\sigma, \vec{\pi})$ in form of an $O(4)$ rotation.

We would like to point out that as it stands, Eq. (2.9) is equivalent to the purely fermionic formulation Eq. (2.1). In particular, since we have performed the partial bosonisation at the cutoff scale, also this formulation depends on Λ.

Apart from its relation to the NJL model one can also consider the partially bosonised action as the definition of an independent effective model. It is then not necessary to introduce a cutoff - the model is renormalisable. It is usually referred to as the *quark-meson (QM) model*.

In practice the action Eq. (2.9) is usually augmented by a kinetic term for the mesonic fields and a more general mesonic potential $U(\bar{\phi})$ obeying the symmetries. Also wave-function renormalisations $Z_{\psi,\phi}$ for the quark and meson fields can be introduced

$$S_{\mathrm{QM}} = \int d^4x \left\{ Z_\psi\bar{\psi}i\partial\!\!\!/\psi + \frac{1}{2}Z_\phi(\partial_\mu\bar{\phi})^2 + i\bar{h}\bar{\psi}(\sigma + i\vec{\tau}\cdot\vec{\pi}\gamma_5)\psi + U(\bar{\phi}) \right\}. \tag{2.10}$$

The connection to the NJL model is then recovered by requiring $Z_\psi|_\Lambda = 1$, $Z_\phi|_\Lambda = 0$, $\bar{\lambda}_\psi = \frac{\bar{h}^2}{\bar{m}^2}\Big|_\Lambda$ and $U(\bar{\phi}) = \frac{1}{2}\bar{m}^2\bar{\phi}^2$. In particular, the presence of the meson fields and the Yukawa interaction allows to partially resolve the momentum dependence of the four-fermion interaction $\lambda_\psi(p)$, see also our discussion in Sec. 4.3.3. Hence, by this generalisation, interactions beyond the point-like approximation $\lambda_\psi(|p| \ll k)$ are included.

From the Lagrange equations of motion for the meson fields we find that $\langle\sigma\rangle = -i\frac{\bar{h}}{\bar{m}^2}\langle\bar{\psi}\psi\rangle$ acts as an order parameter for the spontaneous breaking of chiral symmetry in this formu-

lation. To discuss this in more detail, we extend the mesonic potential by a term quadratic in the boson fields $\sim \bar{\lambda}_\phi \bar{\phi}^4$ with $\bar{\lambda}_\phi > 0$. Since the mass parameter $\bar{m}^2$ describes the curvature of the chiral order parameter potential at the origin, the sign of $\bar{m}^2$ is related to the question whether chiral symmetry is broken in the ground state or not. In the case $\bar{m}^2 > 0$, the effective potential possesses one stable minimum at $\langle\sigma\rangle = 0$. For $\bar{m}^2 < 0$, on the other hand, the potential has the form of a "Mexican hat", i.e. it develops a family non-trivial minimum $\langle\sigma\rangle \neq 0$. In the ground state, the system spontaneously chooses one of these minima, hence chiral symmetry is broken. The expectation value $\langle\sigma\rangle \neq 0$ then acts as a mass term for the quark fields via the Yukawa term $i\bar{h}\langle\sigma\rangle\bar{\psi}\psi$. Hence, the value $\bar{m}^2 = 0$ separates the chirally broken ($\bar{m}^2 < 0$) from the chirally symmetric ($\bar{m}^2 > 0$) regime. In terms of the NJL formulation this corresponds to

$$\bar{\lambda}_\psi = \frac{\bar{h}^2}{\bar{m}^2} \to \infty \quad \text{as} \quad \bar{m}^2 \to 0\,. \tag{2.11}$$

In fact, the two criteria are equivalent in the large-N_c limit due to the absence of fluctuation effects of the Goldstone modes [92].

Now it is clear why the fermionic formulation in the point-like approximation, as given in Eq. (2.1) is not well-suited for a study of low-energy observables: At the chiral symmetry breaking scale $k_{\rm cr}$ the four-fermion coupling diverges and thus prevents a study of the chirally broken phase. It is, however, possible to study the onset of chiral symmetry breaking within the NJL-type formulation, as will be demonstrated in Chap. 4. In the partially bosonised formulation, on the other hand, no divergence occurs and we are finally in a position to study both, the chirally symmetric and the chiral symmetry broken phase.[2]

The QM model is expected to lie in the same universality class as QCD and has been studied extensively in the literature, see e.g. [93–97]. In the present work we mostly employ the following ansatz for the meson potential in the ultraviolet

$$U(\bar{\phi}) \;=\; \frac{\lambda}{4}(\sigma^2 + \vec{\pi}^2 - v)^2 - c\sigma\,. \tag{2.12}$$

In this ansatz, finite bare quark masses are introduced via a term linear in the sigma field. Note that within the renormalisation group approach applied in this thesis, Eq. (2.12) should *not* be understood as restricting the potential to quartic order in $\bar{\phi}$. Rather, it corresponds to a more general ansatz taking into account all powers of the chiral invariant ρ complying with $O(4)$ symmetry. While we specify the quadratic and quartic couplings explicitly in the UV, all higher (perturbatively non-renormalisable) couplings, such as those of six- and eight-boson operators, are set to zero at the UV scale Λ. During the RG evolution, these couplings can dynamically acquire non-vanishing values, which is accounted for in our numerical implementation.

2.2. Statistical Confinement

While the NJL and QM models are well-established effective models for the chiral sector of QCD, they do not include any gluonic degrees of freedom and hence are unable to describe

[2] Note that it is also possible to extend the purely fermionic formulation such, that the chirally broken phase becomes feasible. In this thesis we, however, prefer to use the partially bosonised formulation.

confinement. In the recent years, extensions of these models by Polyakov-loop variables have been put forward, see e.g. [98, 99] that include confinement in a statistical sense.

As discussed in Sec. 1.1, the fundamental Polyakov-loop acts as an order parameter for confinement in the pure gauge system. Lattice simulations of QCD with dynamical quarks have moreover confirmed that this quantity shows a crossover behaviour from the low-temperature, confined to the high-temperature phase also in the presence of dynamical quarks. It hence seems well-justified to extend the chiral effective models by introduction of Polyakov-loops to include some aspects of confinement.

The augmentation of the QM model by the Polyakov-loop discussed in the following is referred to as the *Polyakov–quark-meson (PQM) model*. A similar construction can be performed in the NJL model, resulting in the so-called Polyakov–Nambu–Jona-Lasinio (PNJL) model.

In practise, an effective potential term $\mathcal{U}(\Phi, \bar{\Phi})$ for the Polyakov-loop is added to the action of the QM model. This potential mimics a background of gluons in which the quarks and mesons interact. Furthermore, by implicitly assuming the use of Polyakov-Landau-DeWitt gauge[3], the temporal component of the gluon field is coupled to the quarks in a minimal fashion

$$\begin{aligned} S_{\mathrm{PQM}} &= \int d^4x \Big\{ Z_\psi \bar{\psi}(i\partial\!\!\!/ + \bar{g}\gamma_0 A^\mu \delta^0_\mu)\psi + \frac{1}{2} Z_\phi (\partial_\mu \bar{\phi})^2 + i\bar{h}\bar{\psi}(\sigma + i\vec{\tau}\cdot\vec{\pi}\gamma_5)\psi \\ &\quad + U(\bar{\phi}) + \mathcal{U}\left(\Phi, \bar{\Phi}\right) \Big\} \ . \end{aligned} \tag{2.13}$$

For the effective Polyakov-loop potential $\mathcal{U}(\Phi, \bar{\Phi})$, a Landau-Ginzburg like ansatz is made. The requirements that are imposed are $U(1)$ and Z_{N_c} symmetry. While the potential itself is symmetric under Z_{N_c} transformations, in the regime of spontaneous breaking of center symmetry, its ground state need not. In this thesis we consider this potential for $N_c = 3$ colours only, hence it has to accommodate the associated first-order phase transition at finite temperature that is observed in lattice studies of the pure Yang-Mills system.[4] With these requirements, a minimal polynomial ansatz for the Polyakov-loop potential reads

$$\frac{\mathcal{U}_{\mathrm{poly}}}{T^4} = -\frac{b_2(T;T_0)}{2}\Phi\bar{\Phi} - \frac{b_3}{6}\left(\Phi^3 + \bar{\Phi}^3\right) + \frac{b_4}{4}\left(\Phi\bar{\Phi}\right)^2 \ , \tag{2.14}$$

with the temperature dependent coefficient

$$b_2(T) = a_0 + a_1\left(\frac{T_0}{T}\right) + a_2\left(\frac{T_0}{T}\right)^2 + a_3\left(\frac{T_0}{T}\right)^3 \ . \tag{2.15}$$

On the lattice, the Polyakov-loop as well as thermodynamic quantities such as the free energy can be measured. This data is used to fix parameters in the ansätze Eq. (2.14) and Eq. (2.15). This was done for example in [101] by a fit to pure Yang-Mills lattice data and results in

$$a_0 = 6.75 \ , \ a_1 = -1.95 \ , \ a_2 = 2.625 \ , \ a_3 = -7.44 \tag{2.16}$$

[3] With this choice of gauge, A_0 is an element of the Cartan subalgebra of $SU(N_c)$, which subsequently allows to express the explicit gluon contribution in the covariant derivative in terms of Polyakov-loops, see e.g. [100].

[4] For $N_c = 2$ a second-order transition is observed, see also our discussion in Chap. 4.

and

$$b_3 = 0.75\,, \quad b_4 = 7.5\,. \tag{2.17}$$

These values will also be used in the present work. The parameter T_0 denotes the scale of the deconfinement transition and is deduced from the lattice to be $T_0 = 270$ MeV in the pure gauge system. The influence of dynamical quarks on this parameter is an essential point and will be discussed in detail in Sec. 3.2.

Presently, there are also other versions of the Polyakov-loop potential on the market, such as a logarithmic version [44], that includes the Haar-measure of the gauge group. A benefit of the logarithmic potential is, that it automatically restricts the Polyakov-loops to the physical domain $\Phi, \bar{\Phi} \leq 1$. In contrast, the polynomial version allows also for $\Phi, \bar{\Phi} > 1$, cf. [99], and one has to apply a suitable normalisation to ensure $\Phi, \bar{\Phi} \to 1$ for asymptotically high temperatures.

The Polyakov-loop potential proposed by Fukushima [98] takes into account not only the longitudinal, but also the transverse parts of the gluon field since these are expected to contribute to the pressure at high temperatures. Apart from the discrepancy at high temperatures it is found that all three versions agree reasonably well at moderate temperatures, cf. [37]. In view of the project discussed in Chap. 3 we want to add that Fukushima's parametrisation of the Polyakov-loop potential is different from the polynomial and logarithmic versions in one aspect: the deconfinement scale T_0 is not directly accessible in this variant.

The results shown in the subsequent chapters were achieved by use of the polynomial potential. The general features persist also when the other versions are used. However, we want to add that Fukushima's parametrisation is not well suited for our present application.

By now it is also possible to compute the glue potential using functional methods, see e.g. [16, 75] for results from the RG. Functional results can on the one hand be used as additional crosschecks of the employed approximation. On the other hand, they provide new input to augment the ansatz for the potential towards the full theory. These computations are rather sophisticated, thus we resort to the above introduced parametrisation of the glue potential in this thesis.

Let us briefly elaborate on the statistical confinement introduced by the Polyakov-loop. This can already be understood in a mean-field approximation, where the meson fields are replaced by their expectation values $\langle\sigma\rangle \equiv \sigma, \langle\vec{\pi}\rangle \equiv 0$. The remaining integration over the quark fields is Gaußian and can be performed analytically. The grand potential of the PQM model in this approximation is given by

$$\Omega_{\mathrm{MFA}}(\sigma, \Phi, \bar{\Phi}) = \Omega_{q\bar{q}}(\sigma, \Phi, \bar{\Phi}) + U(\sigma) + \mathcal{U}(\Phi, \bar{\Phi})\,, \tag{2.18}$$

with the quark contribution

$$\begin{aligned}
\Omega_{q\bar{q}}(\sigma, \Phi, \bar{\Phi}) &= -2N_f N_c \int \frac{d^3p}{(2\pi)^3} E_q \\
&- 2TN_f \int \frac{d^3p}{(2\pi)^3} \Big\{ \log\Big(1 + 3\Phi e^{-(E_q-\mu)/T} + 3\bar{\Phi} e^{-2(E_q-\mu)/T} + e^{-3(E_q-\mu)/T}\Big) \\
&+ \log\Big(1 + 3\bar{\Phi} e^{-(E_q+\mu)/T} + 3\Phi e^{-2(E_q+\mu)/T} + e^{-3(E_q+\mu)/T}\Big)\Big\}\,.
\end{aligned} \tag{2.19}$$

The first term in Eq. (2.19) is known as the fermion vacuum term. In the standard mean-field approximation this term is neglected. However, it was shown recently [53, 102] that this term indeed has crucial influence on the phase structure. In the chiral limit, the QM model shows a first-order chiral phase transition at vanishing chemical potential if the vacuum term is neglected, contradicting universality arguments [103]. After proper renormalisation and inclusion of this term one indeed observes the expected second-order chiral transition.

For the time being we are only interested in the implementation of confinement in the PQM model. To study this aspect, we can safely neglect the vacuum term, which carries no explicit dependence on the Polyakov-loop. Hence we do not expect it to have a large influence on our subsequent discussion. Note, however, that in the FRG study presented in the following chapters, this term is naturally included.

From Eq. (2.19) it can be seen that at low temperatures, where the Polyakov-loops assume small values, $\Phi, \bar{\Phi} \approx 0$, the argument of the logarithm simplifies

$$\Omega_{q\bar{q}} \sim -4TN_f \int \frac{d^3p}{(2\pi)^3} \left\{ \log\left(1 + e^{-3(E_q-\mu)/T}\right) \right\} . \tag{2.20}$$

This expression corresponds to the occupation number of a system of baryon-like degrees of freedom, characterised by three times the energy of a quark: $E \sim 3E_q$. One- and two-quark excitations are suppressed by the Polyakov-loop variable in this regime, which is interpreted as *statistical confinement*. In the high-temperature region, on the other hand, the Polyakov-loop tends to unity and we find

$$\begin{aligned} \Omega_{q\bar{q}} &\sim -2TN_f \int \frac{d^3p}{(2\pi)^3} \left\{ \log\left(1 + 3e^{-(E_q-\mu)/T} + 3e^{-2(E_q-\mu)/T} + e^{-3(E_q-\mu)/T}\right) \right. \\ &+ \left. \log\left(1 + 3e^{-(E_q+\mu)/T} + 3e^{-2(E_q+\mu)/T} + e^{-3(E_q+\mu)/T}\right) \right\} , \\ &= -2TN_f \int \frac{d^3p}{(2\pi)^3} 3 \left\{ \log\left(1 + e^{-(E_q-\mu)/T}\right) + \log\left(1 + e^{-(E_q+\mu)/T}\right) \right\} , \end{aligned} \tag{2.21}$$

Hence, also one- and two-quark states are excited at high temperatures, which is interpreted as deconfinement in the statistical sense.

The same mechanism is present also in the FRG approach to the PQM model.

2.3. Connection of the PQM Model to full QCD

We would like to take a moment to stress the relation of the above presented PQM model to full two-flavour QCD. To this end, consider the RG flow equation of two-flavour QCD shown in Fig. 2.1. The loops correspond to the gluon, ghost, quark and mesonic contributions, respectively. The signs and prefactors reflect the statistics of the fields. In the depicted flow equation, the ghost loop results from gauge fixing and the explicit meson degrees of freedom are introduced by partial bosonisation. Recall, that while the FRG flow equations always are of one-loop structure, they are not of one-loop order in the perturbative sense. In particular, the system in Fig. 2.1 is fully coupled and exact, i.e. no higher contributions are omitted.

The simple additive structure has important consequences for the PQM model: We

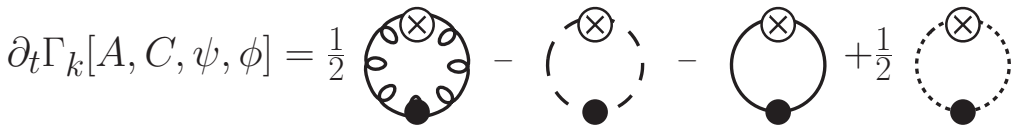

Figure 2.1.: FRG flow equation for two-flavour QCD after partial bosonisation and gauge fixing. The loops represent the gluon, ghost, quark and meson contributions, respectively, while the signs and prefactor reflect the statistics of the corresponding fields.

can easily identify the different parts of the model in terms of full QCD fluctuations. For example, the fluctuating quark-meson sector of the model is given by the last two diagrams in Fig. 2.1. In turn, the glue and ghost loops in Fig. 2.1, evaluated in the background of a Polyakov-loop Φ, give the Polyakov-loop potential in full QCD.

We are hence in the position to write down the flow equation of QCD, where the gluonic degrees of freedom have been integrated out. It is composed of a flow for the free energy which only involves the last two loops in Fig. 2.1 and the first two loops lead to the Polyakov-loop glue potential Ω_{glue}. Furthermore, there are modifications of the matter interaction which are included in the initial conditions in the quark-meson sector that capture the correct vacuum physics. The resulting effective potential for QCD can be cast in the following form

$$\Omega_{\text{QCD}}(\Phi,\bar{\Phi},\sigma,\vec{\pi}) = \Omega_{\text{glue}}(\Phi,\bar{\Phi}) + \int_{\Lambda}^{0} dk\, \partial_k \Omega_{\text{matter,k}}(\Phi,\bar{\Phi},\sigma,\vec{\pi}) + \Omega_{\text{matter},\Lambda}(\Phi,\bar{\Phi},\sigma,\vec{\pi})\,. \tag{2.22}$$

Let us stress that the glue potential implicitly depends on the matter sector due to the coupled nature of the flow equation. This is in contradistinction to the Polyakov-loop potential discussed previously, whose parameters are obtained by fitting to pure Yang-Mills lattice data. The glue potential, on the other hand, only agrees with the Yang-Mills potential if we neglect the matter fluctuations, such as the vacuum polarisation, cf. Fig. 2.2. This entails that with Fig. 2.2 we have access to the change of the Polyakov-loop potential in the presence of matter fluctuations. In Chap. 3 we will highlight the effect of the backcoupling on the phase structure and point out a way to reintroduce it in the Polyakov-loop potential.[5]

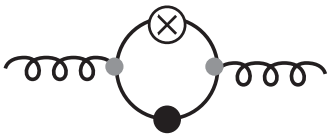

Figure 2.2.: Quark loop contribution to the gluon propagator that adds to the backcoupling of the matter sector to the gauge sector.

[5] As pointed out above, by now it is also possible to calculate the glue potential in an FRG approach directly from the flow equation shown in Fig. 2.1, cf. [75]. These results can be used as inputs to effective models in order to improve the description of the glue sector.

The matter part of Eq. (2.22) is indeed given by the PQM flow equation to be derived below, subject to the approximation of classical dispersions of quarks and mesons. At sufficiently large initial cut-off scale Λ the initial matter part of the free energy, $\Omega_{\mathrm{matter},\Lambda}$, is just a local Yukawa-type action of quarks and mesons, its parameters are fixed to phenomenology in the vacuum with f_π, m_π and m_σ. We also remark that the independence of the full free energy from the initial cut-off scale Λ, that is $\partial_\Lambda \Omega_{\mathrm{QCD}} = 0$, enforces Λ-dependent terms in $\Omega_{\mathrm{matter},\Lambda}$. These terms can be determined from the flow at Λ, see the reviews [92, 104–108] and our discussion below. Phenomenologically, they can be understood as the high-energy part of the vacuum fluctuations, see [53, 102].

Due to this close relation of the RG flow of the PQM model to full QCD it is possible to systematically enhance the model towards full QCD. This path will be followed in the subsequent chapter, where we discuss the influence of fluctuations on QCD matter in terms of the PQM model.

3. Impact of Quantum and Thermal Fluctuations

In the previous chapter the PQM model was introduced as a powerful effective model for QCD. Furthermore, it was argued that it is closely related to full QCD and this connection can be understood on the basis of the FRG flow equation. This circumstance will be exploited in the present chapter when we study the influence of fluctuations on the phase structure and thermodynamics.

First, the Wetterich equation in the PQM truncation to leading order in the derivative expansion is introduced. This yields a flow equation for the effective potential which provides the basis to calculate the phase structure and thermodynamics, in analogy to standard statistical physics. In this context, special emphasis is put on the influence of the matter backcoupling on the gauge sector, which will be introduced below.

Moreover, in order to understand the mechanisms at work in QCD, it is interesting to study the reaction of the system to systematic deformations. Here, we vary the pseudo Goldstone boson mass in order to study the mass sensitivity of the phase structure. Interesting differences to the physical mass point are observed at high chemical potentials. Finally, we close this chapter by critical comments on the model and its limitations.

Some of the results presented in this chapter have been published in [46, 48].

3.1. Fluctuations in the PQM Model

As the basis for our study of the PQM model, we consider the flow equation in lowest order derivative expansion, Eq. (A.16), for the meson fields. To this end, we set the wave-function renormalisations to a constant $Z_{\phi,\psi} \equiv 1$ and $Y_{\phi,\psi} \equiv 0$. Then, we are left with the standard kinetic terms and the effective average potential Ω_k, resulting in the ansatz for the effective average action[1]

$$\Gamma_k = \int d^4x \left\{ \bar{\psi}(\not{D} + \mu\gamma_0 + ih(\sigma + i\gamma_5 \vec{\tau}\vec{\pi}))\psi + \frac{1}{2}(\partial_\mu \phi)^2 + \Omega_k[\sigma, \vec{\pi}, \Phi, \bar{\Phi}] \right\} , \tag{3.1}$$

with $D^\mu = \partial^\mu + \bar{g}A^0\delta_0^\mu$. The only scale dependent quantity in this expression is $\Omega_k[\sigma, \vec{\pi}, \Phi, \bar{\Phi}]$ and its flow is calculated by plugging this ansatz into the flow Eq. (A.15). A derivation of the resulting flow equation can be found in [100], where the proper-time renormalisation group was used. As pointed out above, within the present truncation the proper-time flow equation is exactly the same as the ERGE.

[1] Note that since we take the wave-function renormalisations to be scale-independent and constant in this case, there is no distinction between the renormalised and unrenormalised quantities and we will leave out the bars for simplicity.

The resulting flow equation for the two-flavour PQM model finally reads [46, 100, 109]

$$\begin{aligned}\partial_t \Omega_k &= \frac{k^5}{12\pi^2}\left\{\frac{1}{E_\sigma}\coth\left(\frac{E_\sigma}{2T}\right)+\frac{3}{E_\pi}\coth\left(\frac{E_\pi}{2T}\right)\right.\\ &- \left.\frac{4N_cN_f}{E_q}\left[1-N_q(T,\mu;\Phi,\bar\Phi)-N_{\bar q}(T,\mu;\Phi,\bar\Phi)\right]\right\}. \end{aligned} \tag{3.2}$$

The structure of this equation is rather intuitive: the first line contains the contributions for the sigma and three pion modes, while the second line describes the coupling of the quarks and antiquarks to the Polyakov-loops. Note the different sign between the mesonic and fermionic contributions, which denotes the different statistics. One can also nicely see the factorisation of the thermal contribution to the threshold function accomplished by use of the optimised RG regulator function.

In the fermionic contributions, Polyakov-loop enhanced quark/anti-quark occupation numbers appear which are explicitly given by

$$\begin{aligned} N_q(T,\mu;\Phi,\bar\Phi) &= \frac{1+2\bar\Phi e^{(E_q-\mu)/T}+\Phi e^{2(E_q-\mu)/T}}{1+3\bar\Phi e^{(E_q-\mu)/T}+3\Phi e^{2(E_q-\mu)/T}+e^{3(E_q-\mu)/T}}\,,\\ N_{\bar q}(T,\mu;\Phi,\bar\Phi) &\equiv N_q(T,-\mu;\bar\Phi,\Phi)\,. \end{aligned} \tag{3.3}$$

In the limit of vanishing background gluon fields, i.e., when $\Phi,\bar\Phi\to 1$, the extended occupation numbers simplify to the usual Fermi-Dirac distribution functions for quarks and antiquarks

$$N_q(T,\mu;1,1) = \frac{1}{1+\exp((E_q-\mu)/T)}\,, \tag{3.4}$$

$$N_{\bar q}(T,\mu;1,1) = \frac{1}{1+\exp((E_q+\mu)/T)}\,, \tag{3.5}$$

and the flow of the quark-meson model [94, 110] is recovered.

Furthermore, the quasi-particle energies in Eq. (3.2) are given by $E_i=\sqrt{k^2+m_i^2}$, $i=q,\pi,\sigma$, and the masses are defined as

$$\begin{aligned} m_q^2 &= h^2\rho\,,\\ m_\pi^2 &= 2\Omega_k'\,,\\ m_\sigma^2 &= 2\Omega_k'+4\rho\Omega_k''\,. \end{aligned} \tag{3.6}$$

Here and in the following, primes denote derivatives with respect to the chiral invariant $\rho=\phi^2$. Note that we use screening masses, that are defined at vanishing momentum, in this work. Recently it has been pointed out in a two-colour study [111, 112] that the use of pole masses might result in quantitative corrections. An extension of the present system including pole masses is postponed to future work.

Since the flow Eq. (3.2) includes that of the QM model as a limiting case, see Eqs. (3.4) and (3.5), we expect to describe the essential physics of the chiral phase transition properly. Moreover, our extension by the Polyakov-loops allows in addition to study

the impact of statistical confinement on the chiral sector. Also critical exponents can be computed with remarkable accuracy within this truncation, cf. [113]. The boson anomalous dimension, which is related to the wave-function renormalisation, on the other hand, vanishes. However, its value is expected to be small and hence we neglect its influence for the time being. In Chap. 5 we discuss an extension of the present truncation including these effects.

Let us emphasis that we do not specify the form of Ω_k any further. In particular, we do not introduce an expansion in powers of the chiral invariant ρ to derive the β-functions of the arising coefficients, as is done in e.g. [109]. Rather, we consider the scale dependence of the full effective potential. For the numerical solution, we discretise the chiral invariant ρ in a grid. In this manner, the full effective potential is at our disposal. Especially, this enables the study of the first-order phase transition we expect at high chemical potentials. First-order transitions manifest themselves via multiple minima in the effective potential. Within a Taylor expansion of the effective potential it is, not possible to resolve more than one minimum. Using the above mentioned discretisation, on the other hand, this is feasible.

We remark furthermore that in this study the Yukawa coupling is considered to be scale independent. In Ref. [94] it was shown that the contribution of the running Yukawa coupling has only small influence at vanishing chemical potential. At high chemical potential, a scale dependence of this coupling is expected to yield a better description of the quark Fermi surface, which will be in the focus of Chap. 5.

It remains to determine the initial effective action Γ_Λ or, more precisely, the effective potential Ω_Λ at the arbitrary initial scale Λ, for which we have chosen $\Lambda = 950$ MeV. For the computation of thermodynamic quantities, the UV scale Λ provides a restriction on the accessible temperature range, since thermal modes with $2\pi T \geq \Lambda$ are excluded. The inclusion of the missing high-momentum modes can be achieved in an effective way by adding to the original flow, Eq. (3.2), a flow equation for an interacting Polyakov-loop quark system for scales $k > \Lambda$: $\Omega_\Lambda^\infty[\sigma, \vec{\pi}, \Phi, \bar{\Phi}]$. This term is not only relevant for the correct thermodynamics but also includes fermionic vacuum fluctuations. Note that an explicit gluon contribution to the flow equation is neglected here because the effective Polyakov-loop potential is fitted to reproduce the Stefan Boltzmann (SB) limit at high temperatures. In total, the field-dependent part of Ω_Λ consists of a sum of the quark-meson potential Eq. (2.12), the external glue input in form of the Polyakov-loop potential $\mathcal{U}$ and the UV term

$$\Omega_\Lambda[\sigma, \vec{\pi}, \Phi, \bar{\Phi}] = U(\sigma, \vec{\pi}) \; + \; \mathcal{U}(\Phi, \bar{\Phi}) \; + \; \Omega_\Lambda^\infty[\sigma, \vec{\pi}, \Phi, \bar{\Phi}] \,. \tag{3.7}$$

To be precise, $\Omega_\Lambda^\infty[\sigma, \vec{\pi}, \Phi, \bar{\Phi}]$ is computed by integrating

$$\partial_k \Omega_\Lambda^k(T, \mu) \;\; = \;\; -N_c N_f \frac{k^4}{3\pi^2 E_q} \left[1 - N_q(\Phi, \bar{\Phi}; T, \mu) - N_{\bar{q}}(\Phi, \bar{\Phi}; T, \mu)\right] \,, \tag{3.8}$$

from $k = \infty$ to $k = \Lambda$, cf. [46, 109, 114]. In the high-temperature regime, where this contribution is relevant, we employ $E_q = \sqrt{k^2 + m_q^2}$ with the constituent quark mass $m_q \approx 0$, cf. Eq. (3.6). The fermion zero-mode contribution up to the cutoff is already included in the RG flow Eq. (3.2) and we expect the additional contribution from the UV

term at large scales to be small. Furthermore, this term carries no temperature, chemical potential or meson field dependence and is hence neglected.

Using the above defined initial condition Eq. (3.7), Eq. (3.2) can be solved numerically, as indicated above, resulting in $\Omega_{k\to 0}$, i.e. the effective potential in the infrared.[2] This quantity serves as the basis for the equations of motion (EoM) that define the order parameters $\chi_0 = \{\sigma_0, \Phi_0, \bar{\Phi}_0\}$:

$$\left.\frac{\partial\Omega_{k\to 0}}{\partial\sigma}\right|_{\chi_0}(T,\mu) = \left.\frac{\partial\Omega_{k\to 0}}{\partial\Phi}\right|_{\chi_0}(T,\mu) = \left.\frac{\partial\Omega_{k\to 0}}{\partial\bar{\Phi}}\right|_{\chi_0}(T,\mu) = 0\,. \tag{3.9}$$

For the numerical solution of the coupled Eqs. (3.9), we utilise a stochastic technique. This is necessary, since standard multi-dimensional root-finding algorithms, e.g. Newton solvers, do not yield high enough accuracy within tolerable runtime in the present case. Especially for the computation of thermodynamical quantities it is, however, important to have good control over the EoM. The algorithm used in this project yields a speedup of at least a factor 10 and is outlined in App. D.

3.2. Backcoupling of the Matter Sector

In the PQM model, the coupling of the gauge and matter sectors is realised via the fermion determinant. As discussed previously, in order to describe full QCD properly, the Polyakov-loop potential should mimic the glue potential of QCD. It is important to note that the full glue potential includes also vacuum polarisation contributions from the matter sector, see e.g. Fig. 2.2 for an example of a quark loop modifying the gluon propagator. Such contributions are expected to have crucial influence on the phase structure, especially at finite chemical potential. This is related to the fact that the presence of dynamical quarks lowers the deconfinement transition temperature.

In the standard ansatz for the Polyakov-loop potential Eq. (2.14), however, the arising coefficients are fitted to pure-gauge lattice results. Within the RG framework, this corresponds to the loops shown in Fig. 3.1. In this approximation, no modifications by

$$\partial_t\Gamma_k[A,C] = \tfrac{1}{2}$$

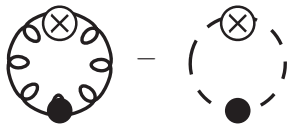

Figure 3.1.: Flow equation for the pure YM system that is used as input for the Polyakov-loop potential.

the matter sector are taken into account. Especially, polarisation contributions, such as Fig. 2.2 are neglected. Furthermore, the deconfinement scale in the effective model, denoted by T_0, is related to the dynamical scale of QCD: $T_0 \sim \Lambda_{\mathrm{QCD}}$. By use of the pure gauge system Fig. 3.1 , this scale is replaced by the one of Yang-Mills (YM) theory

[2] For practical applications, it is useful to note that the flow effectively freezes for scales below the lightest particle in the system, i.e in the present case for $k < m_\pi$. This can be seen analytically from the threshold functions, cf. App. C. It is hence sufficient to evolve the potential to scales below m_π.

$T_0 \sim \Lambda_{\rm YM}$. If the dynamics of the quarks are included, this scale should be lowered. This effect is not accounted for in the standard construction of the Polyakov-loop potentials. In contrast, in full QCD the glue potential is defined via the first two loops in Fig. 2.1, which by the coupled nature of the flow equation includes the matter backreaction. One should thus expect that the scale T_0 receives a flavour N_f and chemical potential μ dependence[3] in full QCD

$$T_0 \longrightarrow T_0(N_f, \mu)\,. \tag{3.10}$$

This generalisation is necessary in order to capture the relevant effects of QCD and in particular, the backcoupling is not included in the fermion determinant, hence Eq. (3.10) does not represent a double counting.

For an estimate of the N_f and μ dependence, hard dense and hard thermal loop arguments are well-suited and we use perturbative arguments to fix the relative scales [46, 99]. To this end, consider the perturbative one-loop beta-function of QCD

$$\beta(\alpha) = -b(N_f)\alpha^2 \tag{3.11}$$

with coefficient

$$b(N_f) = \frac{1}{6\pi}\left(11N_c - 2N_f\right)\,. \tag{3.12}$$

depending on the number colours and flavours. We assume an RG-scheme that minimises part of the higher-order effects. The gauge coupling is then given in leading order by

$$\alpha(p) = \frac{\alpha_0}{1 + \alpha_0 b(N_f)\ln(p/\Lambda)} + O(\alpha_0^2)\,, \tag{3.13}$$

with initial value $\alpha_0 = \alpha(\Lambda)$ at some UV-scale Λ. The scale $\Lambda_{\rm QCD} = \Lambda e^{-1/(\alpha_0 b(N_f))}$ is determined by the Landau pole in Eq. (3.13).

Making use of the identification $p \sim T$ we find that the temperature dependence of the coupling is also governed by Eq. (3.13), resulting in the relation

$$T_0(N_f) = \hat{T} e^{-1/(\alpha_0 b(N_f))}\,, \tag{3.14}$$

where $\hat{T}$ and α_0 are free parameters, cf. [46,99]. With Eq. (3.14) we can now determine the N_f-dependence of the critical temperature $T_0(N_f)$. We fix $\hat{T}$ at the τ-scale, $\hat{T} = T_\tau = 1.77$ GeV, which constitutes a reasonable UV scale. The pure Yang-Mills input, $T_0(N_f = 0) = 270$ MeV, is used to fix the initial value $\alpha_0 = 0.304$. Using these values we find that our ratio T_0/T_χ in the chiral limit compares well with that computed in a two-flavour QCD calculation with the RG, see [115]. The N_f-dependent critical temperature T_0 in the Polyakov-loop potential is summarised in Tab. 3.1.

The presence of massive flavours leads to suppression factors in the β-function of the order $T_0^2/(T_0^2 + m^2)$. For example for $2 + 1$ flavours, Tab. 3.1 shows the result for a current strange quark mass $m_s \approx 150$ MeV. Furthermore, the QCD calculation in the chiral limit [115] can be used to estimate the systematic error of our estimate for $T_0(N_f)$ and we find the error to be of the order $^{+15}_{-20}$ MeV.

As argued previously, in addition to the flavour dependence of T_0 we introduce a chem-

[3] In general, also a dependence on the quark mass m_q should be taken into account, see Tab. 3.1 and the following discussion.

N_f	0	1	2	2+1	3
T_0 [MeV]	270	240	208	187	178

Table 3.1.: Critical Polyakov-loop temperature T_0 for N_f flavours.

ical potential dependence via a μ-dependent coefficient b in the running coupling, which should push the confinement-deconfinement transition temperature down close to the chiral transition line. This can be achieved by defining

$$T_0(N_f, \mu) = T_\tau e^{-1/(\alpha_0 b(N_f,\mu))} \tag{3.15}$$

with

$$b(N_f, \mu) = b(N_f) - b_\mu \frac{\mu^2}{(\hat{\gamma}\ T_\tau)^2}\ . \tag{3.16}$$

The factor $\hat{\gamma}$ determines the curvature of $T_0(\mu)$ and $b_\mu \simeq \frac{16}{\pi} N_f$. Similar to the N_f-dependence discussed above, the μ-dependence in Eq. (3.15) compares well to that found in QCD [115].

We remark that the resulting chemical potential dependence of T_0 also agrees well with the parametrisation determined in [116] by the requirement to reproduce the experimental freeze-out behaviour characterised by several thermodynamic observables computed from the statistical model.

3.3. Phase Structure

From the order parameters obtained by solving the coupled EoM Eqs. (3.9) the phase structure in the (T, μ)-plane can be computed. To this end, we fix the parameters h, λ, v and c of the effective potential at the initial scale Λ such, that physical values of the low-energy observables

$$\begin{aligned} f_\pi &= 93 \text{ MeV}\,, \\ m_\pi &= 138 \text{ MeV}\,, \\ m_\sigma &= 540 \text{ MeV}\,, \\ m_q &= 297 \text{ MeV} \end{aligned} \tag{3.17}$$

are reproduced in the vacuum $T = \mu = 0$ MeV. Several comments concerning these parameters are in order. First, the pion decay constant and pion mass are not independent. Using chiral perturbation theory, they can be related to the explicit chiral symmetry breaking parameter c via $m_\pi^2 f_\pi = c$. Moreover, the quark mass in this approach is given by $m_q = h\sigma_0$, cf. Eq. (3.6). The expectation value of the massive sigma field is related to the pion decay constant $\sigma_0 = f_\pi$. Hence, the Yukawa coupling is easily fixed by the desired values of the IR observables: $h = m_q/f_\pi$. The remaining two parameters then determine the meson masses.

In this approach, we consider the three pseudo Goldstone bosons (pions) as well as the

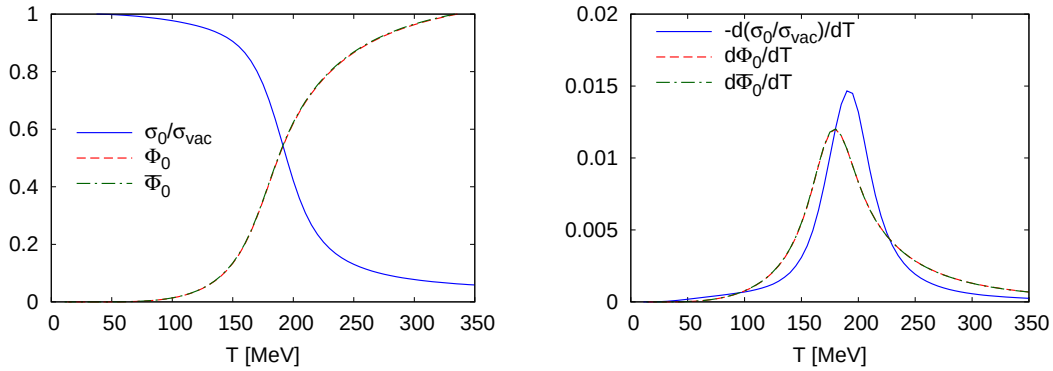

Figure 3.2.: Order parameters (left) and their temperature derivatives (right) for the parameter set defined in Eq. (3.17) at vanishing chemical potential. The chiral and deconfinement transitions, defined via the peak in the temperature derivative of the order parameter, happen at approximately the same temperature.

massive sigma meson, $\sigma = f_0(600)$. The experimental value for the mass of the sigma meson spans the region $400 \leq m_\sigma \leq 1200$ MeV with a width of $\Gamma = 250 - 500$ MeV. However, most results hint at a pole position near $(500 - i\,250)$ MeV, cf. [117], hence the low choice of m_σ.

After fixing the parameters of the initial action in the vacuum, these values are left untouched when the system is solved at finite temperature and chemical potential. These results are then predictions of the model.

Once the initial condition are fixed completely, the EoM can be solved numerically, cf. App. D, resulting in the order parameters $\sigma_0, \Phi_0, \bar{\Phi}_0$ as well as their derivatives as a function of temperature and chemical potential. The resulting curves for $\mu = 0$ are presented in Fig. 3.2. In the left panel the order parameters are shown, where the chiral condensate[4] was normalised by its vacuum value $\sigma_{\text{vac}} = 93$ MeV. While the normalised chiral order parameter is non-vanishing at low temperatures and decreases strongly in the transition region $150 \leq T \leq 250$ MeV, the Polyakov-loop does just the opposite.[5] As expected, at vanishing chemical potential the Polyakov-loop and its conjugate are degenerate.

Remark 3.1:
Due to the crossover nature, the phase transition temperatures are not well-defined. In this work, we choose the peak position of the temperature derivative of the order parameter - corresponding to the inflection point - to define the curves $T_\chi(\mu)$, $T_d(\mu)$, see also Fig. 3.2 (right). In agreement with lattice simulations [118, 119] we observe a crossover transition in all variables at approximately the same temperatures $T_\chi = 194$ MeV and $T_d = 180$ MeV.

[4] Recall that we have $\langle\bar{\psi}\psi\rangle \sim \langle\sigma\rangle =: \sigma_0$.

[5] Center-symmetry breaking is one of the rare phenomena, where the low-temperature phase is the one with restored symmetry, signalled by the (almost) vanishing order parameter.

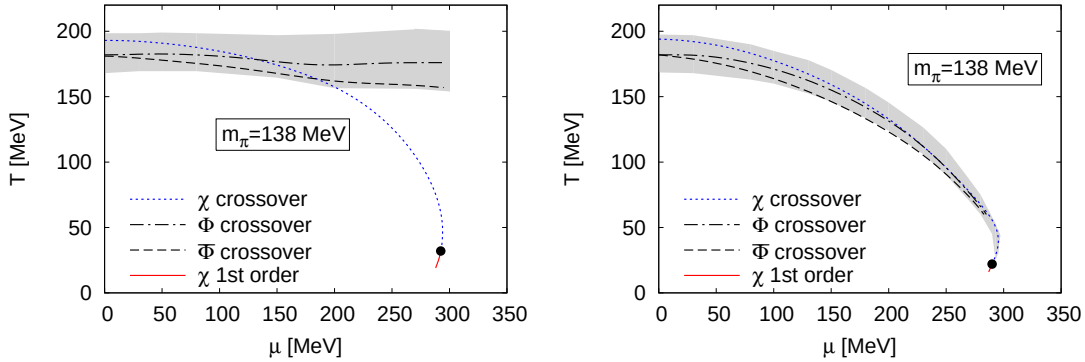

Figure 3.3.: Chiral and deconfinement phase transition lines without matter backcoupling (left) and with matter backcoupling $T_0(\mu)$ (right) at physical pion mass. The inclusion of $T_0(\mu)$ results in a shrinking of the quarkyonic phase characterised in this context by confinement, but chiral symmetry restoration.

Remark 3.2:
We want to emphasis that we sometimes refer to the transition defined by the Polyakov-loops as the deconfinement transition, even though our model is not confining in the strict sense. This is to be interpreted as a language simplification only.

Comparing the present FRG results to those from a mean-field calculation, see e.g. [99], shows that by the inclusion of meson fluctuations, the transition region is broadened. The order parameters (de-)increase more gradually when the mesonic fluctuations are taken into account. This tendency is already observed when fermionic fluctuations are included via the vacuum term in the mean-field approximation.

The phase structure for the present parameter set Eq. (3.17) is summarised in Fig. 3.3, where we also demonstrate the impact of the matter backcoupling. Let us start by discussing the result for μ-independent $T_0 = 208$ MeV, shown in the left panel of Fig. 3.3. The blue (short-dashed) line denotes the chiral crossover transition, while the black (long dashed and dashed-dotted) lines correspond to the Polyakov-loop and its conjugate. As explained above, the degeneracy of Φ and $\bar{\Phi}$ is lifted at finite chemical potential and even the peaks in the two temperature derivatives do not exactly agree. Nevertheless, they lie rather close to each other and overall show the same trend. The gray band denotes the width of $d\Phi/dT$ at 80 % of its maximum height and serves as an indicator of the strength of the transition. With constant T_0 the deconfinement transition is almost independent of chemical potential, while the chiral transition bends towards the $T = 0$ axis at higher chemical potential, as expected. Due to this effect, starting from $\mu \approx 200$ MeV, the deconfinement transition line lies above the chiral one and a 'confined' phase with partially restored chiral symmetry opens up. This phase is sometimes referred to as the quarkyonic phase.

At high chemical potential and low temperatures we find a critical point of second order that separates the chiral crossover from the first-order chiral transition region. The critical endpoint (CEP) is located at $(\mu_{\mathrm{CEP}}, T_{\mathrm{CEP}}) \approx (293, 32)$ MeV. In comparison to the results from a standard mean-field approximation one observes, that neglecting fluctuations, the

CEP lies at much higher temperatures and smaller chemical potentials. Already the proper inclusion of the fermion vacuum term, cf. [102], however, pushes the CEP towards higher chemical potential and low temperature.

The fact that the chiral transition bends inwards at high chemical potential and low temperature is characteristic for RG studies. Despite this fact, at $T = 0$ the chiral transition hits the chemical potential axis perpendicularly, in agreement with the Clausius-Clapeyron relation.

Let us now turn to the phase structure after inclusion of the matter backcoupling, i.e. with $T_0(\mu)$. The resulting phase structure is shown in the right panel of Fig. 3.3. Due to the lowering of the deconfinement scale T_0 when the chemical potential is increased, the transition lines defined by the Polyakov-loops acquire a stronger μ-dependence. In fact, they bend approximately equally strong as the chiral transition and the two transitions (almost) coincide throughout the whole phase diagram. In particular, the chirally restored but confined (quarkyonic) phase present in the previous case is not observed any more. Also, when we consider the gray shaded band, signaling the strength of the transition, we observe that this band shrinks as we approach the critical point. This indicates that both transitions get sharper towards the CEP located at $(\mu_{\mathrm{CEP}}, T_{\mathrm{CEP}}) \approx (292, 23)$ MeV. The influence of the backcoupling on thermodynamic quantities is discussed in one of the next sections.

Furthermore, consider the curvature κ of the chiral transition line defined via

$$\frac{T_\chi(\mu)}{T_\chi(0)} = 1 + \kappa \left(\frac{\mu}{T_\chi(0)}\right)^2 + \mathcal{O}\left(\left(\frac{\mu}{T_\chi(0)}\right)^4\right) . \tag{3.18}$$

This observable can also be calculated in lattice simulations despite the fermion sign problem. In Tab. 3.2 we collect the results for the curvature at $\mu = 0$ of this work and compare to other functional approaches and lattice results. Within the functional approaches, good agreement is observed. Different FRG calculations with constant $T_0 = 208$ MeV result in almost coinciding values of κ, while the inclusion of the matter backcoupling increases its value and brings our result close to the Dyson-Schwinger (DSE) result of Ref. [73]. Despite the nice agreement within the functional approaches, there is a rather large discrepancy to the lattice, which is significantly smaller. In part, this deviation may be related to finite volume effects on the lattice, see e.g. [120] for a FRG model study of finite volume effects on the curvature. On the other hand, it may also hint at the existence of physical effects not included in the present models.

3.4. Mass Sensitivity

Next, we study the mass sensitivity of the chiral phase structure. It turns out that at small Goldstone-boson mass, and especially in the chiral limit, an interesting phase structure emerges that is not observed at physical pion mass.

As discussed above, the vacuum masses of, e.g., the Goldstone bosons can be varied by changing the UV parameters of the flow Eq. (3.2). In order to maintain comparability with the results at the physical mass point presented above, we fix λ, v and h to their values at the physical point also when studying the mass sensitivity in this section. Only the explicit symmetry breaking parameter c, that is directly related to the pion mass is

Method	Ref.	κ
PQM FRG (T_0 fixed)	this work	$-0.1434(39)$
PQM FRG ($T_0(\mu)$)	this work	$-0.2889(47)$
PQM MFA (T_0 fixed)	[60]	-0.17^*
PQM FRG (Taylor, T_0 fixed)	[60]	-0.156^*
DSE (2-flavour, HTL)	[73]	-0.23^*
DSE (2-flavour)	[73]	-0.37^*
DSE ((2+1)-flavour)	[73]	-0.28^*
lattice ((2+1)-flavour)	[31]	$-0.059(2)(4)$

Table 3.2.: Curvature of the chiral transition line at $\mu = 0$ MeV from different approaches. [* no error bars available]

changed.

Note that by keeping all parameters apart from c fixed, the sigma meson mass is also lowered considerably to $m_\sigma \approx 250$ MeV in the chiral limit. The dependence of the chiral phase transition, and in particular the location of the CEP, on m_σ has previously been studied, see [121].

3.4.1. Chiral Limit

The chiral limit is defined as the limit of vanishing explicit chiral symmetry breaking and is hence characterised by a vanishing pion mass. In this case, the chiral transition at zero chemical potential in our FRG approach is a well-defined transition of second order, in agreement with $O(4)$-universality arguments, cf. [103]. Fig. 3.4 shows the chiral and deconfinement order parameters (left) as well as their temperature derivatives (right) at $\mu = 0$. The chiral condensate goes to zero continuously and vanishes exactly for $T \geq T_\chi$. The Polyakov-loop variables, however, show a crossover transitions also in this limit due to the broken center symmetry at $m_q < \infty$.

For the chiral condensate, chiral perturbation theory (χPT) predicts the behaviour [122]

$$\frac{\langle\bar{\psi}\psi\rangle(T)}{\langle\bar{\psi}\psi\rangle(T=0)} = 1 - \frac{T^2}{8f_\pi^2} - \mathcal{O}\left(\left(\frac{T}{f_\pi}\right)^4\right) \tag{3.19}$$

at low temperatures. This is shown as the short-dashed line in Fig. 3.4. We observe, that the chiral condensate in the PQM model is flatter at low T. This seems to be related to the coupling to the Polyakov-loop: In the pure QM model, $\sigma(T)$ has been found to agree very well with the χPT prediction [123].

As can be seen in the right panel of Fig. 3.4, the sharp transition in the chiral sector leaves its traces also in the deconfinement sector. Since the two transitions do not agree exactly in this case, the second order chiral transition induces an additional sharp peak in $d\Phi/dT$. Due to this supplementary structure, the exact determination of the Polyakov-loop transition and its width is not easily possible. In Fig. 3.5 (left) our result for the phase

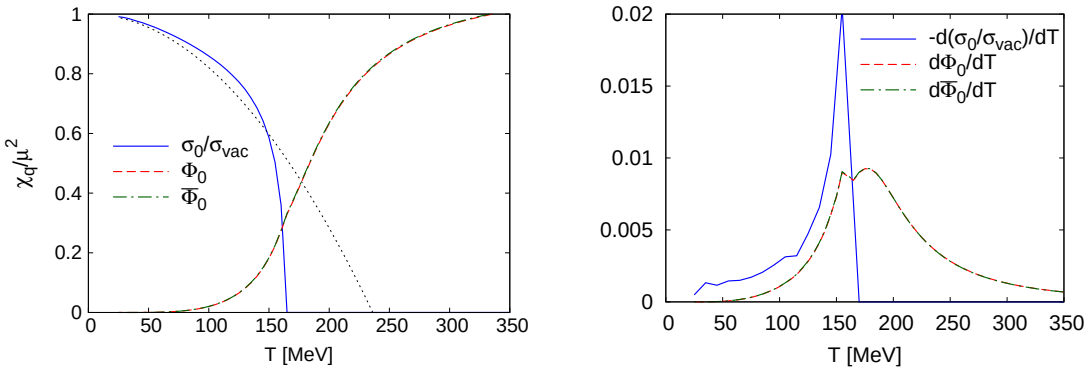

Figure 3.4.: Order parameters (left) and their temperature derivatives (right) in the chiral limit at vanishing chemical potential. The short-dashed line in the left figure denotes the chiral perturbation theory result.

structure is shown. The gray (solid) line denotes the chiral second order transition while the black (dashed and dashed-dotted) lines correspond to the Polyakov-loop transitions, as before. The light-gray band again indicates the width of the transition associated with the Polyakov-loop Φ at 80 % of its maximum height. Due to the superposition of the chirally induced peak, the lower boundary of this region is pushed towards lower temperatures. Note that the chirally induced peak persists throughout the phase diagram and agrees within $\sim \pm 2$ MeV with the chiral transition line defined via the peak in $d\sigma/dT$.

In the following we concentrate on the chiral phase transition. Compared to physical masses, the chiral transition temperature $T_\chi(\mu = 0)$ goes down by approximately 20 MeV:

$$\begin{aligned} T_\chi(\mu = 0)|_{m_\pi = 138 \text{ MeV}} &= 194 \text{ MeV}, \\ T_\chi(\mu = 0)|_{m_\pi = 0 \text{ MeV}} &= 171 \text{ MeV}, \end{aligned} \tag{3.20}$$

which is expected due to the decrease in constituent quark mass as $m_\pi \to 0$.

Increasing the chemical potential, we find that at low temperatures a new structure emerges: the chiral transition splits into two branches.[6] On the inner branch of the transition we find a critical point at $(\mu_{\text{CP}}, T_{\text{CP}}) = (255, 27)$ MeV below which the transition is of first order. The outer branch, however, remains of second order. In contradistinction to the results of Ref. [95], only one critical point is found in the present work. We want to point out that this is not an effect of the coupling to the Polyakov-loop. Rather we observe that by increasing the UV cutoff, the two critical points merge.

Moreover, the chiral splitting modifies the behaviour of the sigma meson mass with chemical potential. At low temperatures two minima, corresponding to the two branches of the chiral transition, appear in the $m_\sigma(\mu)$. This is illustrated in Fig. 3.5 (right) for $T = 30$ MeV, i.e. just above the critical point. In contrast to the sigma mass, the pion mass remains zero until chiral symmetry is completely restored at the outer transition branch.

[6] A similar behaviour had previously been observed in a RG study of the pure quark-meson model [95].

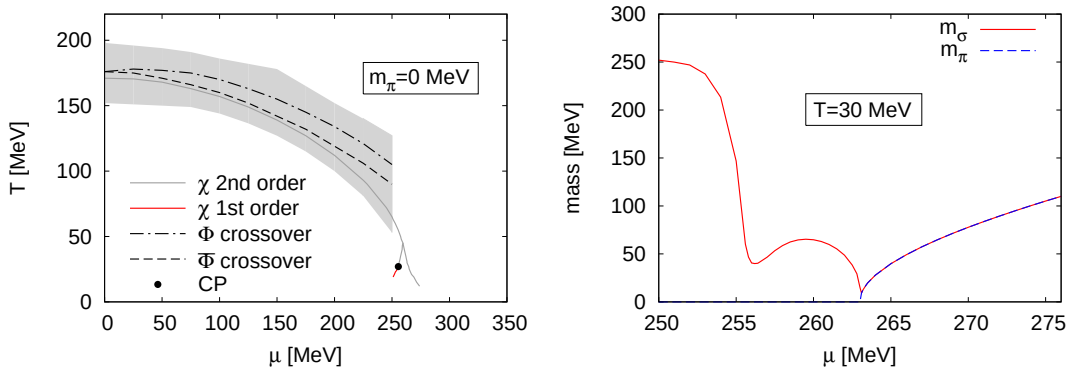

Figure 3.5.: Left: Phase structure in the chiral limit, $m_\pi = 0$ MeV. In contrast to the physical point, a splitting in the chiral transition occurs at low temperatures and high chemical potential. Right: Pion and sigma meson mass in the splitting region ($T = 30$ MeV) in the chiral limit. The splitting is reflected by two minima in the sigma meson mass, while m_π stays zero until the second transition branch is reached.

3.4.2. Small Pion Mass

In the previous section we discussed a novel feature of the chiral phase structure that arises at vanishing pion mass, namely the splitting of the transition line at high chemical potentials. In the following it will be demonstrated how this splitting region changes when the pion mass is increased towards the physical mass point.

To this end, the chiral phase structure for $m_\pi = 50$ MeV is shown in Fig. 3.6 (left). Due to the non-vanishing explicit chiral symmetry breaking, the transition is of crossover type at low μ once again. In the low temperature/high chemical potential region, we still observe a splitting in the chiral transition and also the second minimum in the sigma meson mass persists. As the vacuum pion mass is increased towards its physical value, however, the outer branch of the transition is weakened. This effect can for example be studied via the chemical potential dependence of the sigma meson mass, see Fig. 3.6 (right). In this figure we compare $m_\sigma(\mu)$ at a fixed temperature ($T = 24$ MeV) in the splitting region, for several vacuum pion masses: $m_\pi = 0,\ 25,\ 50,\ 75,\ 138$ MeV. Note that for all values of the pion mass, the first transition branch is of first order at this temperature. While there are two sharp minima in the chiral limit, one can clearly see how the depth of the outer minimum decreases as we approach physical pion masses. Even at the physical mass point some remnants of the splitting remain, see also uppermost line in Fig. 3.6 (right). However, the derivative of the chiral order parameter, which we use to pin down the transition line, does not show two distinct peaks anymore. This is why no splitting region is shown in our phase diagram for the physical mass point, see Fig. 3.3.

Note also that the position of the critical point in temperature direction, T_{CEP}, is hardly affected by the change in the pion mass. In all considered cases we find a critical point at $T_{\mathrm{CEP}} \approx 20 - 30$ MeV. This is in contradistinction to previous results in the PQM model that showed a strong dependence of $(\mu_{\mathrm{CEP}}, T_{\mathrm{CEP}})$ on m_σ when f_π, m_π and m_q are kept fixed, see [121] for mean-field results. When fluctuations beyond the mean-field

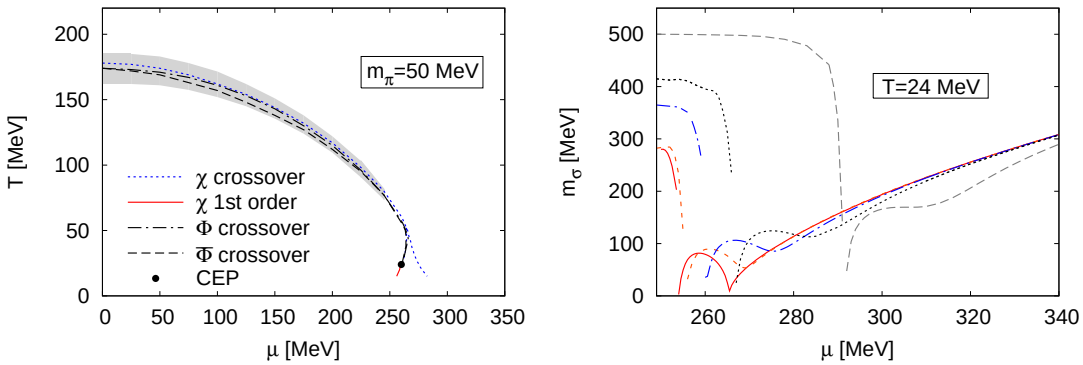

Figure 3.6.: Left: PQM phase structure for $m_\pi = 50$ MeV. Observe, that for small values of the vacuum pion mass, the splitting in the chiral transition persists. Right: Sigma mass in the splitting region ($T = 24$ MeV) for $m_\pi = 0, 25, 50, 75, 138$ MeV from left to right. As m_π increases, the second minimum is weakened.

approximation are taken into account, this observation still holds.

The location of the critical point along the chemical potential axis, μ_{CEP}, on the other hand, is changed more drastically as m_π is varied. This can be understood by noting that the critical chemical potential at vanishing temperature, $\mu_\chi(T = 0)$, is related to the quark Fermi surface and hence the quark mass. This mass, however, increases with m_π, and as a result so does $\mu_\chi(T = 0)$, and subsequently μ_{CEP}.

3.5. Equilibrium Thermodynamics

In order to get a more profound insight into the nature of the phase transitions and also to study the impact of the Polyakov-loop, we calculate some thermodynamic observables. Moreover, these results can be compared to existing lattice data at vanishing and small chemical potential.

3.5.1. Thermodynamic Observables

Evolving the flow equation Eq. (3.2) for the effective average potential to the infrared and evaluating it on the EoM, Eqs. (3.9), one obtains the thermodynamic grand potential

$$\Omega(T, \mu) = \Omega_{k\to 0}(T, \mu)|_{\chi_0} \,. \tag{3.21}$$

As the basis for the thermodynamic quantities discussed in this work, the pressure is defined as the negative value of the grand potential,

$$p(T, \mu) = -\Omega(T, \mu) + \Omega(0, 0) \,, \tag{3.22}$$

which is additively normalised to zero in the vacuum. All thermodynamic observables follow from this expression in the standard way. For example, the first derivatives of the

$\epsilon = -p + Ts$	energy density
$c_V = \frac{\partial \epsilon}{\partial T}$	specific heat
$c_S^2 = \frac{\partial p}{\partial \epsilon}\Big\vert_s = \frac{s}{c_V}$	speed of sound
$\chi_q = \frac{\partial^2 p}{\partial \mu^2}$	quark number susceptibility

Table 3.3.: Collection of some thermodynamic observables.

pressure with respect to T and μ yield the entropy and quark number density

$$\begin{aligned} s &= \frac{\partial p(T,\mu)}{\partial T}\,, \\ n_q &= \frac{\partial p(T,\mu)}{\partial \mu}\,, \end{aligned} \tag{3.23}$$

respectively. For normalisation we use the Stefan-Boltzmann pressure corresponding to a gas of free, massless quarks and gluons. This expression is expected to be approached at high temperatures and densities. For N_f flavours and N_c colours this yields

$$\frac{p_{\mathrm{SB}}}{T^4} = \frac{N_f N_c}{6}\left[\frac{7\pi^2}{30} + \left(\frac{\mu}{T}\right)^2 + \frac{1}{2\pi^2}\left(\frac{\mu}{T}\right)^4\right] \; + \; (N_c^2 - 1)\frac{\pi^2}{45}\,. \tag{3.24}$$

The term in the brackets denotes the fermionic contribution while the last term corresponds the gluonic pressure. Appropriate derivatives of this expression will be used to normalise other thermodynamic observables.

In addition to the entropy and quark number densities we consider the trace anomaly

$$\frac{\Delta}{T^4} = \frac{\Theta^\nu_\nu}{T^4} = \frac{\epsilon - 3p}{T^4}\,, \tag{3.25}$$

which is related to the trace of the energy-momentum tensor $\Theta^{\mu\nu}$, which vanishes in a scale invariant theory. This quantity thus yields a measure for the breaking of conformal invariance in the system. Sometimes this quantity is also referred to as interaction measure, since it quantifies the deviation from the equation of state of an ideal gas $\epsilon = 3p$, as can be seen from the second equality in Eq. (3.25).

Some more thermodynamic quantities are collected in Tab. 3.3. Of these, especially the quark number susceptibility is of interest, since it is related to the correlation length $\chi_q \sim \xi^{2-\eta}$ with η denoting the anomalous dimension. The correlation length ξ governs the exponential decay of the corresponding correlation function, hence its divergence at a second-order transition is indicative for the prevailing long-range order. Thus, a strongly peaked, and actually diverging, susceptibility signals the presence of a critical endpoint of second order, which might be present in the QCD phase diagram.

3.5.2. Physical Mass Point

First, we consider some thermodynamic observables at the physical mass point. Fig. 3.7 shows the pressure, normalised by the Stefan-Boltzmann pressure, without (left) and with

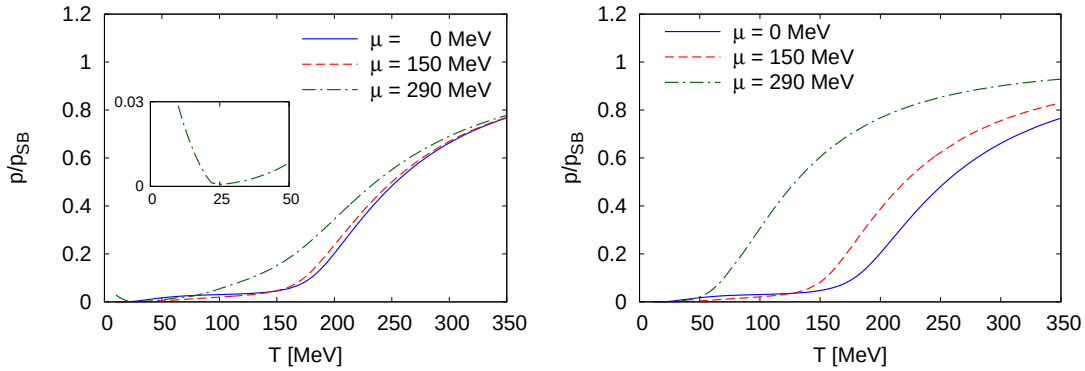

Figure 3.7.: Pressure normalised by the Stefan-Boltzmann pressure with constant $T_0 = 208$ MeV (left) and $T_0(\mu)$ (right), both for physical masses. Including the matter backcoupling, the pressure rises already at lower temperatures owing to the decreased deconfinement temperature.

the matter backcoupling (right) for three values of chemical potential. At low temperatures, the pressure is dominated by the lightest degrees of freedom, i.e the pions. Around the chiral phase transition, the sigma meson and also the quark masses decrease. At even higher temperatures, the sigma meson degenerates with the pions due to the restoration of chiral symmetry. The mesons acquire a large thermal mass $\sim 2\pi T$ and decouple from the system. In this region, the almost massless quarks are the dominant degrees of freedom that govern the pressure. Exactly this effect is seen in Fig. 3.7 (left) with constant T_0. Note also that the pressure is a monotonically rising function of temperature. Only at $\mu = 290$ MeV a non-monotonic behaviour is observed in Fig. 3.7, which can be understood by the fact that at this chemical potential the very low temperature region is chirally symmetric and the chirally broken regime is entered for $T \approx 30$ MeV, cf. Fig. 3.3. Furthermore, the transition at low temperature is of first order, resulting in a kink in the pressure, as shown in the subplot. At high temperatures, the pressure reaches approximately 80 % of its Stefan-Boltzmann value for constant T_0 and all considered chemical potentials.

Turning on the matter backcoupling to the glue sector, we find a pressure as shown in the right panel of Fig. 3.7. The overall behaviour is of course similar to the one with constant T_0. However, one can now clearly see the impact of the deconfinement transition. Due to the fact that $T_\chi \approx T_d$ holds for all chemical potentials, the pressure rises more rapidly. This is most drastically seen at $\mu = 290$ MeV: with constant T_0 the pressure is suppressed up to $T \approx 150$ MeV, which is the region where the Polyakov-loops start to rise significantly. Including $T_0(\mu)$, the Polyakov-loop transition moves down to $T_d \approx 90$ MeV and p increases much earlier. Furthermore, the pressure reaches more than 90 % of its Stefan-Boltzmann value at high temperatures.

A similar behaviour is observed in the entropy density shown in Fig. 3.8, again for fixed T_0 (left) and $T_0(\mu)$ (right). The entropy density measures the active degrees of freedom in the system and hence rises at the deconfinement transition. The first-order transition, is hence signalled by a jump in the entropy density, cf. Fig. 3.8, green (dashed-dotted) line. Also in this observable a strong impact of the matter backcoupling is observed: the

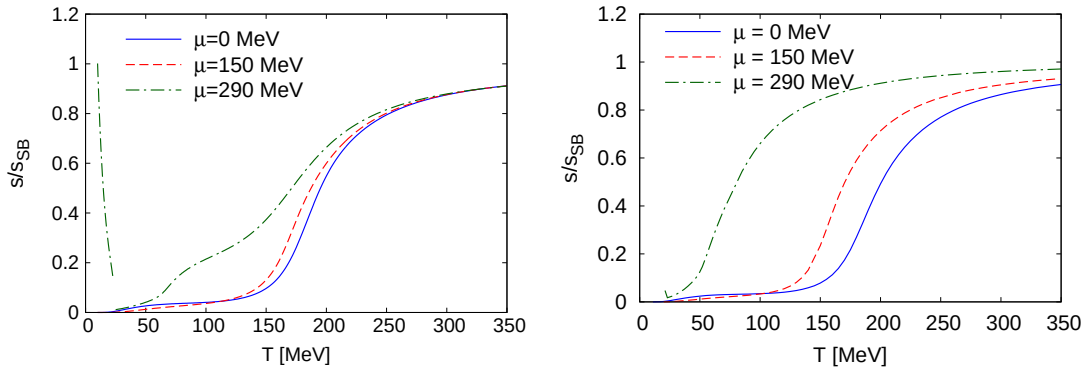

Figure 3.8.: Entropy density normalised by the Stefan-Boltzmann value with $T_0 = \text{const.}$ (left) and $T_0(\mu)$ (right) at the physical point. The impact of the matter backcoupling is similar to its effect on the pressure.

entropy density rises much earlier due to the lowered deconfinement temperature at $\mu > 0$.

Remark 3.3:
These results confirm our previous arguments, that the matter backcoupling to the gauge sector is an essential effect that needs to be included in our study of the phase structure as well as in the computation of thermodynamic quantities. Therefore, all results shown in the following contain $T_0(\mu)$.

In the left panel of Fig. 3.9 the interaction measure Δ/T^4 is shown. This quantity measures the departure of the system from an ideal gas, where $\epsilon = 3p$ and corresponds to $\Delta \equiv 0$. At low temperature, Δ/T^4 vanishes, but has a peak at higher temperatures, after which goes to zero like $1/T^2$. On the lattice the same behaviour is observed [118, 124]. There, the inflection point, rather than the peak of the interaction measure is identified with the phase transition temperature. This agrees nicely with our definition of T_χ via the inflection point of the order parameter.

The equation of state (EoS) measure p/ϵ and the speed of sound c_S^2 are additional observables that quantify the behaviour of the system. In the case of a free gas, $p/\epsilon \to 1/3$ since $\epsilon = 3p$. This is indeed the case in our model for high temperatures, cf. Fig. 3.9 (right), solid curve. Around the phase transition temperature, both observables have a minimum in agreement with lattice results [118, 124]. This observation can be related to the fact that the specific heat c_V is expected to diverge at the CEP and to show a peak at the crossover transition. The speed of sound is proportional to the inverse of c_V, hence the minimum at the critical temperature.

Within a different truncation of the grand potential, where the mean-field Polyakov-loop EoM instead of the RG EoM have been used, it was possible to calculate thermodynamic observables also at high chemical potential and low temperature, see Fig. 3.10. In this figure the quark number density (left) and the quark number susceptibility (right) around the critical endpoint are shown, both including the matter backcoupling. As expected, the slope of the quark number density increases as the CEP of second order is approached from above. Directly at the CEP, the slope is infinite within numerical accuracy, leading

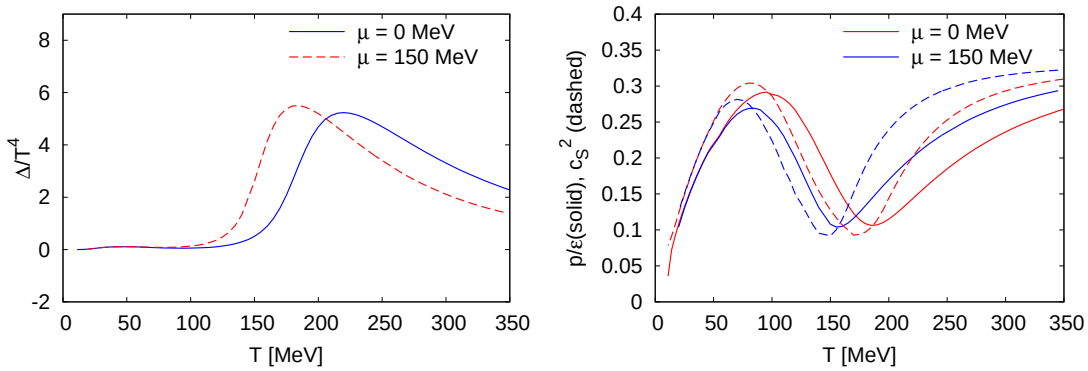

Figure 3.9.: Interaction measure Δ/T^4 (left) and a combined plot (left) of the equation of state measure p/ϵ (solid line) with the speed of sound (dashed line). The matter backcoupling is included in both figures and $m_\pi = 138$ MeV.

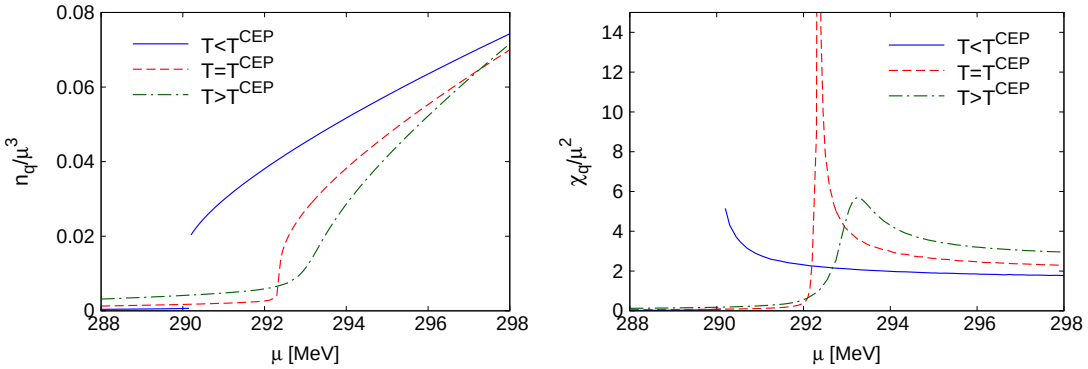

Figure 3.10.: Quark number density (left) and quark number susceptibility (right) around the CEP for physical masses and including the matter backcoupling.

to a diverging susceptibility, cf. right panel. For $T < T_{\mathrm{CEP}}$ a first order transition is present, resulting in a jump in the quark number density.

3.5.3. Small Pion Mass

In order to study the mass sensitivity of thermodynamic quantities, the pressure and some derived observables[7] were computed at $m_\pi = 50$ MeV.

Fig. 3.11 shows the pressure (left) and entropy density (right) in this case. In general, the same structure as at physical masses is observed. Note, however, that the plateau in the pressure at vanishing chemical potential and intermediate temperatures is at a higher value than at the physical point. This is due to the fact that pions, which are lighter in the present case, dominate the pressure in this regime. Moreover, the pressure is normalised to $p(0,0) = 0$, like at the physical mass point. This forces the curve to go to zero at vanishing temperature and chemical potential. Judging from the interaction measure,

[7] Also in this section and the following, the matter backcoupling is included in all shown results.

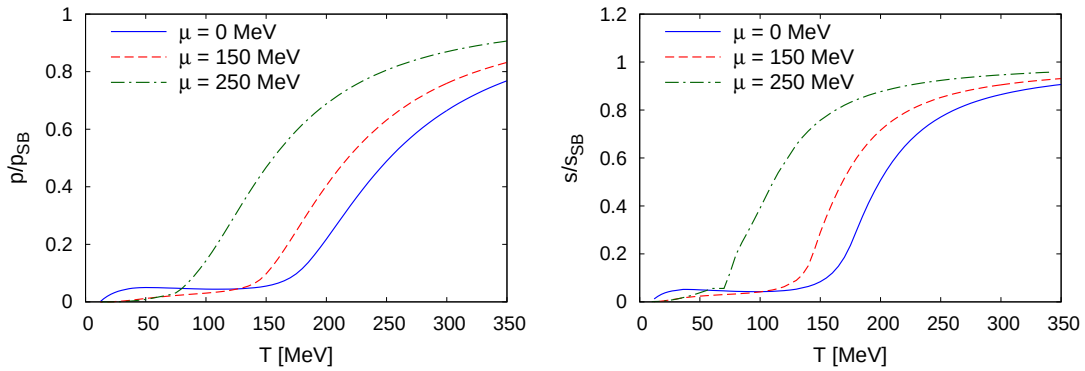

Figure 3.11.: Pressure (left) and entropy density (right), both normalised by the corresponding Stefan-Boltzmann expression for $m_\pi = 50$ MeV. The same trends as for physical masses are seen.

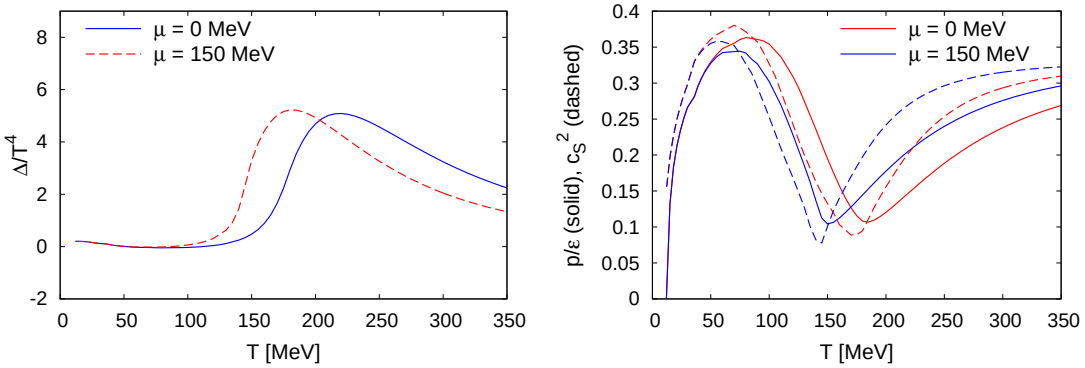

Figure 3.12.: Interaction measure (left) and EoS measure p/ϵ together with the speed of sound (right) for a pion mass $m_\pi = 50$ MeV.

Fig. 3.12 (left), this may, however, not be the proper normalisation. We observe, that Δ/T^4 decreases slightly at low temperatures. The numerical complexity of the system, however, thus far prohibits a more precise study of the low temperature region.

Interestingly, the pressure initially decreases as μ is increased at low temperatures, see Fig. 3.11 (left). In fact, this is also observed at physical pion mass and in the pure QM model. This effect is enhanced as the pion mass is lowered, cf. Fig. 3.13 below.

For completeness we also show the EoS measure and the speed of sound for this vacuum pion mass in Fig. 3.12 (right). It is observed, that the peak preceding the minimum at approximately $T = T_\chi$ increases in height as the pion mass is lowered, compare e.g. to Fig. 3.9. This effect is observed in both quantities p/ϵ as well as c_S^2. The depth of the minimum as well as the high-temperature limit, on the other hand, are unchanged.

3.5.4. Chiral Limit

We end our discussion with the thermodynamics in the chiral limit and show the pressure and entropy density in Fig. 3.13. Due to the vanishing pion mass for $T < T_\chi$, the pressure

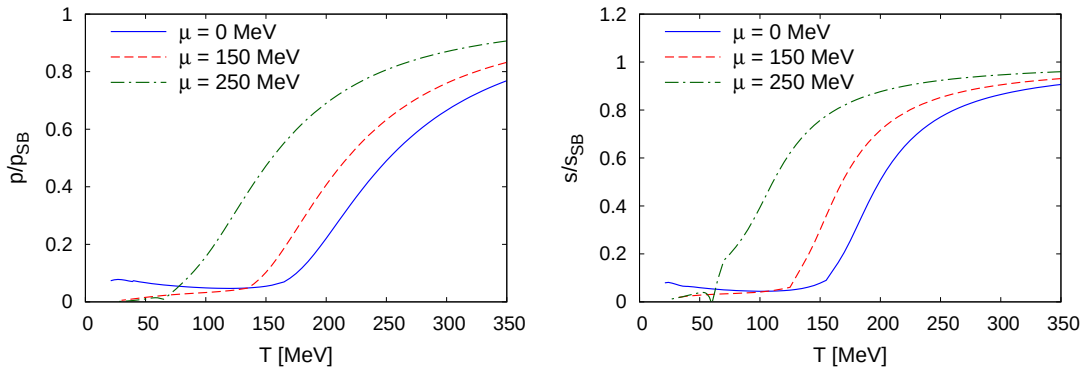

Figure 3.13.: Normalised pressure (left) and entropy density (right) in the chiral limit.

behaves approximately like that of a free gas of pions, $p/T^4 = 3\frac{\pi^2}{90}$. However, instead of a flat plateau, we observe a slight, unphysical decrease in $p(T)$ at vanishing chemical potential below the phase transition. It could not be clarified thus far, what induces this unphysical behaviour. However, we observe an inversion of the mass hierarchy in this region: At the physical point, we have $m_\sigma > m_q > m_\pi$ in the low temperature domain. In the chiral limit, however, we have $m_q > m_\sigma > m_\pi$ in the same region. Owing to this effect, the contributions to the pressure change. Already at $m_\pi = 50$ MeV there exists a temperature region where $m_\sigma < m_q$. This could be checked e.g. by defining the chiral limit as $m_\pi = 0$ with all other vacuum observables as at the physical point. If the behaviour of $p(\mu = 0)$ should indeed be related to the mass ordering in the system, it would also be interesting to check the influence of pole masses on this effect.

Turning to the entropy density, Fig. 3.13 (right), we note a kink in s/s_{SB} at high chemical potential and low temperature. This effect seems to be related to the influence of the chiral second-order transition on the Polyakov-loop sector. As we already discussed, the sharp transition induces an additional peak in $d\Phi/dT$, cf. Fig. 3.4. Similarly, it influences the thermodynamic observables around the phase transition. Hence, we refrain from showing higher thermodynamic observables in the chiral limit.

3.5.5. Low Temperature Region

After discussing some thermodynamic observables and their mass dependence vs. temperature in the last section, we now turn to a study of the low T/high μ region. This regime is especially interesting, since a critical point appears in this region whose properties should be studied in detail. However, the computation of thermodynamic quantities in this region is seriously hampered not only by computational demands, but also by some shortcomings of the Polyakov-loop potential. These will be illustrated in the following.

Let us start by discussing the pressure and quark number density at physical pion mass and temperatures $T \leq 50$ MeV, where the lowest temperature is chosen slightly above the critical endpoint, see Fig. 3.14. The subplot shows the pressure normalised by the Stefan-Boltzmann value. While the pressure rises monotonically at $T = 50$ MeV, as it should, below this temperature a non-monotonicity appears. This effect was already pointed out in [48]. In the quark number density shown in Fig. 3.14, this effect is seen more drastically

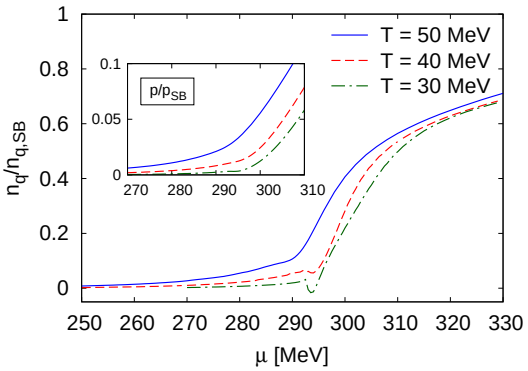

Figure 3.14.: Quark number density in the low temperature region for physical pion mass. The insert shows the pressure. At low temperatures the pressure develops a non-monotonicity that results in negative densities. Discussion see text.

than in the pressure. Already at $T = 40$ MeV, the non-monotonic behaviour of p yields a bump in n_q just before the phase transition. As the temperature decreases, this effect becomes more and more pronounced and eventually leads to negative pressure values and densities. This effect is clearly unphysical and unfortunately inhibits the study of the critical endpoint and, e.g., its universality.

We attribute this effect to an unrealistic implementation of the Polyakov-loop potential. In mean-field studies with or without the vacuum term [53,102], no similar effect had been observed. It thus seems that the influence of the Polyakov-loop potential on the mesonic potential, including fluctuations, is too strong. Note also that the same phenomenon is found when the logarithmic version of the Polyakov-loop potential is used.

As discussed in Sec. 2.2, the parameters of the Polyakov-loop potential are fitted to lattice data from the pure Yang-Mills system. Moreover, the Polyakov-loop is a well-defined order parameter for the deconfinement transition in exactly this limit, corresponding to infinitely heavy quarks. Physical quark masses or even the chiral limit, on the other hand, are far away from this regime, suggesting that some modifications are in order when finite masses are considered. The influence of dynamical quarks is to some extent taken into account by our modification $T_0(N_f, \mu)$, but a fully dynamical treatment within the FRG is still missing. A comparison to the glue potential in full QCD discussed in [75] indeed shows that our Polyakov-loop potential is steeper. This might result in the observed unphysical behaviour.

For smaller pion mass we observe that the decrease in the pressure as a function of μ sets in at even higher temperatures, see Fig. 3.15 for results with $m_\pi = 50$ MeV. Already at $T = 90$ MeV a significant drop in the pressure, and subsequently in the quark number density, is observed. Despite this problem we show the quark number susceptibility χ_q in this case in Fig. 3.15 (right). Of course the drop in the density leads to an additional oscillation in the susceptibility. Note, however, that at $T = 30$ MeV (green, dashed-dotted curve), we pass through the chiral splitting region in the phase diagram and observe two peaks in χ_q, corresponding to the two transition branches. At this temperature, the two transitions are of similar strength, leading to peaks of comparable height. As the critical point is approached, we expect that the related peak increases, and eventually the

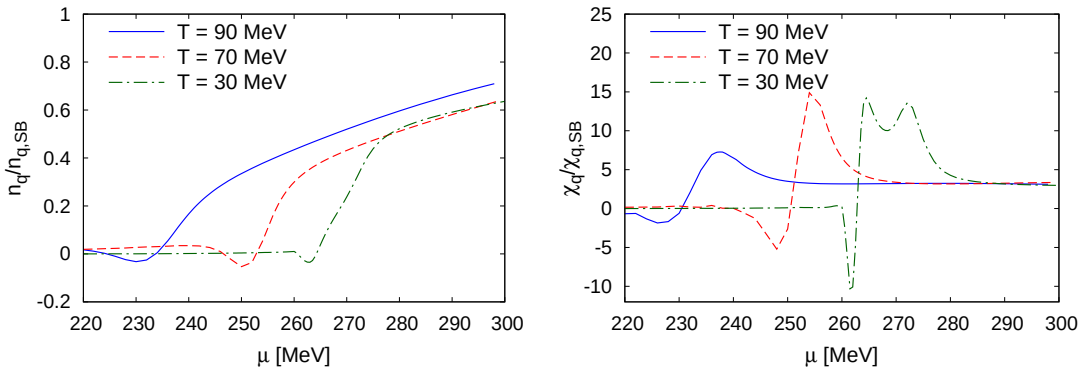

Figure 3.15.: Quark number density (left) and quark number susceptibility (right) above and in the chiral splitting region with $m_\pi = 50$ MeV. At smaller than physical pion mass, the decrease in the pressure sets in at even higher T than at physical pion mass. Despite this effect, a double-peak structure in the susceptibility is observed that can be related to the splitting in the chiral transition line.

susceptibility should diverge at a critical endpoint of second order.

3.6. Comment on the Applicability of the Model

We want to close this chapter with a comment on the applicability of the presented model and its results.

One finding of particular interest from the theoretical as well as the experimental viewpoint is the presence of a critical point at low temperature and $\mu = \mu_q > 200$ MeV. With regard to the location of the CEP, one should, however, always keep in mind that the present model neglects baryonic degrees of freedom completely. Especially in the high chemical potential region, where the CEP is located in our computation, baryons and their fluctuations are certainly of importance for a correct description of QCD. These are expected to have an influence the location of the CEP as well.

On the other hand, we clearly observe that the inclusion of mesonic fluctuations has the tendency to push the CEP towards higher chemical potential as compared to the mean-field approximation without the fermionic vacuum term. Already the inclusion of the fermion vacuum fluctuations beyond the standard mean-field approach shows a similar trend of lowering the temperature coordinate of the CEP, T_{CEP}. Note that in the RG approach presented here, the vacuum contribution is always included.

Furthermore, the presently predicted locations of a QCD critical point within lattice QCD are well within the region of reliability of the PQM model. In view of these results we can exclude a CEP at low $\mu/T \approx 1 - 2$.

4. Gauge Theories with Matter in Different Representations

In the present chapter, we study the interrelation of chiral symmetry breaking and deconfinement in gauge theories with non-trivial center.

One factor that has an impact on the interplay of these two phenomena has already been identified in the previous chapter, namely the matter backcoupling to the gauge sector. Here, we restrict ourselves to the case of vanishing chemical potential and study a different influence, namely the colour representation of the matter fields. It is well-known, that basic properties of the theory can change when we vary the representation of the matter content: quarks in the adjoint representation, for example, do not break the center symmetry of the gauge sector. The presence of quarks in the fundamental representation, however, does break center symmetry explicitly. Since center-symmetry breaking is connected to the question of quark confinement, see e.g. [125] and our discussion in Sec. 1.1, one may expect that a variation of the representation of the quark fields leaves its imprints in the phase structure of the theory. In fact, it has been found in lattice simulations of $SU(N_c)$ gauge theory with adjoint quarks [23–25] that the chiral phase transition temperature is significantly larger than the deconfinement phase transition temperature, in contradistinction to QCD with two light quark flavours in the fundamental representation.

The renormalisation group represents a valuable tool also in this application. In particular, the fixed-point structure of four-fermion interactions is used in the following to achieve an analytical understanding of the mechanism relating the two transitions. Furthermore, a Hubbard-Stratonovich transformation, as discussed in Sec. 2.1.2, allows to connect the purely fermionic formulation to a partially bosonised version, which is better suited for the study of low-energy observables. This enables us to put forward a phase diagram in the plane spanned by the temperature and, e.g., the pion decay constant, which can be compared to other methods, in particular also lattice simulations, since no sign problem is present in this case.

This chapter follows closely our discussion in [126].

4.1. Extended Matter Sector of QCD

In order to analyse the interplay of chiral symmetry restoration and deconfinement at finite temperature in QCD, it is convenient to add a relevant coupling to the theory which can be considered as an external parameter. In particular, we introduce a four-fermion coupling $\bar{\lambda}_\psi$

$$S_{\mathrm{QCD}} \to S_{\mathrm{QCD}} + \int d^4x\, \bar{\lambda}_\psi \left(\bar{\psi}\mathcal{C}\psi\right)^2 ,$$

where S_{QCD} denotes the classical action of QCD, cf. Sec. 1.1. The operator $\mathcal{C}$ will be determined below. In QCD, similar four-fermion interactions are generated by gluon

exchange. For a description of the low-energy regime, it makes therefore sense to include these types of interactions explicitly. Loosely speaking, such a deformation allows us to "detune" the chiral and the confining dynamics of the theory. For lattice studies of this class of theories, see e. g. Refs. [127, 128].

The above defined theory is referred to as λ_ψ-*deformed QCD*. Due to the additional coupling, this theory effectively depends on two parameters: $\bar{\lambda}_\psi$ and Λ_{QCD}.[1] In particular, they both influence the values of low-energy observables. By tuning $\bar{\lambda}_\psi$ we can hence produce different values of, e.g. the pion decay constant f_π. The limit $\bar{\lambda}_\psi \equiv 0$, takes us back to usual QCD, where the only input parameter is given by Λ_{QCD}, or equivalently by the value of the strong coupling α_s at some high momentum scale. In this case, Λ_{QCD} solely sets the scale for all physical observables $\mathcal{O}$: $\mathcal{O} \sim \Lambda_{\mathrm{QCD}}$.

Subsequently, the dependence on the two parameters Λ_{QCD} and $\bar{\lambda}_\psi$ is exploited. A model will be set up which shares many aspects with the full theory, but can also be analysed analytically to a large extent.

Also in beyond the standard model applications, similar theories with an additional relevant parameter have attracted a lot of attention in recent years, see e.g. [128, 129]. Especially, the case of $SU(2)$ gauge theory with two adjoint quark flavours is of interest there, since it is a candidate for minimal walking technicolor, see e.g. [130–133].

Remark 4.1:
A word of caution should be added with regard to our results presented in the following. In Secs. 4.2 and 4.3, we mostly study the case of $SU(2)$ gauge theory with two massless adjoint quarks. We are aware of the fact that this theory could already lie in the conformal window.[2] *In this work, however, we assume that the zero-temperature ground state of $SU(2)$ gauge theory with two adjoint quarks is governed by dynamical chiral symmetry breaking. Actually, this indeed appears to be the case within our present approximations, in accordance with Refs. [129, 134]. As a first step, it is therefore natural to consider this theory in our numerical studies. Even if the present approximations should turn out to be insufficient to describe correctly the chiral ground-state properties of $SU(2)$ gauge theory with two massless adjoint quarks, we still expect that our results will be similar for gauge groups of higher rank and broken chiral symmetry in the zero-temperature limit, see also our discussion in Secs. 4.2 and 4.3.*

Let us now discuss the field-theoretical setup in the matter sector, where we employ the following ansatz for the quantum effective action Γ, cf. Sec. 1

$$\Gamma_k[\bar{\psi}, \psi, \langle A_0 \rangle] \;=\; \int d^4x \Big\{ Z_\psi \bar{\psi} \left(\mathrm{i}\partial\!\!\!/ + \bar{g}\gamma_0 \langle A_0 \rangle \right) \psi + \frac{\bar{\lambda}_\psi}{2} \left[(\bar{\psi}\psi)^2 - (\bar{\psi}\vec{\tau}\gamma_5\psi)^2 \right] \Big\} . \quad (4.1)$$

Here, Z_ψ is the fermion wave-function renormalisation and we again restrict ourselves to $N_f = 2$ massless quark flavours. The matter fields are assumed to transform under a representation R of the gauge group. In particular, we discuss the case of an $SU(N_c)$ gauge group.

[1] Here and in the following we consider the chiral limit, i.e. the current quark masses are set to zero.

[2] The term "conformal window" for a $SU(N_c)$ gauge theory refers to the range of flavours N_f for which the theory is asymptotically free at large energies while its low-energy region is conformally invariant.

Since the ansatz (4.1) is *perturbatively* non-renormalisable, we define it with an UV cutoff Λ which then represents an additional parameter. This setup also implies that the regularization scheme belongs to the definition of the model. The role of Λ for the fixed-point structure will be discussed in detail in Sec. 4.3.

Concerning the background field $\langle A_0 \rangle$, we *do not* use the approximation $\mathrm{tr}_\mathrm{R}\, L_\mathrm{R}[\langle A_0 \rangle] = \langle \mathrm{tr}_\mathrm{R}\, L_\mathrm{R}[A_0] \rangle$ which underlies most PNJL/PQM model studies,[3] see e. g. Chap. 3. Although this assumption is convenient and opens up the possibility to incorporate lattice results for $\langle \mathrm{tr}_\mathrm{R} L_\mathrm{R}[A_0] \rangle$, it may be problematic in quark representations other than the fundamental one and away from the limit of infinitely many colours, $d_\mathrm{R} \to \infty$, see our discussion below. Moreover, it has been found for fundamental matter that PNJL/PQM-type studies are to some extent sensitive to different parametrisations of the potential for $\langle \mathrm{tr}_\mathrm{F} L_\mathrm{F}[A_0] \rangle$, see e. g. Ref. [137]. Hence it is important to analyse at least some of the consequences arising from the approximation $\mathrm{tr}_\mathrm{R}\, L_\mathrm{R}[\langle A_0 \rangle] = \langle \mathrm{tr}_\mathrm{R}\, L_\mathrm{R}[A_0] \rangle$ underlying these model studies.

For the analytic studies presented here, we will rather make use of the exact relations given in Sec. 1.1.3. For the numerical evaluation of the quantum effective action, we then use the numerical results for $\langle A_0 \rangle$ from a non-perturbative first-principles RG study of the order-parameter potential in Polyakov-Landau-DeWitt gauge, see Refs. [19, 20].

For the investigation of the RG flow of the four-fermion coupling $\bar{\lambda}_\psi$, we employ the Wetterich Eq. (A.15). In general, our ansatz Eq. (4.1) in the matter sector can be considered as the leading order in a systematic derivative expansion. The associated expansion parameter is the anomalous dimension $\eta_\psi = -\partial_t \ln Z_\psi$ of the quark fields. This "parameter" is small as has been found in various previous studies [85, 88, 138, 139]. In fact, it is identical to zero when we consider the four-fermion coupling in the so-called point-like limit, $\lambda_\psi(|p| \ll k)$, see e. g. Ref. [92]. This is true even if we allow for dynamical gauge degrees, provided that one considers the class of Landau gauges [140], such as Polyakov-Landau-DeWitt gauge. As we have discussed above, the latter gauge is implicitly assumed in this work, see Sec. 1.1.3.

Apart from an expansion in derivatives, the effective action can be expanded in operators, such as n-fermion operators, cf. Sec. A.2. Regarding four-fermion operators, we note that the ansatz Eq. (4.1) for the effective action is not complete with respect to Fierz transformations, not even in the limits $\langle A_0 \rangle \to 0$ and $T \to 0$, cf. our discussion in Sec. 2.1.1. From a consideration of a Fierz-complete basis, however, we only expect quantitative corrections to our results presented here. The main qualitative aspects are expected to persist since the general structure of the loop integrals remains unchanged. For a Fierz-complete study of the RG flow of four-fermion couplings in QCD, the reader is referred to e.g. [87, 92, 141].

Note that it can be shown that higher fermion operators, such as eight-fermion operators, do not contribute to the RG flow of the four-fermion couplings in the point-like limit. Beyond the point-like limit, however, these higher-order operators may very well contribute to the flow of the four-fermion interactions, see, e. g., our discussion in Sec. 4.3.

In the subsequent section it will be shown that the purely fermionic formulation of our ansatz Eq. (4.1) for the matter sector is convenient for a general discussion of the interplay of the chiral and the deconfinement phase transitions, independent of the fermion

[3] Note that there are also PNJL/PQM-type model studies which do not use this approximation but consider an integration over the group $\mathrm{SU}(N_c)$, see e. g. Refs. [135, 136].

representation. In order to compute low-energy observables, however, a purely fermionic formulation may not be the first choice since this requires to resolve the momentum-dependence of the fermionic vertices. In this case, a partially bosonised formulation of our ansatz might be better suited. The Hubbard-Stratonovich transformation resulting in such a description has already been discussed in Sec. 2.1.2. For the present case this yields

$$\Gamma_k[\bar{\psi},\psi,\bar{\phi},\langle A_0\rangle] = \int d^4x \left\{ Z_\psi \bar{\psi}\left(\mathrm{i}\partial\!\!\!/ + \bar{g}\gamma_0\langle A_0\rangle\right)\psi + i\bar{h}\bar{\psi}(\sigma + i\vec{\tau}\cdot\vec{\pi}\gamma_5)\psi \right. \\ \left. + \frac{1}{2}Z_\phi\left(\partial_\mu\bar{\phi}\right)^2 + \frac{1}{2}\bar{m}^2\bar{\phi}^2 \right\}. \tag{4.2}$$

Recall, that chiral symmetry breaking is now signaled by a non-vanishing expectation value of $\sigma \sim \langle\bar{\psi}\psi\rangle$.

Studying this action, we choose the initial conditions for the couplings such that

$$\lim_{k\to\Lambda}\bar{m}^2 > 0\,, \quad \lim_{k\to\Lambda} Z_\phi = 0\,, \quad \lim_{k\to\Lambda} Z_\psi = 1\,. \tag{4.3}$$

Together with the identity

$$\bar{\lambda}_\psi = \frac{\bar{h}^2}{\bar{m}^2}\,, \tag{4.4}$$

cf. Sec. 2.1.2, the ansatz Eq. (4.2) can then be mapped to the ansatz Eq. (4.1) at the initial UV scale Λ. Thus, only the ratio of the Yukawa coupling $\bar{h}$ and the mass parameter $\bar{m}$ acquires a physical meaning. As discussed in Sec. 2.1.2, a large (i. e. diverging) four-fermion coupling signals the onset of chiral symmetry breaking.

We conclude that the fixed-point structure of the coupling $\bar{\lambda}_\psi$ - or, equivalently, of the couplings $\bar{m}$ and $\bar{h}$ - is directly linked to the question of chiral symmetry breaking in the IR limit. In the following, we analyse how this fixed-point structure is related to the order parameter for center-symmetry breaking. This will eventually allow us to gain insights into the relation of chiral symmetry breaking and center-symmetry breaking at finite temperature.

4.2. Dynamical Locking Mechanism and the Fermionic Fixed-Point Structure

Now we perform an analysis of the interplay of center-symmetry breaking and chiral symmetry breaking using the purely fermionic formulation Eq. (4.1). In this study, the value of the background field $\langle A_0\rangle$ is considered an external input, which is given by the ground state of the corresponding order-parameter potential. As discussed above, the position $\langle A_0\rangle$ of the ground state is then directly related to the order parameter for center-symmetry breaking, namely $\mathrm{tr}_\mathrm{R} L_\mathrm{R}[\langle A_0\rangle]$.

The RG flow equation of the four-fermion coupling in the point-like approximation can be computed similar to the derivation shown in App. B and for quarks living in any

representation. We find

$$\beta_{\lambda_\psi} \equiv \partial_t \lambda_\psi = (2+2\eta_\psi)\lambda_\psi - \frac{2}{\pi^2}\Big(2+\frac{1}{d_{\mathrm{R}}}\Big)\sum_{l=1}^{d_{\mathrm{R}}} l_1^{(\mathrm{F})}(\tau, \nu_l^{(\mathrm{R})}|\phi|, 0)\,\lambda_\psi^2\,, \tag{4.5}$$

where the dimensionless renormalised coupling λ_ψ is defined as

$$\lambda_\psi = Z_\psi^{-2} k^2 \bar{\lambda}_\psi\,. \tag{4.6}$$

For convenience, we have introduced the eigenvalues $\nu_l^{(R)}$ of the Hermitean matrix given in Eq. (1.19):

$$\nu_l^{(\mathrm{R})} = \mathrm{spec}\left\{(T^a v^a)_{ij} \;|\; v^2 = 1\right\}\,. \tag{4.7}$$

The coupling λ_ψ depends on the background field $\langle A_0\rangle$ and the dimensionless temperature $\tau = T/k$. The threshold function $l_1^{(\mathrm{F})}$ describes a regularised one-particle irreducible (1PI) Feynman diagram with two internal fermion lines, see Fig. 4.1. The definition of this function can be found in App. C.

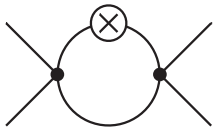

Figure 4.1.: 1PI Feynman diagram corresponding to the threshold function $l_1^{(F)}$ appearing in the β-function of the four-fermion interaction λ_ψ.

The RG flow Eq. (4.5) has two fixed-points: a Gaußian fixed-point ($\lambda_\psi \equiv 0$) and a non-trivial fixed-point $\lambda_\psi^*(\tau, \langle A_0\rangle)$, see Fig. 4.2. The non-Gaußian fixed-point can be computed analytically

$$\begin{aligned}\lambda_\psi^*(\tau,\langle A_0\rangle) \;&=\; \left(\frac{1}{\pi^2}\left(2+\frac{1}{d_{\mathrm{R}}}\right)\sum_{l=1}^{d_{\mathrm{R}}} l_1^{(\mathrm{F})}(\tau, 0, \nu_l^{(\mathrm{R})}|\phi|)\right)^{-1} \qquad (4.8)\\ &= \lambda_\psi^*\left(1+\frac{1}{d_{\mathrm{R}}}\sum_{n=1}^{\infty}(-d_{\mathrm{R}})^n\left[\mathrm{tr}_{\mathrm{R}}(L_{\mathrm{R}}[\langle A_0\rangle]^n)+\mathrm{tr}_{\mathrm{R}}(L_{\mathrm{R}}^\dagger[\langle A_0\rangle]^n)\right]\left(1+\frac{n}{\tau}\right)\mathrm{e}^{-\frac{n}{\tau}}\right)^{-1}\end{aligned}$$

where

$$\lambda_\psi^* \equiv \lambda_\psi^*(0,0) = \frac{6\pi^2}{(2d_{\mathrm{R}}+1)}\,. \tag{4.9}$$

In the limit of large d_{R}, the rescaled fixed-point $d_{\mathrm{R}}\lambda_\psi^*$ approaches a constant value. Note that we have dropped terms depending on η_ψ on the right-hand side of Eq. (4.8). As discussed above, in the presently used point-like limit this is not an approximation.

Remark 4.2:
At finite temperature, the non-Gaußian fixed-point is rather a pseudo fixed-point, i. e. the fixed-point inherits an implicit scale dependence from the dimensionless tempera-

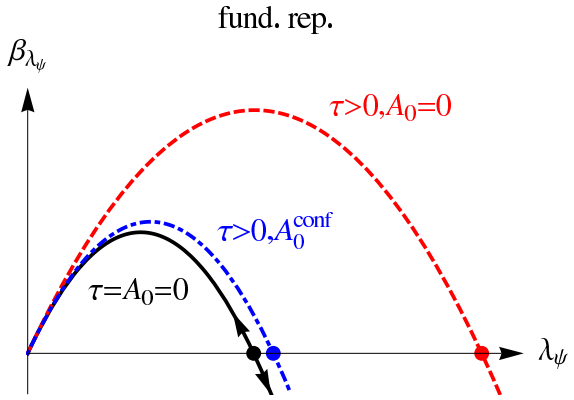

Figure 4.2.: Sketch of the β_{λ_ψ}-function of the four-fermion coupling λ_ψ for vanishing temperature (black/solid line), finite temperature and $\langle A_0\rangle = 0$ (red/dashed line), and finite temperature and $\langle A_0\rangle > 0$ (blue/dashed-dotted line) at finite $d_{\rm R}$, see Eq. (4.5). The arrows indicate the direction of the RG flow towards the infrared.

ture $\tau = T/k$ as well as a dependence on $\langle A_0\rangle$. Moreover, the line of pseudo fixed-points $\lambda_\psi^*(\tau, \langle A_0\rangle)$ does not represent a separatrix in the (λ_ψ, τ)-plane. However, it represents a strict upper bound for the separatrix in this plane [92].

Remark 4.3:
The fixed-point value is not a universal quantity, as can be seen from its dependence on the regularisation scheme. However, the statement about the existence of the fixed-point and its qualitative dependence on the temperature and $\langle A_0\rangle$ is universal.

Vanishing $\langle A_0\rangle$

Before we turn to the case of finite temperature, we briefly discuss a few basic aspects of the zero-temperature limit. In order to solve the RG flow Eq. (4.5), we have to choose an initial value $\lambda_\psi^{\rm UV}$ at the scale $k = \Lambda$. For $\lambda_\psi^{\rm UV} < \lambda_\psi^*$, we find that the four-fermion coupling approaches the Gaußian fixed-point in the IR limit, i. e. the theory becomes non-interacting and chiral symmetry remains intact. This can be seen from the black (solid) curve in Fig. 4.2, where the arrows denote the direction of the RG flow towards the IR. For $\lambda_\psi^{\rm UV} > \lambda_\psi^*$, on the other hand, we observe that the four-fermion coupling grows rapidly and diverges at a finite scale $k_{\rm SB}$. This scale signals the onset of chiral symmetry breaking. Below this scale, the point-like approximation is no longer justified: the formation of a quark condensate and the appearance of Nambu-Goldstone modes requires that we resolve the momentum dependence of the four-fermion coupling in this regime. For example, this can be done by means of partial bosonisation techniques, see Secs. 2.1.2 and 4.3. In any case, the chiral symmetry breaking scale $k_{\rm SB}$ sets the scale for all chiral low-energy observables $\mathcal{O}$

$$\mathcal{O} \sim k_{\rm SB}^{d_\mathcal{O}} \sim \left[1 - \left(\frac{\lambda_\psi^*}{\lambda_\psi^{\rm UV}}\right)\right]^{\frac{d_\mathcal{O}}{|\Theta|}} \theta(\lambda_\psi^{\rm UV} - \lambda_\psi^*)\,. \tag{4.10}$$

Here, $d_{\mathcal{O}}$ is the canonical mass dimension of the observable $\mathcal{O}$ and the critical exponent Θ is defined as

$$\Theta = -\frac{\partial \beta_{\lambda_\psi}}{\partial \lambda_\psi}\bigg|_{\lambda_\psi^*} = 2 \tag{4.11}$$

in this one-dimensional case. In general, when there are several couplings $g = (g_1, \ldots, g_n)$ present, the critical exponents are the eigenvalues of the stability matrix

$$\mathcal{S}_{ij} = -\frac{\partial \beta_{g_i}}{\partial g_j}\bigg|_{g=g^*}, \tag{4.12}$$

which arises when we linearise the flow equations in the vicinity of a fixed-point

$$\partial_t g_i = \sum_j \mathcal{S}_{ij}(g_j - g_j^*) + \ldots . \tag{4.13}$$

The critical exponents Θ_j and associated eigenvectors describe the behaviour of the RG flow near the fixed-points. By use of the standard theory of linear partial differential equations, we can conclude that the critical exponents can be used to classify the directions in the categories *relevant* (infrared repulsive, $\Theta_j > 0$), *irrelevant* (infrared attractive, $\Theta_j < 0$) and *marginal* ($\Theta_j = 0$), cf. Sec. 1.3.1. For the study of marginal operators, higher orders in the expansion around the fixed-point need to be taken into account.

Coming back to the case of Eq. (4.11), we see that $\Theta = 2$ corresponds to a relevant, infrared repulsive direction, which is indicated by the arrows pointing away from the non-Gaußian fixed-point in Fig. 4.2. Note that while the position of the fixed-point is not universal, the value of the critical exponents are. Indeed, they are just the critical exponents associated with a quantum phase transition at $T = 0$.

Now we return to our discussion of the properties of the β-function Eq. (4.5) and fix $\lambda_\psi^{\mathrm{UV}} > \lambda_\psi^*$ at $T = 0$ in the following. The value of $\lambda_\psi^{\mathrm{UV}}$ then determines the symmetry breaking scale k_{SB} and, in turn, the values of the chiral low-energy observables. For our study of finite-temperature effects and influence of the confining dynamics parametrised by the background field $\langle A_0 \rangle$, we leave our choice for $\lambda_\psi^{\mathrm{UV}}$ unchanged. This ensures comparability of our results at zero and finite temperature for a theory defined by a given value of $\lambda_\psi^{\mathrm{UV}}$.

At finite temperature the fixed-point structure of the theory is deformed compared to the zero-temperature limit. In this case, the pseudo fixed-point is shifted to larger values at finite temperature, $\lambda_\psi^*(\tau, 0) > \lambda_\psi^*$, see Eq. (4.8). For a given initial value $\lambda_\psi^{\mathrm{UV}} > \lambda_\psi^*$, this implies that a critical temperature T_χ exists, above which chiral symmetry is restored. Strictly speaking, the critical temperature T_χ is defined to be the temperature for which $1/\lambda_\psi \to 0$ for $k \to 0$. From the RG flow Eq. (4.5) one can then obtain a simple analytic expression for T_χ:

$$T_\chi = \left(\frac{\Lambda}{\pi}\right)\left[1 - \left(\frac{\lambda_\psi^*}{\lambda_\psi^{\mathrm{UV}}}\right)\right]^{\frac{1}{2}} \theta(\lambda_\psi^{\mathrm{UV}} - \lambda_\psi^*)\,, \tag{4.14}$$

which is accordance with our general statement in Eq. (4.10). To derive this expression, we have assumed that $T/\Lambda \ll 1$.

Non-Vanishing $\langle A_0 \rangle$ in the Large d_R-Limit

Let us now turn to the case of finite $\langle A_0 \rangle$. For fermions in the fundamental representation, for example, we have $\mathrm{tr}_\mathrm{F}\left(L_\mathrm{F}[\langle A_0 \rangle]^n\right) \to 0$ in the center symmetric phase for $n \in \mathbb{N}$ and $d_\mathrm{F} = N_c \to \infty$, see Eq. (1.24). Thus, the temperature-dependent corrections to $\lambda_\psi^*(\tau, \langle A_0 \rangle)$ vanish identically and we have

$$\lambda_\psi^*(\tau, \langle A_0 \rangle) \equiv \lambda_\psi^*(0,0) \quad \text{for} \quad T \leq T_\mathrm{d}\,. \tag{4.15}$$

We shall refer to this as a *locking mechanism* for the chiral phase transition. Loosely speaking, this means that the chiral phase transition is locked in due to the confining dynamics. For $T > T_\mathrm{d}$, we have $\mathrm{tr}_\mathrm{F} L_\mathrm{F}[\langle A_0 \rangle] > 0$ and the fixed-point is again shifted to larger values. This implies that $T_\chi \geq T_\mathrm{d}$ in the limit $N_c \to \infty$, see also Refs. [26, 142, 143].

Remark 4.4:
We will refer to the temperature T_d as the deconfinement phase transition temperature, even if we study theories with quarks in other representation than the fundamental. It has been discussed in Sec. 1.1.3 that there exist representations for which the quark-antiquark potential is not linearly rising at large distances, independent of the temperature. Below T_d, however, center symmetry is restored also in these cases. In any case, free, static colour charges are screened to form colour-neutral states below T_d for all representations considered here.

In the case of adjoint fermions and $d_\mathrm{A} \gg 1$, the temperature-dependent corrections in Eq. (4.8) do not vanish on all RG scales k for $T \leq T_\mathrm{d}$, since $\mathrm{tr}_\mathrm{A}(L_\mathrm{A}[\langle A_0 \rangle]^n) < 0$ for these temperatures, see Eq. (1.36). Therefore the (global) sign of the temperature-dependent corrections changes compared to the case with $\langle A_0 \rangle = 0$. This implies that the pseudo fixed-point is shifted to smaller values at finite temperature rather than to larger values.[4] For fixed T and $k \to 0$ (i. e. $\tau \to \infty$), the pseudo fixed-point approaches

$$\lambda_\psi^*(\tau \to \infty, \langle A_0 \rangle) = \frac{\lambda_\psi^*}{1 + \frac{1}{d(\mathrm{A})}}\,, \tag{4.16}$$

and for $d_\mathrm{A} \to \infty$ we have $\lambda_\psi^*(\tau \to \infty, \langle A_0 \rangle) \to \lambda_\psi^*$ from below. Since $\mathrm{tr}_\mathrm{A} L_\mathrm{A}[\langle A_0 \rangle] \to 1$ for $T \gg T_\mathrm{d}$, the fixed-point is "released" and shifted to larger values. For a given initial value $\lambda_\psi^\mathrm{UV} > \lambda_\psi^*$, it then follows again that $T_\chi \geq T_\mathrm{d}$ for $d_\mathrm{A} \to \infty$.

This analysis can in principle be repeated for any fermion representation, including fermion representations for which $\mathrm{tr}_\mathrm{R} L_\mathrm{R}[\langle A_0 \rangle] > 0$ for $T < T_\mathrm{d}$, such as the ten-dimensional representation, see Eq. (1.41). In the latter case, the temperature-dependent corrections do not vanish for large values of d_R. However, the finite-temperature shift of the fixed-point is still suppressed by a factor of $1/d_\mathrm{R}$ compared to the case with $\langle A_0 \rangle = 0$. As a consequence, the chiral transition temperature is increased, but it is not necessarily pushed above the deconfinement phase transition. Therefore, a strict statement about the relation of the chiral and the deconfinement phase transition cannot be made for this class of theories, not even in the large-d_R limit.

[4] Note that an external magnetic field deforms the fixed-point structure in a similar way [61, 144].

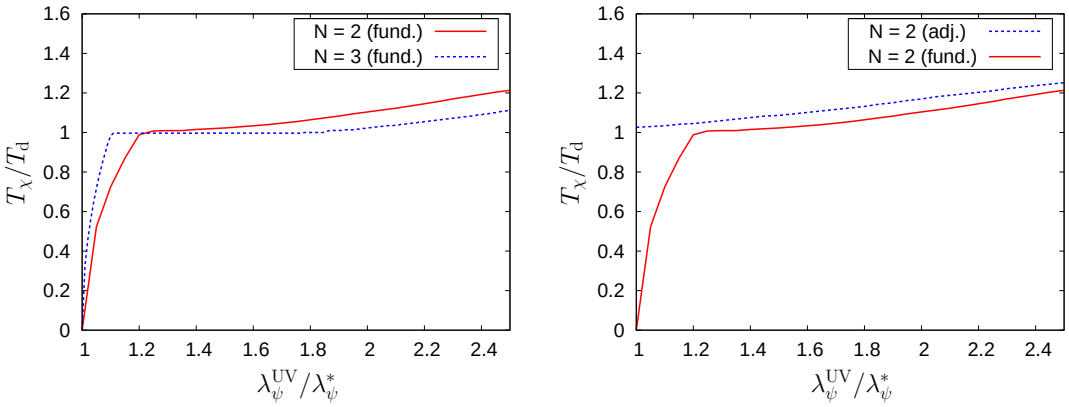

Figure 4.3.: Left: Phase diagram in the plane spanned by the temperature and the rescaled coupling $\lambda_\psi^\mathrm{UV}/\lambda_\psi^*$ for $N_f = 2$ massless quark flavours in the fundamental representation and $N_c = 2$ colours (red/solid line) as well as for $N_c = 3$ (blue/dashed line), see also Ref. [26]. Note that there is no splitting of the phase boundary (i. e. $T_\chi \simeq T_\mathrm{d}$) for small λ_ψ^UV in the large-N_c limit, see Eq. (4.17) and discussion thereof. Right: T_χ/T_d as a function of $\lambda_\psi^\mathrm{UV}/\lambda_\psi^*$ for $N_f = 2$ massless quarks in the fundamental representation ($N_c = 2$) (red/solid line) as well as for quarks in the adjoint representation (blue/dashed line).

From the flow Eq. (4.5) we can derive an implicit equation for the chiral phase transition temperature T_χ provided that we neglect a possible RG scale dependence of $\mathrm{tr}_\mathrm{R} L_\mathrm{R}[\langle A_0\rangle]$

$$T_\chi^2 = \frac{1}{\mathcal{P}_\mathrm{R}(T_\chi)} \left(\frac{\Lambda}{\pi}\right)^2 \left[1 - \left(\frac{\lambda_\psi^*}{\lambda_\psi^\mathrm{UV}}\right)\right] \theta(\lambda_\psi^\mathrm{UV} - \lambda_\psi^*), \tag{4.17}$$

where

$$\mathcal{P}_\mathrm{R}(T) = -\frac{6}{d(\mathrm{R})\pi^2} \sum_{n=1}^{\infty} \frac{1}{n^2} (-d_\mathrm{R})^n \left[\mathrm{tr}_\mathrm{R}(L_\mathrm{R}[\langle A_0\rangle]^n) + \mathrm{tr}_\mathrm{R}(L_\mathrm{R}^\dagger[\langle A_0\rangle]^n)\right]. \tag{4.18}$$

In order to derive this equation, we have again assumed that $T/\Lambda \ll 1$. For $\langle A_0\rangle \to 0$, we find $\mathcal{P}_\mathrm{R}(T) = 1$, as expected from Eq. (4.14). Since $\mathrm{tr}_\mathrm{R} L_\mathrm{R}[\langle A_0\rangle]$ depends on T_d, Eq. (4.17) relates the chiral phase transition temperature T_χ to the deconfinement phase transition temperature T_d.

For fermions in the fundamental representation and $N_c \to \infty$, we have $\mathcal{P}_\mathrm{F}(T) = 0$ for $T \leq T_\mathrm{d}$ and $\mathcal{P}_\mathrm{F}(T) > 0$ for $T > T_\mathrm{d}$. Thus, no finite solution of Eq. (4.17) exists for $T_\chi < T_\mathrm{d}$. In accordance with our fixed-point analysis, we conclude that $T_\chi \geq T_\mathrm{d}$.

For fermions in the adjoint representation and $d_\mathrm{A} \gg 1$, we have $\mathcal{P}_\mathrm{A}(T) \approx -1/d_\mathrm{A}$ for $T \leq T_\mathrm{d}$. As in the case of fundamental matter fields, this implies again that $T_\chi \geq T_\mathrm{d}$. For fermion representations with $0 < \mathcal{P}_\mathrm{R}(T) < 1$ for $T < T_\mathrm{d}$, we observe that the chiral phase transition temperature is still shifted to larger values compared to the case with $\langle A_0\rangle = 0$. However, a definite statement about the ordering of the two phase transitions temperatures cannot be made in this case.

Non-Vanishing $\langle A_0 \rangle$ at Finite d_R

Let us now turn to the case of finite values of $d_{\rm R}$. For fermions in the fundamental representation, we then find $\mathcal{P}_{\rm F}(T) = 1/N_c^2 > 0$ for $T \leq T_{\rm d}$. For $T > T_{\rm d}$, $\mathcal{P}_{\rm F}(T)$ increases monotonically from $\mathcal{P}_{\rm F}(T_{\rm d}) = 1/N_c^2$ to $\mathcal{P}_{\rm F}(T \to \infty) \to 1$. In fact, right above the deconfinement phase transition, the quantity $\mathcal{P}_{\rm F}(T)$ increases rapidly since $\mathrm{tr}_{\rm F} L_{\rm F}[\langle A_0 \rangle]$ increases rapidly. Since $\mathcal{P}_{\rm F}(T)$ is finite for all temperatures, we find a regime where $T_\chi < T_{\rm d}$ for $\lambda_\psi^{\rm UV}/\lambda_\psi^* \gtrsim 1$. In the left panel of Fig. 4.3, we show our numerical results for $T_\chi/T_{\rm d}$ as a function of $\lambda_\psi^{\rm UV}/\lambda_\psi^*$. For larger values of $\lambda_\psi^{\rm UV}/\lambda_\psi^*$, a window in parameter space opens up in which the chiral and the deconfinement phase transition (almost) coincide. In the limit $N_c \to \infty$, this locking window extends down to $\lambda_\psi^{\rm UV}/\lambda_\psi^* = 1$, as illustrated by a comparison of our results for $N_c = 2$ and $N_c = 3$ in Fig. 4.3. Note that the locking window for $\lambda_\psi^{\rm UV}/\lambda_\psi^*$ can be related to a locking window for low-energy observables, such as the pion decay constant. We shall come back to this in Sec. 4.3.

In the case of adjoint fermions and finite $d_{\rm A}$, we have $\mathcal{P}_{\rm A}(T) \leq 0$ for $T \leq T_{\rm d}$. For example, we have $\mathcal{P}_{\rm A}(T) = -1$ for $N_c = 2$. For $T \gtrsim T_{\rm d}$, $\mathcal{P}_{\rm A}(T)$ increases rapidly and changes its sign. For $T \gg T_{\rm d}$, it then approaches $\mathcal{P}_{\rm A}(T) = 1$. Since we have $\mathcal{P}_{\rm A}(T) \leq 0$ even for finite N_c, we find that the chiral phase transition temperature is larger than the deconfinement phase transition temperature. This is independent of our choice for $\lambda_\psi^{\rm UV}/\lambda_\psi^* > 1$ and $N_c \geq 2$, see right panel of Fig. 4.3 for our numerical results for $N_c = 2$. Note that this observation is compatible with lattice results of $SU(2)$ gauge theory with two adjoint quarks, see Refs. [23–25]. In our analysis, it can be traced back to the deformation of the fermionic fixed-point structure in the presence of gauge dynamics.

Remark 4.5:
To obtain the numerical results in Fig. 4.3, we have employed data for $\langle A_0 \rangle(T)$ as obtained from an RG study of the associated order parameter potential for $SU(2)$ and $SU(3)$ Yang-Mills theory [19,20]. However, we did not take into account the backreaction of the matter fields on the order-parameter potential associated with $\langle A_0 \rangle$, as discussed e.g. in Sec. 3.2. In the case of fundamental matter, we expect that this backreaction will shrink the size of the locking window, since it further increases the quantity $\mathcal{P}_{\rm F}(T)$ at low temperatures. For adjoint quarks, the backreaction will also increase $\mathcal{P}_{\rm A}(T)$. Nevertheless, it may remain negative over a wide range of temperatures. Therefore, we may still have $T_\chi > T_{\rm d}$ for all values of $\lambda_\psi^{\rm UV}/\lambda_\psi^* > 1$, at least for $N_c = 2$.

Before we now enter the discussion of the RG flows of the partially bosonised formulation of the matter sector, we would like to comment on the number of parameters in our study. Up to this point, our discussion suggests that our study only relies on a single parameter in the matter sector, apart from the UV cutoff Λ, namely on the initial value $\lambda_\psi^{\rm UV}$. Strictly speaking, however, the non-trivial fixed-point of the four-fermion interaction is an artifact of our point-like approximation. In the following we will resolve part of the momentum dependence of the four-fermion interaction with the aid of the partially bosonised formulation. We will then find that the matter sector depends on three parameters: the Yukawa coupling $\bar{h}$, the bosonic mass parameter $\bar{m}$ and the UV cutoff Λ, see Eq. (4.2). This is a substantial difference to, e. g., fermion models in $d < 4$ space-time dimensions, where we only have a single parameter in both formulations, see e. g. Ref. [145]. There,

the non-trivial fixed-point of the four-fermion coupling can be mapped onto a corresponding non-trivial fixed-point in the plane spanned by the renormalised Yukawa coupling h and the dimensionless renormalised bosonic mass parameter m. In the present case, the role of the non-trivial fixed-point in the purely fermionic formulation is taken over by a separatrix in the (h^2, m^2)-plane in the partially bosonised formulation, see Figs. 4.4 and 4.5 below. The shift of the non-trivial fixed-point of the four-fermion coupling due to the gauge dynamics then turns into a corresponding shift of this separatrix.

Being aware of this subtlety, the discussion of the fermionic fixed-point structure is still useful and nicely illustrates the mechanism underlying the interplay of the chiral and the deconfinement phase transition.

4.3. Partial Bosonisation and the Large-d_{R} Expansion

In this subsection, we briefly discuss how our study of fermionic RG flows is related to the gap equation for the fermion mass in the large-d_{R} limit.

4.3.1. Gap Equation

Starting from the partially bosonised action given in Eq. (4.2), we can derive the gap equation for the vacuum expectation value $\bar{\phi}_0 = (\langle\sigma\rangle, \vec{0})$ of the scalar fields. To this end, we first consider the classical action $S \simeq \Gamma_{k\to\Lambda}$ which appears in the functional integral. Since only bilinear combinations of the fermions occur in the action S, these fields can be integrated out straightforwardly. From the resulting expression, we obtain the fully bosonised effective action $\Gamma_{\mathrm{B}}[\sigma, \vec{\pi}]$, which is a highly non-local object. From the stationary condition,

$$\left.\frac{\delta\Gamma_{\mathrm{B}}[\sigma,\vec{\pi}]}{\delta\sigma}\right|_{\bar{\phi}_0} \stackrel{!}{=} 0\,, \tag{4.19}$$

we then find the gap equation for $\langle\sigma\rangle$:[5]

$$1 \;=\; 8\left(\frac{\bar{h}_\Lambda^2}{\bar{m}_\Lambda^2}\right)\mathrm{Tr}\int\frac{d^3p}{(2\pi)^3}\left[G_F(\vec{p}^{\,2},\bar{g}\langle A_0\rangle,\langle\sigma\rangle) - G_F(\Lambda^2,\bar{g}\langle A_0\rangle,\langle\sigma\rangle)\right]\theta(\Lambda^2-\vec{p}^{\,2})\,, \tag{4.20}$$

with the fermion propagator

$$G_F(\vec{p}^{\,2},\bar{g}\langle A_0\rangle,\langle\sigma\rangle) = \frac{1}{\vec{p}^{\,2} + (\omega_{n,F} + \bar{g}\langle A_0\rangle)^2 + \bar{h}^2\langle\sigma\rangle^2} \tag{4.21}$$

depending additionally on the fermionic Matsubara frequencies $\omega_{n,F} = (2n+1)\pi T$. In the above equation, the trace Tr runs over colour as well as Matsubara indices

$$\mathrm{Tr}\cdots = \mathrm{tr}_{\mathrm{R}}\, T\sum_{n=-\infty}^{\infty}\cdots\,. \tag{4.22}$$

[5] Here and in the following we assume that the ground state is homogeneous.

In Eq. (4.20) we have dropped the trivial solution $\langle\sigma\rangle = 0$. The integral on the right-hand side of the gap equation represents a Feynman integral with two internal fermion lines and two Yukawa vertices. In order to regularise this integral, we have employed a regularization scheme[6] which corresponds to the one used to derive the RG flow equation for the four-fermion coupling $\bar{\lambda}_\psi$ in the previous section, see Eq. (4.5). The structure of the loop integral in the gap equation and on the right-hand side of the flow Eq. (4.5) is indeed identical.[7] However, the prefactor on the right-hand side of the gap equation is only correct in leading order in the large-d_{R} expansion, in contrast to the associated prefactor in the flow Eq. (4.5) of the four-fermion coupling - loosely speaking, the trace tr_{R} yields a factor of d_{R}. Our general arguments concerning the relation of the chiral and the deconfinement phase transition in the previous section are not affected by this prefactor. The latter plays only a qualitative, but no quantitative role. Therefore our findings concerning the interplay of the chiral and the deconfinement phase transition can be obtained from the gap Eq. (4.20) as well, as it should be. In fact, the fixed-points of the (dimensionless) four-fermion coupling can be viewed as critical values for the dimensionless quantity $\Lambda^2\bar{h}_\Lambda^2/\bar{m}_\Lambda^2$. This follows also from our discussion below Eq. (4.2).

4.3.2. RG Flow at Large d_{R}

Next, we discuss the fixed-point structure and the locking mechanism in the partially bosonised formulation of the matter sector, see Eq. (4.2). This formulation has the advantage that it allows us to systematically resolve the momentum dependence of the four-fermion interaction by means of a derivative expansion. Eventually, this enables us to relate the initial value $\lambda_\psi^{\mathrm{UV}}$ of the four-fermion coupling to physical low-energy observables, such as meson masses and the pion decay constant f_π. The phase diagrams in the $(\lambda_\psi^{\mathrm{UV}}, T)$ plane can then be translated into phase diagrams in, e. g., the (f_π, T) plane. In other words, the partially bosonised formulation gives us access to the phase with broken chiral symmetry in the ground state.

From the effective action Eq. (4.2), we obtain the RG flow equations for the partially bosonised formulation In leading order of an expansion in powers of d_{R}, we find the following equations for the chirally symmetric regime

$$\partial_t m^2 = (\eta_\phi - 2)m^2 + \frac{4}{\pi^2}\sum_{l=1}^{d_{\mathrm{R}}} l_1^{(\mathrm{F})}(\tau, 0, \nu_l|\phi|)h^2\,, \tag{4.23}$$

$$\partial_t \lambda_\phi = 2\eta_\phi\lambda_\phi - \frac{8}{\pi^2}\sum_{l=1}^{d_{\mathrm{R}}} l_2^{(\mathrm{F})}(\tau, 0, \nu_l|\phi|)h^4\,, \tag{4.24}$$

$$\partial_t h^2 = (2\eta_\psi + \eta_\phi)h^2\,, \tag{4.25}$$

$$\eta_\phi = \frac{2}{3\pi^2}\sum_{l=1}^{d_{\mathrm{R}}} m_4^{\mathrm{F}}(\tau, 0, \nu_l|\phi|)h^2\,, \tag{4.26}$$

[6] Often, a sharp cutoff is used to regularise the gap equation. In this case, the Λ-dependent term in the square brackets in Eq. (4.20) is absent, cf. e.g. Ref. [92].

[7] Recall also that $\bar{h}_\Lambda^2/\bar{m}_\Lambda^2$ can be identified with $\bar{\lambda}_\psi^{\mathrm{UV}} \equiv \bar{\lambda}_{\psi,\Lambda}$.

$$\eta_\psi \;=\; 0\,, \tag{4.27}$$

with the renormalised couplings

$$h^2 = Z_\phi^{-1} Z_\psi^{-2} \bar{h}^2, \quad m^2 = k^{-2} Z_\phi^{-1} \bar{m}^2 \quad \text{and} \quad \lambda_\phi = Z_\phi^{-2} \bar{\lambda}_\phi\,. \tag{4.28}$$

The threshold functions can be found in App. C. We add that despite the fact that the heat-bath distinguishes a direction at finite temperature, we do not distinguish between wave-function renormalisations longitudinal ($Z^{\parallel}_{\psi,\phi}$) and transversal ($Z^{\perp}_{\psi,\phi}$) to the heat-bath. In the following we identify the corresponding wave-function renormalisations, $Z^{\parallel}_{\psi,\phi} = Z^{\perp}_{\psi,\phi} \equiv Z_{\psi,\phi}$. In Ref. [139], it has indeed been found for the case $\langle A_0 \rangle = 0$ that the difference is small at low temperatures and only yields mild corrections to, e. g., the thermal masses close to and above the chiral phase transition. In our study of the partially bosonised formulation, we also include the RG flow of the four-boson coupling $\bar{\lambda}_\phi$ associated with an additional term $\sim (\bar{\lambda}_\phi/8)\bar{\phi}^4$ in the ansatz Eq. (4.2). Since we have $\bar{\phi} \sim (\bar{\psi}\mathcal{O}\psi)$, this type of interaction parametrises higher-order fermionic self-interaction terms. These interactions are generated dynamically in the RG flow due to Yukawa-type quark-meson interactions. The initial value of the associated coupling is set to zero in our studies, i. e. $\bar{\lambda}_\phi\big|_{k=\Lambda} = 0$. This allows us to map the partially bosonised theory onto our purely fermionic ansatz for the matter sector at the initial RG scale Λ.

In the large-d_{R} limit, the flow of the four-boson coupling (and also of higher bosonic self-interactions $\sim \bar{\phi}^{2n}$) does not contribute to the RG flows of Z_ϕ, Z_ψ, h and m, at least in the chirally symmetric regime. This corresponds to the fact that the RG flow of the four-fermion coupling is decoupled from the RG flow of fermionic n-point functions of higher order, such as eight-fermion interactions.

Remark 4.6:
Since we consider the large-d_{R} limit in this subsection, we only have purely fermionic loops appearing on the right-hand side of the flow equations. We would like to stress that the large-d_{R} expansion should not be confused with the widely used local potential approximation (LPA) where the running of the wave-function renormalisations is not taken into account.

Let us now relate the RG flow of the partially bosonised formulation to the RG flow of the purely fermionic formulation. Using Eq. (4.4) together with the flow Eqs. (4.23) and (4.25), we recover the flow equation Eq. (4.5) of the four-fermion coupling λ_ψ in the large-d_{R} limit, i. e.

$$\partial_t \left(\frac{h^2}{m^2} \right) \Bigg|_{d_{\mathrm{R}}\to\infty} \equiv \partial_t \lambda_\psi \Big|_{d_{\mathrm{R}}\to\infty}\,, \tag{4.29}$$

see also Eq. (4.47). Thus, only our choice for the ratio h^2/m^2 at the initial RG scale determines whether chiral symmetry is broken in the IR limit $k \to 0$. Since the flow equation for the ratio h^2/m^2 is identical to the one for λ_ψ, we already anticipate that our statements concerning the ordering of the chiral and the deconfinement transition temperatures still hold in the partially bosonised formulation.

After having shown the equivalence of the RG flow of h^2/m^2 and λ_ψ in the chirally

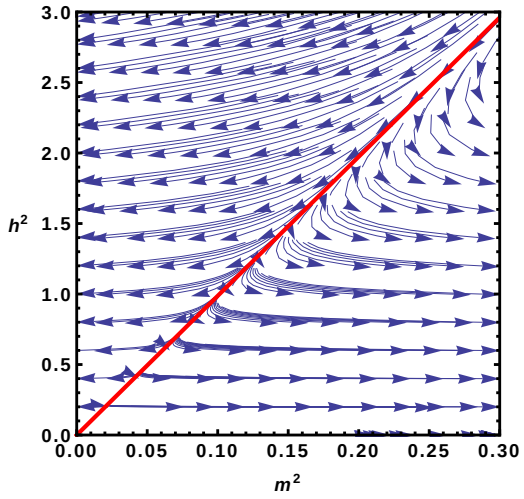

Figure 4.4.: $T = 0$ RG flow for fundamental fermions and $N_c = 3$ in leading order in the $1/d_R$-expansion in the (h^2, m^2)-plane. The red (solid) line represents the separatrix (critical manifold). The arrows indicate the direction of the RG flow towards the infrared, see text for an interpretation.

symmetric regime, we now discuss the number of parameters in the matter sector of our model. Relation Eq. (4.29) seems to suggest that we only have one parameter, namely the ratio h^2/m^2 at the initial RG scale. Indeed, the value of the symmetry breaking scale k_{SB} depends only on our choice for h^2/m^2 at the initial RG scale. This connotes that a non-trivial IR repulsive fixed-point also exists in the plane spanned by the couplings h^2 and m^2. From the above set of flow equations, however, we read off that the system has only a Gaußian (non-interacting) fixed-point $(h_*^2, m_*^2)_{\mathrm{Gauß}} = (0, 0)$, but no non-Gaußian fixed-point. This seems to be in contradiction to Eq. (4.29) and to our results from the purely fermionic formulation. However, apart from the Gaußian fixed-point, we also observe that a separatrix exists in the plane spanned by h^2 and m^2. The latter separates the (h^2, m^2)-plane into two disjoint regimes, see Fig. 4.4. In the large-d_{R} limit, the functional form of the separatrix can be computed analytically. At $T = 0$ we find

$$h^2_{\mathrm{sep.}}(m^2) = \frac{3\pi^2 m^2}{d_{\mathrm{R}}} \equiv \lambda^*_{\psi,\infty} m^2 \,, \tag{4.30}$$

where $\lambda^*_{\psi,\infty}$ is the value of the fixed-point λ^*_ψ in the large-d_{R} limit.

Choosing initial conditions $(h^2_\Lambda, m^2_\Lambda)$ in the domain to the left of the separatrix, we find that the system flows into the regime with $m^2 < 0$, in which chiral symmetry is broken in the ground state. On the other hand, the system remains in the chirally symmetric regime, if we initialise the flow in the domain to the right of the separatrix, see Fig. 4.4. Loosely speaking, we have found that the separatrix takes over the role of the non-Gaußian fixed-point λ^*_ψ which is present in the point-like approximation of the purely fermionic formulation.

To further clarify the fate of the seemingly missing non-trivial fixed-point in the (h^2, m^2)-plane, we briefly consider the case $2 < d < 4$. In this case, a non-trivial fixed-point

indeed exists in NJL-type and Gross-Neveu-type models, see e. g. Ref. [145]. This follows immediately from a consideration of the RG flow of the dimensionless renormalised Yukawa coupling $h^2 = k^{d-4} Z_\phi^{-1} Z_\psi^{-2} \bar{h}^2$

$$\partial_t h^2 = (d - 4 + \eta_\phi + 2\eta_\psi) h^2 \,. \tag{4.31}$$

This differential equation has a Gaußian fixed-point and a non-Gaußian fixed-point h^2_* for $2 < d < 4$ since $\eta_\phi \sim h^2$ and $\eta_\phi > 0$, as shown in [145]. In the (h^2, m^2)-plane, we therefore have a non-trivial fixed-point with an IR attractive and IR repulsive direction for $2 < d < 4$. This non-trivial fixed-point represents the intersection point of two separatrices in the (h^2, m^2)-plane and corresponds to the non-trivial fixed-point of the associated four-fermion coupling. For $d \to 4$, this fixed-point merges with the Gaußian fixed-point.

The non-existence of the non-Gaußian fixed-point in $d = 4$ implies that the Yukawa coupling h and the UV cutoff Λ should be considered as parameters of the theory, in addition to the ratio $h^2_\Lambda / m^2_\Lambda$. In fact, for any finite UV cutoff we can define a critical value for the ratio $h^2/m^2 \sim \lambda_\psi$, above which spontaneous chiral symmetry breaking occurs in the long-range limit $k \to 0$. However, since no non-trivial fixed-point with an IR attractive direction exists in the (h^2, m^2)-plane, the value of the Yukawa coupling at the symmetry breaking scale k_{SB} depends strongly on the initial conditions for the bosonic mass parameter and the Yukawa coupling itself. Once the system enters the regime with $m^2 < 0$, the RG flow of the Yukawa coupling effectively "freezes". In this low-energy regime, the fermions acquire a mass and fermionic loops are therefore generically suppressed, see also our discussion below. Hence we have three parameters in our simplified model ansatz for the matter sector, namely $h^2_\Lambda / m^2_\Lambda$, h^2_Λ and Λ.

Let us now analyse the dynamics at finite T and $\langle A_0 \rangle$. Our discussion of Eq. (4.29) and of the RG flow in the (h^2, m^2)-plane at zero temperature already suggest that our general arguments concerning the relation of the deconfinement and the chiral phase transition from Sec. 4.2 are still valid. This is not too surprising: the point-like approximation in the purely fermionic formulation is a reasonable approximation in the chirally symmetric regime where the bosonic mass parameter m^2 is large over a wide range of scales and therefore suppresses the non-trivial momentum-dependence of the vertices.[8] In any case, we now have to study the behaviour of the separatrix in the (h^2, m^2)-plane for finite temperature T and finite $\langle A_0 \rangle$. To this end, we may even consider the dimensionless temperature $\tau = T/k$ as an additional coupling of the theory. Thus, the separatrix is no longer a one-dimensional manifold as it is the case at zero temperature. It rather represents a two-dimensional manifold. Again, the functional form of this critical manifold can be computed analytically. For $\tau = T/\Lambda \ll 1$, we find

$$h^2_{\mathrm{sep.}}(m^2, \tau) = \frac{\lambda^*_{\psi,\infty} m^2}{1 - \pi^2 \mathcal{P}_{\mathrm{R}}(T) \tau^2} \,, \tag{4.32}$$

where $\mathcal{P}_{\mathrm{R}}(T)$ is defined in Eq. (4.18). We observe that the shape of the critical manifold depends on the temperature and the order parameter for center-symmetry breaking, see

[8] Recall that the bosons mediate the interaction between the fermions in the partially bosonised formulation. In this spirit, the boson propagators parametrise the momentum dependence of the four-fermion coupling, see e. g. Ref. [92] for a detailed discussion.

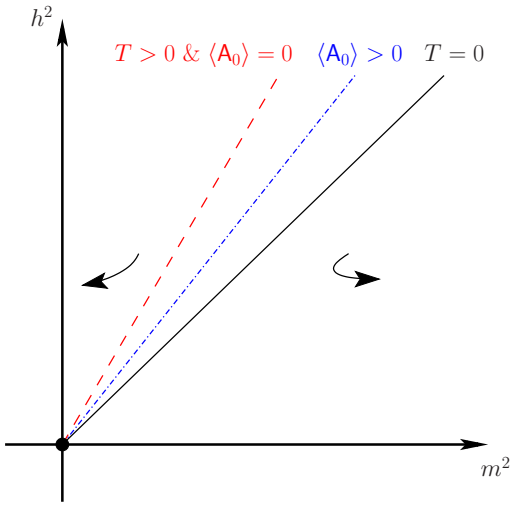

Figure 4.5.: Sketch of the separatrices of the RG flow in leading order in the $1/d_{\mathrm{R}}$-expansion in the (h^2, m^2)-plane. The black dot denotes the Gaußian fixed-point. The separatrices are sketched for three different cases: vanishing temperature (black/solid line), finite temperature and $\langle A_0 \rangle = 0$ (red/dashed line), and finite temperature and $\langle A_0 \rangle > 0$ (blue/dashed-dotted line). The dependence of the separatrices on the temperature and $\langle A_0 \rangle$ reflects the behaviour of the non-Gaußian fixed-point of the four-fermion coupling, see Fig. 4.2. The arrows indicate the direction of the RG flow towards the infrared.

Fig. 4.5.

The critical manifold allows us to define a necessary condition for chiral symmetry breaking at finite temperature. Solving Eq. (4.32) for τ, we obtain $\tau_{\text{sep.}}(m^2, h^2)$. Choosing now $\tau < \tau_{\text{sep.}}$ for a given set of initial values $(h_\Lambda^2, m_\Lambda^2)$, the theory necessarily approaches the regime with broken chiral symmetry in the IR limit. For $\tau > \tau_{\text{sep.}}$, on the other hand, the theory remains in the chirally symmetric regime. For a given value of the UV cutoff Λ and $(h_\Lambda^2, m_\Lambda^2)$, the quantity $\tau_{\text{sep.}}$ is therefore nothing but the dimensionless chiral phase transition temperature, $\tau_{\text{sep.}} = T_\chi/\Lambda$. In fact, $T_\chi = \Lambda \tau_{\text{sep.}}$ agrees with the result from Eq. (4.17). Thus, our general statements in Sec. 4.2 concerning the interplay of the chiral and the deconfinement phase transition still hold.

Let us now discuss how the phase diagrams in the $(T, \lambda_\psi^{\mathrm{UV}})$-plane can be translated into phase diagrams in, e. g., the (T, f_π)-plane. To this end, we need to follow the RG flow down to the long-range limit. As discussed in Sec. 4.1, the mass parameter m^2 assumes negative values in the regime with broken chiral symmetry in the ground state and the vacuum expectation value $\langle \phi \rangle \equiv \bar{\phi}_0$ becomes finite. It is therefore convenient to study the RG flow of $\bar{\phi}_0$ and $\bar{\lambda}_\phi$ rather than that of $\bar{m}^2$ and $\bar{\lambda}_\phi$. The flow equation of $\bar{\phi}_0$ can be obtained from the stationary condition

$$\frac{d}{dt}\left[\frac{\partial}{\partial \bar{\phi}^2}\left(\frac{1}{2}\bar{m}^2\bar{\phi}^2 + \frac{1}{8}\bar{\lambda}_\phi \bar{\phi}^4\right)\right]_{\bar{\phi}_0} \stackrel{!}{=} 0\,. \tag{4.33}$$

To be specific, we find the following RG flow equations for the regime with broken chiral

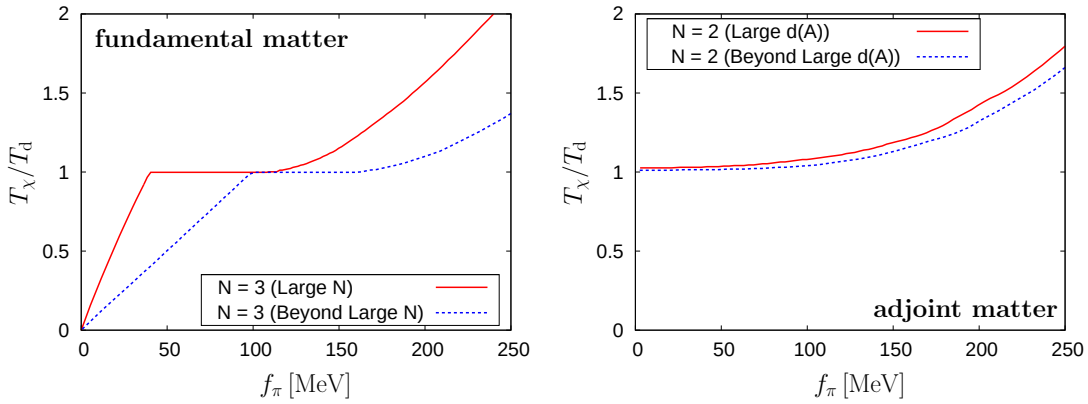

Figure 4.6.: Left: Phase diagram for two massless fundamental quarks and $N_c = 3$ in the plane spanned by the rescaled temperature T_χ/T_{d} and the value of the pion decay constant f_π at $T = 0$. Right: Corresponding phase diagram for two massless quark flavours in the adjoint representation and $N_c = 2$. In both panels, the results from the large-d_{R} approximation are given by the red (solid) line, whereas in the blue (dashed) line corrections beyond the large-d_{R} limit are included.

symmetry in the ground state:

$$\partial_t \phi_0^2 = -(\eta_\phi + 2)\phi_0^2 - \frac{8}{\pi^2}\sum_{l=1}^{d_{\mathrm{R}}} l_1^{(\mathrm{F})}(\tau, m_{\mathrm{q}}^2, \nu_l|\phi|)\frac{h^2}{\lambda_\phi}\,, \tag{4.34}$$

$$\partial_t \lambda_\phi = 2\eta_\phi \lambda_\phi - \frac{8}{\pi^2}\sum_{l=1}^{d_{\mathrm{R}}} l_2^{(\mathrm{F})}(\tau, m_{\mathrm{q}}^2, \nu_l|\phi|)h^4\,, \tag{4.35}$$

$$\partial_t h^2 = (2\eta_\psi + \eta_\phi)h^2\,, \tag{4.36}$$

$$\eta_\phi = \frac{2}{3\pi^2}\sum_{l=1}^{d_{\mathrm{R}}} m_4^{\mathrm{F}}(\tau, m_{\mathrm{q}}^2, \nu_l|\phi|)h^2\,, \tag{4.37}$$

$$\eta_\psi = 0\,, \tag{4.38}$$

where $\phi_0^2 = k^{-2} Z_\phi \bar{\phi}_0^2$ and the dimensionless renormalised constituent quark mass reads

$$m_{\mathrm{q}}^2 = h^2 \phi_0^2\,.$$

In the following, we identify the pion decay constant f_π with $Z_\phi^{1/2}\bar{\phi}_0$ and the dimensionless renormalised meson masses are given by

$$m_\pi^2 = 0 \quad \text{and} \quad m_\sigma^2 = \lambda_\phi \phi_0^2\,.$$

Since we are working in the large-d_{R} limit in this section, the latter do not appear explicitly on the right side of the flow equations.

Recall that the scale for m_{q} and m_σ is set by the symmetry breaking scale k_{SB} which

is determined by our choice for h_Λ^2/m_Λ^2. The role of the Yukawa coupling as an additional parameter becomes now apparent from the relation

$$m_\sigma^2 = \lambda_\phi \phi_0^2 \sim h^4 \phi_0^2 \sim h^2 m_\mathrm{q}^2 \,,$$

which follows from the flow equations of the couplings. Since the flow of the Yukawa coupling is not governed by the presence of a non-trivial IR attractive fixed-point, its value depends on k_SB and the initial value h_Λ, as discussed above. Therefore, the ratio $m_\sigma^2/m_\mathrm{q}^2$ depends on our choice for h_Λ. On the other hand, the initial value of the coupling λ_ϕ does not represent a free parameter of the theory. It is set to zero at $k = \Lambda$ and therefore generated dynamically in the RG flow, see also Eq. (4.2).

Using the flow equations (4.23)-(4.27) and (4.34)-(4.38), we can now proceed and compute the phase diagram in the plane spanned by the temperature and the value of the pion decay constant at $T = 0$. In Fig. 4.6 (left) we show our results for quarks in the fundamental representation and $N_c = 3$. For adjoint matter and $N_c = 2$, our results can be found in the right panel of Fig. 4.6. To obtain these results, we have used $\Lambda = 1\,\mathrm{GeV}$. Moreover, we have again employed the data for the ground-state values of $\langle A_0 \rangle$ as obtained from a RG study of $SU(N_c)$ Yang-Mills theories [19, 20].

In the case of fundamental matter and $N_c = 3$, we observe that the upper end of the locking window ($T_\mathrm{d} \approx T_\chi$) roughly coincides with the physical value of the pion decay constant, provided that we fix the initial condition of the Yukawa coupling such that $m_\mathrm{q} \approx 300\,\mathrm{MeV}$ for $f_\pi \approx 90\,\mathrm{MeV}$, see left panel of Fig. 4.6. This observation is in accordance with results from lattice simulations and general expectations. For $f_\pi \lesssim 30\,\mathrm{MeV}$, we find $T_\chi < T_\mathrm{d}$. More precisely, we observe that $T_\chi \sim f_\pi$ for small values of f_π. For $f_\pi \gtrsim 100\,\mathrm{MeV}$ ($m_\mathrm{q} \gtrsim 350\,\mathrm{MeV}$), we then have $T_\chi > T_\mathrm{d}$. In this regime, the quarks are very heavy and the two phase transitions are disentangled. Concerning the role of the Yukawa coupling, we find that the lower end of the locking window is shifted to smaller values of f_π when we increase the initial value of the Yukawa coupling. Moreover, we find that the size of the window does not strongly depend on our choice for h_Λ. This is not unexpected since we have found in our analysis of the fermionic fixed-point structure that the size of the locking window is solely related to the value of the ratio $h_\Lambda^2/m_\Lambda^2 = \lambda_\psi^\mathrm{UV}$. However, the translation of the upper and lower end of the locking window in λ_ψ^UV-space into values of physical observables does indeed depend on our choice for both h_Λ as well as h_Λ^2/m_Λ^2, as discussed above.

For adjoint matter and $N_c = 2$ as well as $N_c = 3$, we find that $T_\chi > T_\mathrm{d}$, even for very small values of f_π. We refer to Fig. 4.6 for our results for $N_c = 2$. To obtain these results, we have used $h_\Lambda = 3$. However, $T_\chi > T_\mathrm{d}$ holds for arbitrary values of h_Λ in the large-d_R limit, as suggested by our fermionic fixed-point analysis. In fact, our results in the large-d_R limit are in accordance with our results in Fig. 4.3, as it should be. For increasing f_π, we observe that the chiral phase transition temperature increases further. Thus, we have $T_\chi > T_\mathrm{d}$ for all values of f_π.

Finally we want to add that it is also possible to tune the parameters h_Λ^2/m_Λ^2 and m_Λ^2 such that we obtain $T_\chi/T_\mathrm{d} \approx 7.8$ for $N_c = 3$, as found in lattice simulations [24] of adjoint QCD without λ_ψ-deformation. This requires that the UV cutoff Λ is adjusted to larger values in order to ensure that T/Λ is sufficiently small for the temperature range under consideration, see Ref. [146] for a related PNJL model study in a mean-field approximation.

4.3.3. RG Flow Beyond the Large-d_{R} Approximation

In the following we study the robustness of our results of the previous sections with respect to $1/d_{\mathrm{R}}$-corrections. This includes an analysis of the role of Goldstone-mode fluctuations, which are absent in the large-d_{R} limit.

Our RG approach allows us to systematically include $1/d_{\mathrm{R}}$-corrections. Due to the one-loop structure of the Wetterich equation, these corrections correspond to 1PI diagrams with at least one internal boson line. In the chirally symmetric regime ($\phi_0 \equiv 0$), we then find the following set of equations:

$$\partial_t m^2 = (\eta_\phi - 2)m^2 - \frac{3}{2\pi^2} l_1^{(\mathrm{B})}(\tau, m^2)\lambda_\phi + \frac{4}{\pi^2}\sum_{l=1}^{d_{\mathrm{R}}} l_1^{(\mathrm{F})}(\tau, 0, \nu_l|\phi|)h^2\,, \tag{4.39}$$

$$\partial_t \lambda_\phi = 2\eta_\phi\lambda_\phi + \frac{3}{\pi^2} l_2^{(\mathrm{B})}(\tau, m^2)\lambda_\phi^2 - \frac{8}{\pi^2}\sum_{l=1}^{d_{\mathrm{R}}} l_2^{(\mathrm{F})}(\tau, 0, \nu_l|\phi|)h^4\,, \tag{4.40}$$

$$\partial_t h^2 = \eta_\phi h^2 - \frac{2}{\pi^2}\frac{1}{d_{\mathrm{R}}}\sum_{l=1}^{d_{\mathrm{R}}} l_{1,1}^{(\mathrm{FB})}(\tau, 0, \nu_l|\phi|, m^2)h^4\,, \tag{4.41}$$

$$\eta_\phi = \frac{2}{3\pi^2}\sum_{l=1}^{d_{\mathrm{R}}} m_4^{\mathrm{F}}(\tau, 0, \nu_l|\phi|)h^2\,. \tag{4.42}$$

In the regime with broken chiral symmetry ($\phi_0 \neq 0$), the flow of the couplings is determined by the following equations:

$$\partial_t \phi_0^2 = -(\eta_\phi + 2)\phi_0^2 + \frac{3}{2\pi^2} l_1^{(\mathrm{B})}(\tau, m_\sigma^2) + \frac{3}{2\pi^2} l_1^{(\mathrm{B})}(\tau, m_\pi^2) - \frac{8}{\pi^2}\sum_{l=1}^{d_{\mathrm{R}}} l_1^{(\mathrm{F})}(\tau, m_{\mathrm{q}}^2, \nu_l|\phi|)\frac{h^2}{\lambda_\phi}, \tag{4.43}$$

$$\partial_t \lambda_\phi = 2\eta_\phi\lambda_\phi + \frac{9}{4\pi^2} l_2^{(\mathrm{B})}(\tau, m_\sigma^2)\lambda_\phi^2 + \frac{3}{4\pi^2} l_2^{(\mathrm{B})}(\tau, m_\pi^2)\lambda_\phi^2 - \frac{8}{\pi^2}\sum_{l=1}^{d_{\mathrm{R}}} l_2^{(\mathrm{F})}(\tau, m_{\mathrm{q}}^2, \nu_l|\phi|)h^4\,, \tag{4.44}$$

$$\partial_t h^2 = \eta_\phi h^2 - \frac{1}{\pi^2}\frac{1}{d_{\mathrm{R}}}\sum_{l=1}^{d_{\mathrm{R}}}\left[3\, l_{1,1}^{(\mathrm{FB})}(\tau, m_{\mathrm{q}}^2, \nu_l|\phi|, m_\pi^2) - l_{1,1}^{(\mathrm{FB})}(\tau, m_{\mathrm{q}}^2, \nu_l|\phi|, m_\sigma^2)\right] h^4\,, \tag{4.45}$$

$$\eta_\phi = \frac{2}{3\pi^2}\sum_{l=1}^{d_{\mathrm{R}}} m_4^{\mathrm{F}}(\tau, m_{\mathrm{q}}^2, \nu_l|\phi|)h^2\,, \tag{4.46}$$

The appearing threshold functions[9] can be found in App. C. For simplicity, we do not include the running of the fermionic wave-function renormalisation in the present study, although it can be taken into account straightforwardly, as illustrated in, e. g., Refs. [85, 88, 138] for the case $\langle A_0\rangle = 0$. As discussed in the previous subsection, this is *not* an approximation in the large-d_{R} limit. Beyond the large-d_{R} limit, it has been found in

[9] Note that the functions $l_1^{(\mathrm{B})}$, $l_2^{(\mathrm{B})}$ and $l_{1,1}^{(\mathrm{FB})}$ depend implicitly on η_ϕ.

e.g. [85, 88, 138] that the anomalous dimension η_ψ is still small. This can be traced back to the fact that the running of Z_ϕ is solely governed by 1PI diagrams with at least one internal boson and fermion line. Such diagrams are suppressed in the regime with broken chiral symmetry due to the large mass of the fermions, but they are also suppressed in the chirally symmetric regime due to the large mass of the bosons. As a consequence, the running of Z_ψ only yields mild corrections to the symmetry breaking scale k_{SB}. In the following we will only take into account $1/d_{\mathrm{R}}$-corrections in those RG equations which are also non-zero in the large-d_{R} limit. The inclusion of the running of Z_ψ is left to future work.

Remark 4.7:
In the flow equations for the Yukawa coupling and the bosonic wave-function renormalisation, we have dropped terms proportional to ϕ_0. Concerning the Yukawa coupling, it has been found that these terms only yield mild quantitative corrections [85, 147]. With regard to the bosonic wave-function renormalisation, these terms are of crucial importance for an accurate computation of the critical exponents [93, 138] which is beyond the scope of the present work.

Using the flow equations of the Yukawa coupling and the bosonic mass parameter in the chirally symmetric regime, we can study again the RG flow of the ratio h^2/m^2. We now find

$$\begin{aligned}\partial_t\left(\frac{h^2}{m^2}\right) &= (2+2\eta_\psi)\left(\frac{h^2}{m^2}\right)+\frac{3}{2\pi^2}l_1^{(\mathrm{B})}(\tau,m^2)\lambda_\phi\left(\frac{h^2}{m^4}\right) \\ &- \frac{4}{\pi^2}\sum_{l=1}^{d_{\mathrm{R}}}l_1^{(\mathrm{F})}(\tau,m_{\mathrm{q}}^2,\nu_l|\phi|)\left(\frac{h^2}{m^2}\right)^2-\frac{2}{\pi^2}\frac{1}{d_{\mathrm{R}}}\sum_{l=1}^{d_{\mathrm{R}}}l_{1,1}^{(\mathrm{FB})}(\tau,m_{\mathrm{q}}^2,\nu_l|\phi|,m^2)\left(\frac{h^4}{m^2}\right).\end{aligned} \tag{4.47}$$

Making the identification $\lambda_\psi \equiv (h^2/m^2)$, the first term on the right-hand side as well as the terms in the second line can be straightforwardly identified with terms appearing in the RG equation of the four-fermion coupling λ_ψ, see Eq. (4.5). These are the leading order terms of the large-d_{R} expansion. The second term on the right-hand side corresponds to a $1/d_{\mathrm{R}}$-correction and effectively couples the flow of h^2/m^2 ($\sim$ four-fermion coupling) to the flow of the four-boson coupling ($\sim$ eight-fermion coupling). Since it can be shown that the RG flow of fermionic self-interactions is fully decoupled in the point-like limit [92], this term resolves part of the momentum dependence of the four-fermion interaction. The expression in the third line also represents a $1/d_{\mathrm{R}}$-correction and can be traced back to the running of the Yukawa coupling. Without the terms in the third line, it is not possible to reproduce the prefactor of the term $\sim \lambda_\psi^2$ in the flow equation Eq. (4.5) in the limit $m^2 \gg 1$ (point-like limit). As also pointed out in Ref. [26], this can be seen immediately from the relation

$$l_{1,1}^{(\mathrm{FB})}(\tau,m_{\mathrm{q}}^2,\nu_l|\phi|,m^2)\overset{(m\gg1)}{\longrightarrow}\frac{1}{m^2}\,l_1^{(\mathrm{F})}(\tau,m_{\mathrm{q}}^2,\nu_l|\phi|)\,. \tag{4.48}$$

For finite m^2, the expression in the third line on the right-hand side of Eq. (4.47) also resolves part of the momentum structure of the four-fermion vertex beyond the point-like

limit.

Let us now discuss our results for the phase diagrams in the (T, f_π)-plane beyond the large-d_{R} limit. In Fig. 4.6, we show our results for quarks in the fundamental representation and $N_c = 3$ as well as for quarks in the adjoint representation and $N_c = 2$. We have chosen these representations and values for N_c since they play a prominent role from a phenomenological point of view. For quarks in the fundamental representation, we observe that our results agree with those from our large-N_c study, at least on a qualitative level.[10] This means we still have three distinct regimes: one regime with $T_\chi < T_{\mathrm{d}}$ for small values of f_π, one regime with $T_\chi \approx T_{\mathrm{d}}$ (locking window), and a regime with $T_\chi > T_{\mathrm{d}}$ for large values of f_π. Also, the size of the locking window is roughly the same as in the large-N_c approximation. However, the lower and the upper end of the window have been shifted to larger values of f_π. The locking window begins at $f_\pi \approx 100$ MeV and ends at $f_\pi \approx 150$ MeV. Thus, the physical value of the pion decay constant is slightly below the lower end of the locking window. For quarks in the adjoint representation and $N_c = 2$, we find that our results are less strongly affected by corrections arising beyond the large-d_{A} approximation, see Fig. 4.6 (right). To be specific, we observe that $T_\chi > T_{\mathrm{d}}$ for $f_\pi > 0$, even if we take $1/d_{\mathrm{R}}$-corrections into account. The results only differ with respect to the slope of the chiral phase transition temperature as a function of f_π. As in the case of fermions in the fundamental representation, the slope is steeper in the large-d_{A} limit. We conclude that fluctuations of the Nambu-Goldstone modes tend to lower the sensitivity of T_χ on f_π.

The results for adjoint quarks in Fig. 4.6 have been obtained by choosing $h_\Lambda = 3$ for the initial value of the Yukawa coupling. The value of the pion decay constant can then be varied by varying only the initial value of the bosonic mass parameter m_Λ. As in the case of fundamental quarks, it is in principle possible to fix the initial condition for the Yukawa coupling by requiring that the constituent quark mass assumes a given value for a given value of the pion decay constant. For adjoint quarks, we refrain from fixing the initial condition h_Λ in this way but rather illustrate how our results depend on the choice for h_Λ, see Fig. 4.7. We observe that the dependence of T_χ on f_π becomes stronger for larger values of h_Λ. Most importantly, however, we find that $T_\chi > T_{\mathrm{d}}$ for $N_c = 2$, independent of our choice for $h_\Lambda > 0$. We stress that the mechanism underlying this observation is the deformation of the (fermionic) fixed-point structure due to the presence of the confining gauge dynamics.

Let us finally comment on the order of the chiral phase transition in the (T, f_π) phase diagram. In Ref. [26], it was found for fundamental fermions and $N_c = 3$ that the chiral phase transition is of first order within the locking window. To be more precise, we observe that the chiral phase transition is of first order for $100\,\mathrm{MeV} \lesssim f_\pi \lesssim 150\,\mathrm{MeV}$ for $N_c = 3$. Above and below the locking window, the chiral phase transition is of second order. In particular, the observation of a first-order region might be a shortcoming of our approximations: we have simply used the data for $\langle A_0 \rangle(T)$ from a study of pure $SU(3)$ Yang-Mills theory, but neglected the backreaction of the matter sector on the confinement order parameter. Within the locking window, the first-order phase transition in the gauge sector induces a first-order chiral phase transition. As argued in Ref. [26], a first-order

[10] Note that we have fixed the initial value of the Yukawa coupling by requiring that $m_{\mathrm{q}} \approx 300\,\mathrm{MeV}$ for $f_\pi \approx 90\,\mathrm{MeV}$. The same initial value for the Yukawa coupling has then been used to compute the phase transition temperature for all other values of f_π as well. Thus, we have only varied the initial value of the bosonic mass parameter m^2 to change the value of f_π. Recall that $\lambda_\psi \sim h^2/m^2$.

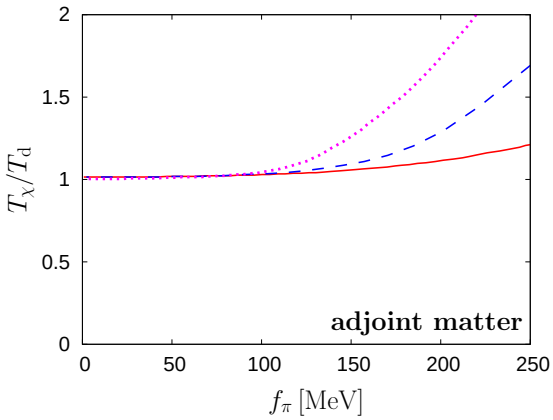

Figure 4.7.: Ratio T_χ/T_d of the chiral and the deconfinement phase transition temperature as a function of the zero-temperature value of the pion decay constant f_π for two massless adjoint quarks and $N_c = 2$. The lines illustrate the dependence of our results on the initial condition (UV value) for the Yukawa coupling. The results have been obtained for $h_\Lambda = 2, 3, 4$ (from bottom to top).

chiral transition may still occur in the (T, f_π)-plane, even if we go beyond the present approximation. However, this would then require that the confinement order parameter rises rapidly for $T \gtrsim T_\mathrm{d}$. A test of this conjecture is beyond the scope of the present work and left to future studies.

For adjoint matter and $N_c = 2$, we observe that $T_\chi > T_\mathrm{d}$ for all values of $f_\pi > 0$. Therefore the dynamics at the chiral phase transition is less affected by the confining dynamics. Loosely speaking, the latter only pushes T_χ above T_d. Within the present approximation, we therefore find that the chiral phase transition is of second order for all values of $f_\pi > 0$. This result is consistent with lattice simulations for $N_c = 2$, see Refs. [23, 24].

5. Scale Dependence of the Yukawa Coupling

In Chap. 3, the RG flow for the effective potential of the PQM model has been studied under extreme conditions, namely at finite temperature and quark chemical potential. While thermal and quantum fluctuations of the meson fields were taken into account, we did make use of the common approximation of a scale-independent Yukawa interaction between quarks and mesons. We have argued that this simplification is justified, since previous studies within a similar truncation have resulted in good values for, e.g. the order parameters or critical exponents. Due to its contribution to the quark mass, however, a better description of Fermi-surface effects is expected in a computation including the running Yukawa coupling.

In the present chapter, which reports on an ongoing project, we will now collect the necessary information to include the scale dependence of the Yukawa coupling in our study of the phase diagram. We discuss the contributing diagrams to the RG flow and compute the corresponding threshold functions. The numerical solution of the system detailed below is still under way, hence numerical results will be presented elsewhere in the future.

5.1. Motivation

Let us first start by a brief discussion of the expected scale evolution of QCD from the UV to the IR at $T = \mu = 0$. This discussion is based on the one given in Ref. [138]. At high momenta, QCD is known to be described via gluon and quark degrees of freedom. As the energy scale is lowered, several effects arise that modify the effective description. We can define the so-called compositeness scale k_ϕ as the scale at which mesons are formed. In this regime, a description of QCD in terms of quarks, gluons and mesons should become valid. In particular, k_ϕ is expected to be well separated from the confinement scale Λ_{QCD}. In the range from k_ϕ down to the chiral symmetry breaking scale k_{cr}, quarks are light and their interaction with the meson degrees of freedom is described via a strong Yukawa coupling. Around k_{cr}, also the lightest scalar mesons contribute significantly to the dynamics, since their mass goes down. Below k_{cr}, the Yukawa coupling decreases again. Its IR value, however, is fixed by the constituent quark mass $m_q = h\sigma_0$ and we find that $h(k \to 0)$ is still rather large. Hence, a description of QCD in terms of quarks and mesons, as also discussed in Chap. 2, seems a reasonable choice. Furthermore, the inclusion of a scale-dependent Yukawa coupling, at least in the chirally symmetric regime is called for.

In the following we will introduce the corresponding flow equations within the PQM model introduced in Chap. 2.

5.2. Contributing Diagrams

In Chap. 4, we have already seen that it is possible to calculate the RG scale dependence of the Yukawa coupling. Furthermore, the associated diagrams can be classified systematically within, e.g., a large-N_c expansion. Here, we will extend the truncation used in Chap. 4 and discuss the arising contributions in more detail.

As initial action for the Polyakov–quark-meson model we use again the following truncation

$$\Gamma_k \quad = \quad \int d^4x \left\{ Z_\psi \bar{\psi} \left[i\partial\!\!\!/ + i\bar{h}(\sigma + i\vec{\pi}\vec{\tau}\gamma_5) + i\gamma_0\mu \right] \psi + \frac{1}{2} Z_\phi (\partial_\mu \bar{\phi})^2 + \Omega_k(\bar{\phi}) \right\} , \tag{5.1}$$

where we restrict ourselves to the case of $N_f = 2$ flavours and $N_c = 3$ colours. The quark and meson degrees of freedom are coupled via a (unrenormalised) Yukawa interaction $\bar{h}$, which acquires a scale dependence in the following. In contradistinction to the truncation used previously, we allow for scale-dependent wave-function renormalisations Z_ψ, Z_ϕ for the quark and meson fields, respectively. This is a step beyond the local potential-like approximation that is often used in (P)QM studies with the FRG, cf. Chap. 3. In particular, the inclusion of running wave-function renormalisations renders the vertices momentum dependent.

At finite temperature, the wave-function renormalisations in general split into components parallel and orthogonal to the heat bath: $Z^{\parallel}_{\psi,\phi}$, $Z^{\perp}_{\psi,\phi}$. For simplicity we will not make such a distinction here, but use $Z^{\perp}_{\psi,\phi} = Z^{\parallel}_{\psi,\phi} \equiv Z_{\psi,\phi}$. Directly at the chiral phase transition temperature we expect the difference between $Z^{\parallel}_{\psi,\phi}$ and $Z^{\perp}_{\psi,\phi}$ to vanish, since there exists only one related critical exponent: $\eta_{\psi,\phi}$. This exponent is also referred to as the anomalous dimension and is defined via

$$\eta_{\psi,\phi} \quad = \quad -\partial_t \ln Z_{\psi,\phi} \, . \tag{5.2}$$

Furthermore, a study within the one-flavour quark-meson model, see Ref. [139], indicates that this approximation is indeed justified.

Now, we determine the contributions to the RG running of the Yukawa coupling in terms of Feynman graphs. The reader is then referred to App. B for an example of how to compute the corresponding analytic expressions. Furthermore, a collection of the arising threshold functions is found in App. C.

To determine the associated graphs, consider the Wetterich Eq. (A.15). This equation has to be projected onto the terms $\sim \bar{\psi}\bar{\phi}\psi$, hence we take derivatives with respect to $\psi, \bar{\psi}$ and $\bar{\phi}$. In this manner, graphs with three external lines, but still one-loop structure are generated. Furthermore, a sum over all vertices allowed by our ansatz Eq. (5.1) has to be performed.

Remark 5.1:
Note once more, that this procedure is not *a one-loop approximation in the perturbative sense. As the Wetterich Eq. (A.15) is fully non-perturbative, so are the present equations derived from it. Higher-loop contributions are resummed in the couplings appearing in the flow equations.*

Figure 5.1.: Pictorial representation of the triangle diagram contributions to the RG flow of the renormalised Yukawa coupling h^2.

This procedure finally yields the diagrams shown in Fig. 5.1. To arrive at this relation, we have introduced the renormalised Yukawa coupling

$$h = \frac{\bar{h}}{Z_\phi^{1/2} Z_\psi}\,. \tag{5.3}$$

Since the wave-function renormalisations depend on the RG scale k, the flow equation of the renormalised Yukawa coupling depends explicitly on the boson and fermion anomalous dimensions $\eta_\phi,\ \eta_\psi$, respectively.

The graphs in Fig. 5.1 denote fermion-boson triangle diagrams, with solid lines denoting the quark and dashed lines the meson propagators. As usual, the cross in a circle indicates the RG regulator insertion. Black dots label renormalised Yukawa vertices $\sim h$, while the gray dots indicate purely mesonic vertices $\sim \Omega_k''$. Primes, as before, label the derivative with respect to the chiral invariant $\rho = \phi^2$, which is related to its unrenormalised counterpart $\bar{\phi}$ via

$$\rho = Z_\phi \bar{\rho} = Z_\phi \bar{\phi}^{\,2}\,. \tag{5.4}$$

Note that in the second and third graphs in Fig. 5.1, external sources $\sim \langle\phi\rangle = \sqrt{\rho}$, denoted by boson lines with a cross, appear. In the chirally symmetric regime, where $\langle\phi\rangle = 0$, these thus do not contribute to the flow.

Furthermore, we want to point out that we *do not* restrict the mesonic potential to e.g., quartic order in the mesonic field. Hence, higher vertices with an odd number of source terms are also included in the above diagrams. Despite the fact that we do not show these graphs explicitly, all contributions of this kind are included in our generalised mesonic coupling $\sim \Omega_k''$. To make this point more explicit, consider for example a potential that is at most cubic in ρ

$$\Omega_\Lambda(\rho) = \frac{m^2}{2}\rho + \frac{\lambda_2}{2}\rho^2 + \frac{\lambda_3}{3!}\rho^3\,. \tag{5.5}$$

The second derivative with respect to the chiral invariant ρ reads

$$\Omega_\Lambda''(\rho) = \lambda_2 + \lambda_3\rho \tag{5.6}$$

and the mesonic vertex appearing in Fig. 5.1 contains not only graphs with one external source $\sim \lambda_2\langle\phi\rangle$, but due to the additional term also with three $\sim \lambda_3\rho\langle\phi\rangle$.

Since they contribute to the flow of the renormalised Yukawa coupling, our next task is to determine the diagrams corresponding to the boson and fermion anomalous dimensions. As before, the corresponding expressions can be derived by taking appropriate derivatives of the Wetterich equation. For η_ϕ, we need two external boson legs, and for η_ψ two fermionic ones.

Fig. 5.2 shows the graphical representation for the flow of the boson wave-function renormalisation. The first diagram is a purely fermionic loop. As is also discussed in Chap. 4, this term is the leading contribution to $\partial_t h$ in a large-N_c expansion.

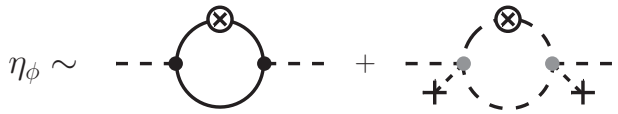

Figure 5.2.: Feynman diagrams contributing to the RG flow of the bosonic wave function renormalisation $\eta_\phi = -\ln \partial_t Z_\phi$.

The second contribution to η_ϕ is purely mesonic. It is given by a meson loop with $2n$, $n \in \mathbb{N}$ sources $\sim \langle \phi \rangle$ attached. As for the triangle diagrams, all these contributions are naturally included in the coupling $\sim \Omega_k''$.

Finally, the Feynman diagrams arising in the flow $\partial_t Z_\psi$ are shown in Fig. 5.3. Due to

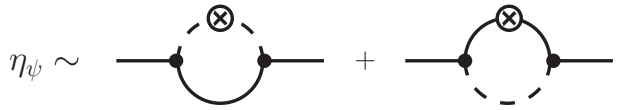

Figure 5.3.: Contributions to the fermionic anomalous dimension η_ψ.

their structure with one internal boson and one internal fermion line, these contributions are suppressed. In the chirally symmetric regime, the meson mass is large, which diminishes the influence of this contribution. In the chirally broken region, on the other hand, the quark mass is large and hence the diagrams are suppressed in this regime as well. Actually, in a purely fermionic formulation in the point-like approximation, as discussed in Sec. 4.2, we have $\eta_\psi \equiv 0$. Furthermore, previous studies indicate that even beyond the point-like limit, the influence of the fermion anomalous dimension is small [85,88,138,139]. Hence, this contribution to the flow of the Yukawa coupling is neglected for the time being. Only η_ϕ and the triangle diagrams are taken into account.

5.3. Flow Equations

Next, the analytic expressions corresponding to the diagrams determined above have to be derived. Some of them we already encountered in Chap. 4. In general, the threshold functions can be derived along the lines of App. B and, e.g., Ref. [138].

Within the truncation introduced above of setting $\eta_\psi \equiv 0$, we find for the flow of the Yukawa coupling

$$\partial_t h = \frac{1}{2}\eta_\phi h - \frac{1}{\pi^2}\frac{1}{N_c}\sum_{l=1}^{N_c}\left\{3\ell_{1,1}^{F,B}(T,\tilde{\mu}_l;m_\pi^2,m_q^2) - \ell_{1,1}^{F,B}(T,\tilde{\mu}_l;m_\sigma^2,m_q^2)\right\} h^3\,, \quad (5.7)$$

where the chemical potential and gauge field dependence is contained in $\tilde{\mu}_l$. For our initial study, we neglect the triangle diagrams with mesonic sources $\sim \langle \phi \rangle$. The triangle diagram

with one internal meson line corresponds to the threshold function $\ell_{1,1}^{F,B}$, which contributes with a prefactor 3 for the three pions. The sigma-contribution comes with the opposite sign.

Note that the running of the Yukawa coupling is rather fast since we have $\partial_t h \sim h^3$. As discussed in Sec. 5.1, a comparison to the constituent quark mass in the infrared leads us to the conclusion that the final value h in the IR is still large. A correspondingly large initial value for the Yukawa coupling hence leads to a fast running of the couplings. In particular it has been discussed in e.g. [138] that this leads to a rapid approach of the couplings to partial IR fixed-points in the symmetric regime. In this manner, the dependence of the system on the detailed choice for the effective potential in the UV is reduced.

The full expression of the boson anomalous dimension reads

$$\eta_\phi = \frac{N_f}{3\pi^2}\sum_{l=1}^{N_c} m_4^F(T,\tilde{\mu}_l;m_q)\,h^2 - \frac{2\rho\,(2\Omega_k'')^2}{3\pi^2 k^2} m_{2,2}^{(B)}(m_\pi,m_\sigma)\,. \tag{5.8}$$

We already encountered the first term in Chap. 4, while the second one was neglected there, since it vanishes in the chirally symmetric phase.

Allowing for a non-vanishing boson anomalous dimension furthermore entails modifications in the flow equation for the effective potential. Explicitly, the mesonic contribution acquires a η_ϕ-dependent prefactor

$$\begin{aligned}\partial_k\Omega_k &= \frac{k^4}{12\pi^2}\left\{\left(1-\frac{\eta_\phi}{5}\right)\left[\frac{3}{E_\pi}\coth\left(\frac{E_\pi}{2T}\right)+\frac{1}{E_\sigma}\coth\left(\frac{E_\sigma}{2T}\right)\right]\right. \\ &- \left.\frac{2\nu_q}{E_q}\left[1-N_q(T,\mu;\Phi,\bar{\Phi})-N_{\bar{q}}(T,\mu;\Phi,\bar{\Phi})\right]\right\}\,.\end{aligned} \tag{5.9}$$

A similar modification would arise in the fermionic sector, if we allowed for a fermion anomalous dimension $\eta_\psi \neq 0$.

Furthermore, an implicit dependence on the running Yukawa coupling and wave-function renormalisation appears via the quasi-particle energies $E_i = \sqrt{k^2+m_i^2}$, $i = q,\sigma,\pi$ with the masses and all other definitions are as given in Sec. 3.1, but substituting $h \to h(k)$.

The coupled flow equations (5.7), (5.8) and (5.9) can now be solved numerically. An implementation thereof is currently under way. Within our approach to discretise the mesonic field on a grid this is, however, more involved than an expansion in a Taylor series: The use of the mesonic grid induces a field-dependence in the Yukawa coupling $h \to h(\rho_i)$, which needs to be taken into account consistently. Despite the additional effort needed, it should be worthwhile to do this also in the present case. Within such an approach the full phase diagram, including the first-order transition region becomes feasible and we can study the impact of the newly introduced fluctuations on the full phase structure.

In Ref. [138] the temperature dependence of the running Yukawa coupling has been studied within the QM model. The authors found a sharp dip in $h(T)$ at the chiral transition temperature in the chiral limit. This dip is induced by the long wavelength fluctuations of the pion modes that lead to a non-analyticity in the corresponding wave-function renor-

malisation. Within the above presented setup we can now study the behaviour of this effect at finite quark masses and finite chemical potential. In particular, the influence on the phase structure and thermodynamic observables can be studied.

Especially at high chemical potential the influence of the Fermi surface should be better described within the present truncation. In [148] the QCD transition at $T = 0$ and non-vanishing chemical potential was studied with the RG within a two flavour QM model. There, the authors showed that the quark number density vanishes at low chemical potential $\mu < m_q$. At $\mu = m_q$ the situation changes and a non-vanishing density develops, while chiral symmetry remains broken. Only at $\mu > m_q$ appears a jump in the density, signalling a phase transition of first order. In this work, however, the running of the Yukawa coupling was neglected in the chirally broken phase. The setup presented here will allow us to extend this investigation and take into account the RG running h for all scales.

Moreover, we plan not only to study the QM, but also the PQM model with running Yukawa coupling. In this manner, we can investigate the combined influences of deconfinement and the scale dependent Yukawa interaction, which has not been done so far.

6. Summary and Outlook

This thesis was conducted with the aim to achieve a more profound understanding of the QCD phase structure. In particular, we are interested in the interplay of chiral symmetry restoration and deconfinement at finite temperature and quark chemical potential. Since the study of the QCD phase structure from first principles still poses a formidable task, we have chosen to employ effective models describing the two effects.

Moreover, for a realistic description of phase transitions, the inclusion of fluctuations is of utmost importance. Hence, we have included thermal and quantum fluctuations by means of the FRG, which is widely applicable and is well-suited for the present task. Notably, this method allows to understand better the relation of effective models to full QCD: By studying the FRG flow of QCD it is possible to improve the effective models towards the full theory in a systematic fashion.

This circumstance has been exploited in Chap. 3, where we have studied the phase structure and thermodynamics of the Polyakov–quark-meson model at finite temperature and quark chemical potential. We have argued that the standard Polyakov-loop potential misses an important effect: the backcoupling of the matter content to the gauge sector. This leads to a deconfinement phase transition temperature T_d that is larger than the chiral restoration temperature T_χ, in contradiction to the lattice results. At finite chemical potential we have moreover observed that T_d hardly changes with μ. Especially, we have found a phase in which chiral symmetry is partially restored while deconfinement persists, a so-called quarkyonic phase.

On the other hand, if the matter backcoupling to the glue sector is included, see Sec. 3.2, we find almost coinciding chiral and deconfinement transition temperatures at zero chemical potential. Moreover, the phase structure at finite chemical potential is modified: The two transition lines lie in close proximity to each other throughout the whole phase diagram. With and without the matter backcoupling we find that both transitions are crossovers at small chemical potentials. On the chiral transition line we find a critical endpoint of second order that separates the crossover from a first-order transition line at small temperature and high chemical potential. Due to the inclusion of fluctuations, the critical point is located at rather low temperatures.

In Sec. 3.4 we have moreover studied the mass sensitivity of the phase structure and thermodynamics. In the chiral limit, a splitting of the chiral transition line into two branches emerges at high chemical potential and low temperature. Also in this limit a critical point is found, which lies on the inner transition branch. The outer branch is of second order, as is the transition at small chemical potential, in agreement universality arguments. As the vacuum pion mass is increased away from the chiral limit, the splitting persist, but the outer branch is weakened. Approaching the physical mass point, it is not possible to pin down a second transition branch anymore.

We have observed that the presently used Polyakov-loop potentials have some difficulties in describing the high chemical potential regions properly. Input from, e.g., first-principle

RG studies [115] could be used to get closer to the glue potential of QCD. Moreover, it is clear that for a correct description of the high chemical potential region, it is necessary to include baryonic degrees of freedom. These, as well as diquarks are expected to influence the phase structure and the location of the critical point.

Chap. 4 of this thesis focuses on the interplay of chiral symmetry breaking and confinement at vanishing chemical potential. In particular we have studied the interrelation of the two finite temperature transitions in gauge theories with non-trivial center. To this end, we have studied the response of the system to a change of the colour representation of the matter content. In particular the fundamental and adjoint representation of $SU(N_c)$ have been studied.

We have used a simple ansatz for the quantum effective action to compute the phase structure in the (λ_ψ, T)-plane. This formulation has the advantage that calculations can be performed analytically to a large extent. For theories with quark fields living in a given representation R, we have found that the interplay of the chiral and the deconfinement phase transition clearly depends on the sign of $\mathrm{tr}_{\mathrm{R}} L_{\mathrm{R}}[\langle A_0 \rangle]$ in the center symmetric phase. The relation of $\mathrm{tr}_{\mathrm{R}} L_{\mathrm{R}}[\langle A_0 \rangle]$ to the standard Polyakov-loop (for a given representation R) has been discussed in detail in Sec. 1.1.3. Our fixed-point analysis in Sec. 4.2 suggests that $T_\chi > T_{\mathrm{d}}$ for adjoint quarks, at least in the large-d_{R} limit. This observation is in accordance with results from lattice simulations [23–25]. For quarks in the fundamental representation, our findings are also compatible with lattice QCD [149], first-principles continuum [72, 75, 115], and earlier analytic (model) studies [26, 142, 143].

A partially bosonised formulation of the system subsequently allowed us to conveniently study low-energy observables, such as the pion decay constant f_π. This made it possible to study the phase structure in the (f_π, T)-plane. We have also investigated how robust our predictions for these phase diagrams are once $1/d_{\mathrm{R}}$-corrections, that are associated with fluctuations of the Nambu-Goldstone modes, are taken into account in the matter sector. For quarks in the fundamental representation, we have found that the locking window ($T_\chi \approx T_{\mathrm{d}}$) is shifted to larger values of f_π, but remains finite. At the physical point ($f_\pi \approx 90\,\mathrm{MeV}$), we have $T_\chi \lesssim T_{\mathrm{d}}$. For adjoint quarks and $N_c = 2$, we have found that $T_\chi > T_{\mathrm{d}}$ for all values of $f_\pi > 0$, even if $1/d_{\mathrm{R}}$-corrections are taken into account. In this respect, the finite-temperature dynamics of gauge theories with adjoint matter appear to be distinct from gauge theories with fundamental matter, at least for $N_c = 2$. This observation is also consistent with lattice studies of $SU(2)$ gauge theory with two flavours of adjoint quarks [23–25].

As an extension of the present analysis one may consider to take into account the backcoupling of the matter fields on the quantity $\mathrm{tr}_{\mathrm{R}} L_{\mathrm{R}}[\langle A_0 \rangle]$. Such contributions will push $\mathrm{tr}_{\mathrm{R}} L_{\mathrm{R}}[\langle A_0 \rangle]$ to larger values in the low-temperature phase. We expect that this will weaken the mechanisms governing the dynamics in our present study. For fundamental quarks, for example, this may shrink the locking window. For adjoint quarks, on the other hand, the quantity $\mathrm{tr}_{\mathrm{R}} L_{\mathrm{R}}[\langle A_0 \rangle]$ may still be negative over a wide range of temperatures. Therefore, $T_\chi > T_{\mathrm{d}}$ may persist for $N_c = 2$, even if we take these backreactions into account. It would be interesting to see whether and how the mechanism governing the interplay of the chiral and deconfinement transitions persists in the presence of a finite quark chemical potential and/or a finite external magnetic field. The latter deforms the fermionic fixed-point structure in a way [61, 144] which is indeed reminiscent of the

deformation discussed here for adjoint quarks.

In Chap. 5 we have presented an extension of the commonly used truncation of the PQM flow equation in which the RG scale dependence of the Yukawa coupling is taken into account. We have argued that this augmentation should result in a better description of the phase structure, especially at finite chemical potential. From the inclusion of a running Yukawa coupling we expect improvements in our description of the quark Fermi surface. In particular, we have derived the contributions to the respective flow equation diagrammatically and in analytic form and discussed their expected influence. Our aim for the near future is to investigate the impact the scale-dependent Yukawa coupling at finite temperature and chemical potential. Modifications of the phase structure and thermodynamic observables will be studied. Furthermore, the inclusion of running wave-function renormalisations allows to resolve partially the momentum dependence of the vertices. As has been shown previously [139], this can further improve the quality of, e.g., critical exponents.

Summarising, in this work we have demonstrated that by the use of effective models, significant insights into the QCD phase structure can be achieved. In particular in combination with the FRG, which allows to include fluctuations, a reliable and realistic description can be gained. Furthermore, a systematic improvement towards the full theory is possible in this approach.

A. Wetterich Equation

A.1. Derivation

The ERGE is a functional differential equation that describes the dependence of the effective average action Γ_k on the RG scale k. It is constructed such that Γ_k interpolates between the initial action at the ultraviolet scale, $\Gamma_\Lambda = S$, and the full quantum effective action in the infrared $\Gamma_{k\to 0} = \Gamma$. Going from microscopic to macroscopic scales, a coarse-graining procedure is introduced which assures that only fluctuations with momenta $q^2 \gtrsim k^2$ are taken into account. This idea is implemented by adding a k-dependent regulator term

$$\Delta S_k[\chi] = \frac{1}{2}\int_q \chi^T(-q) R_k(q) \chi(p) \tag{A.1}$$

to the action. Note that the regulator term (A.1) is quadratic in the fields and hence acts as a mass term for the Fourier modes of the fields χ with momenta smaller than k. In the previous equation, the shorthand notation $\int_p := \int \frac{d^4q}{(2\pi)^4}$ is used. For convenience, we have defined vectors containing all fields and sources present in the theory

$$\chi(p) := \begin{pmatrix} \phi(p) \\ \psi(p) \\ \bar{\psi}^T(-p) \\ \vdots \end{pmatrix} \quad \text{and} \quad J := \begin{pmatrix} j(p) \\ -\bar{\eta}^T(-p) \\ \eta(-p) \\ \vdots \end{pmatrix}, \tag{A.2}$$

where ϕ denotes a set of bosonic fields while $\bar{\psi}, \psi$ are fermionic fields and further fields can be included in the same fashion as needed.

Requirements on the regulator $R_k(q)$ are introduced in order to achieve the desired behaviour of the effective average action. In particular, for fixed q^2 we impose the conditions

$$\lim_{k\to 0} R_k(q) = 0\,, \tag{A.3}$$

$$\lim_{k\to \Lambda} R_k(q) \to \infty\,. \tag{A.4}$$

The first condition ensures that the regulator vanishes in the infrared and the full effective action is reached. In the opposite limit of k approaching the cutoff Λ, or in principle infinity, the regulator diverges, leaving us with $\Gamma_\Lambda = S$. Fig. A.1 (left) shows an example for a regulator function that fulfils the above conditions versus momentum q. The RG scale k is indicated by the vertical dashed line.

We want to mention that, despite the above conditions, there is an arbitrariness in the choice of the regulator function. In a hypothetical world where infinite computer power is available and no truncations have to be made, results should not depend on the choice of

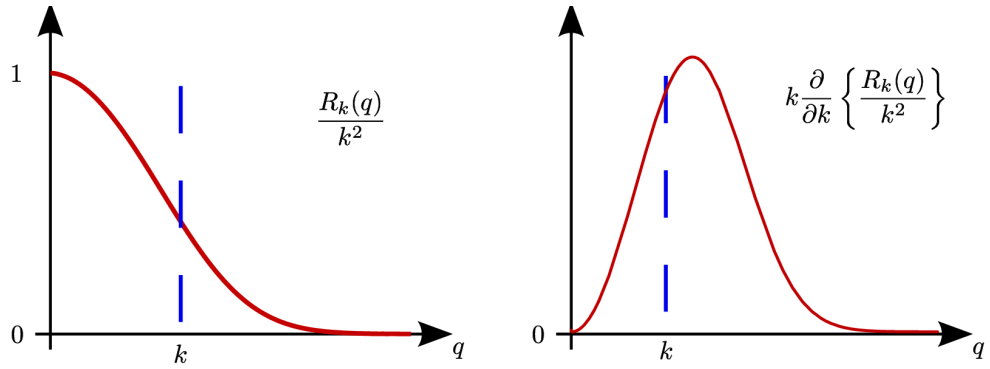

Figure A.1.: An example for the RG regulator (left) and its scale derivative (right) that implement the momentum-shell integration in the ERGE.

the regulator. As is indicated in Fig. 1.4, different regulator functions result in different RG trajectories through theory space, but emanating from the same initial action they should result in the same quantum effective action in the infrared. In practise, however, truncations are necessary in order to turn the RG flow equation into a finite system of ordinary differential equations, see also Sec. A.2. Starting at a finite UV scale Λ, it might be necessary to change the initial conditions in order to reproduce the same IR physics for different regulators. Furthermore, the deep infrared $k = 0$ can never be reached in a numerical computation with finite numerical accuracy and the flow has to be stopped at a finite, if small, scale $k_{\min}$. A variation of the regulator function can be used to obtain an estimate of the truncation error.

When the regulator term (A.1) is added to the action, the partition function acquires a scale dependence

$$Z_k[J] = \mathcal{N} \int \mathcal{D}\chi e^{-S[\chi]-\Delta S_k[\chi]+\int_q J\chi}\,. \tag{A.5}$$

This scale dependence is inherited by the other well-known generating functionals of connected and one-particle irreducible (1PI) Greens functions, respectively

$$W_k[J] = \ln Z_k[J]\,, \quad \text{and} \quad \Gamma_k[\Theta] = \int_q J\Theta - W_k[J] - \Delta S_k[\Theta]\,. \tag{A.6}$$

Here, Θ denotes the classical field

$$\Theta = \langle\chi\rangle = \frac{\overrightarrow{\delta}}{\delta J} W_k[J] \quad \text{and} \quad \Theta^T = \langle\chi^T\rangle = W_k[J]\frac{\overleftarrow{\delta}}{\delta J}\,. \tag{A.7}$$

For convenience we define[1]

$$\tilde{\Gamma}_k[\Theta] = \Gamma_k[\Theta] + \Delta S_k[\chi] \tag{A.8}$$

[1]Recall that $\Gamma_k[\Theta]$ is defined by a Legendre transformation of $W_k[J]$ and the k-dependence appears only in one of the variables J or Θ, here $J = J_k(\Theta)$.

and compute its scale derivative $\partial_t = k\partial_k$, where $t = \log(k/\Lambda)$ denotes the RG-time

$$\partial_t \tilde{\Gamma}_k = \int_q (\partial_t J(q))\Theta(q) - \partial_t W_k[J] - \int_q \frac{\delta W_k}{\delta J(q)} \partial_t J(q)\,. \tag{A.9}$$

By the definition of Θ in Eq. (A.7), the first and last terms cancel. The scale derivative of W_k is calculated from its definition, Eq. (A.6), combined with Eq. (A.5). Since R_k is the only quantity in this expression that depends on the scale we find

$$\partial_t \tilde{\Gamma}_k[\Theta] = \langle \partial_t \Delta S_k[\chi] \rangle = \left\langle \frac{1}{2} \int_{q,p} \chi(q) \partial_t R_k(q,p) \chi(p) \right\rangle , \tag{A.10}$$

with $R_k(q,p) = R_k(q)\delta(p-q)$.

Next we introduce the partially dressed, connected two-point function

$$G_k(q,p) = \frac{\delta^2 W_k}{\delta J(q) \delta J(p)} \tag{A.11}$$

and decompose

$$\langle \chi(q)\chi(p) \rangle = G_k(q,p) + \langle \chi(q) \rangle \langle \chi(p) \rangle \equiv G_k(q,p) + \Theta(q)\Theta(p)\,. \tag{A.12}$$

Plugging this into Eq. (A.10) we find

$$\begin{aligned} \partial_t \tilde{\Gamma}_k[\Theta] &= \frac{1}{2} \int_{q,p} \{ \partial_t R_k(q,p) G_k(p,q) + \Theta(p) \partial_t R_k(p,q) \Theta(q) \} & \text{(A.13)} \\ &= \frac{1}{2} \mathrm{Tr} \{ G_k \partial_t R_k \} + \partial_t \Delta S_k[\Theta]\,. & \text{(A.14)} \end{aligned}$$

It is now straightforward to reformulate this expression in terms of the effective average action Γ_k. Furthermore, we make use of the fact that $\tilde{\Gamma}_k^{(2)} = \Gamma_k^{(2)} + R_k$ is the inverse of $G_k(q,p)$ to arrive at the celebrated Wetterich equation

$$\partial_t \Gamma_k[\Theta] = \frac{1}{2} \mathrm{Tr} \left\{ \left(\Gamma_k^{(2)}[\Theta] + R_k \right)^{-1} \partial_t R_k \right\}. \tag{A.15}$$

This equation is infrared as well as ultraviolet finite, since the infrared modes of the partially dressed propagator $\left(\Gamma_k^{(2)}[\Theta] + R_k \right)^{-1}$ are regularised by the regulator term R_k and its scale derivative $\partial_t R_k$ regularises the ultraviolet, cf. Fig. A.1 (right). The flow equation of higher n-point functions can be obtained from Eq. (A.15) by differentiating with respect to the fields. It turns out that the RG equation for an n-point function always includes the $(n+1)$- and $(n+2)$-point function. In this manner we encounter a similar problem in the ERGEs as in the DSEs: There is no finite, closed subset of equations that could be solved without resorting to truncations.

In Fig. A.2 the pictorial representation of Eq. (A.15) is given. The full dot denotes the partially dressed propagator, meaning that fluctuations down to the RG-scale k are included. As $k \to 0$, we are left with the full, dressed propagator. The circled cross labels the scale derivative of the RG regulator $\partial_t R_k$, also referred to as regulator insertion.

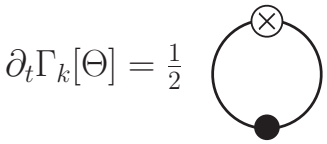

Figure A.2.: Generic structure of the RG flow equation.

Note that while the equation is of one-loop structure, it is not of one-loop order in the perturbative sense, but fully non-perturbative.

A.2. Common Truncation Schemes

Despite its simple structure, the appearance of the partially dressed propagator in the Wetterich Eq. (A.15) makes this object rather complicated - it is a functional partial differential equation. Thus far, no general mathematical techniques for the solution of this kind of equations is known. However, one can reduce the problem to a coupled system of partial differential equations by expanding Γ_k in, e.g., invariants, as discussed in the following. By definition, this system is infinite dimensional, as can also be seen by the fact that the theory space introduced above is infinite dimensional, and one still has to resort to truncations. Such a truncation must on the one hand be of numerically manageable size, but on the other hand it needs to capture the relevant physical effects, which may not be known a priori. As an error estimate, one can subsequently try to increase the chosen truncation and/or take different contributions into account, which provides insights into the stability of the system.

Several expansions of the effective average action have been introduced in the past and we will briefly introduce two common truncation schemes in the following, see e.g. [105] for a more detailed account. Let us, however, stress that the expansions we use are still non-perturbative in nature. In certain regimes it is possible to make contact with perturbative results and use these as crosschecks or even input, but the ERGE results presented here always include non-perturbative information as well.

For simplicity, in the present section we consider a theory with a N-component scalar field ϕ with $O(N)$ invariant $\rho = \phi_a \phi^a$, but an extension to more complicated theories is straightforward.

Derivative Expansion

One possible truncation consists of an expansion of Γ_k in derivatives of the invariant ρ:

$$\Gamma_k[\rho] = \int dx \left\{ \Omega_k(\rho) + \frac{Z_\phi(\rho)}{2} \partial_\mu \phi^a \partial^\mu \phi_a + \frac{Y_\phi(\rho)}{2} \partial_\mu \rho \partial^\mu \rho + \mathcal{O}(\partial^4) \right\} . \tag{A.16}$$

The lowest truncation order, the so-called local potential approximation, takes only the scalar effective potential $\Omega_k(\rho)$ and a standard kinetic term into account, with the wave-function renormalisations $Z_\phi(\rho) \equiv 1$ and $Y_\phi(\rho) \equiv 0$. Higher truncations then involve also the (field-dependent) wave-function renormalisations $Z_\phi(\rho)$ and $Y_\phi(\rho)$ and higher derivative terms.

In this work, we consider models involving quark and/or mesonic fields. For the meson fields are mostly make use of the local potential approximation, cf. Chap. 3. It is well-known that this approximation yields good results for, e.g. critical exponents and order parameters, see e.g. [139,150]. For a quantitative computation of critical exponents, however, a more sophisticated approach, including the anomalous dimensions of the fields is needed [151]. A step in this direction is undertaken in Chap. 5 as well as Chap. 4 of this thesis.

Vertex Expansion

A further possible truncation bases in the so-called vertex expansion. In this approach, the effective average action is expanded in powers of the fields

$$\Gamma_k[\phi] = \sum_{n=0}^{\infty} \frac{1}{n!} \int dx_1 dx_2 \dots dx_n \Gamma_k^{(\mathrm{n})}(x_1, x_2, \dots, x_n)\phi(x_1)\phi(x_2)\cdots\phi(x_n)\,. \tag{A.17}$$

Insertion of this ansatz in the Wetterich Eq. (A.15) yields flow equations for the vertex functions $\Gamma_k^{(\mathrm{n})}$. In particular, the resulting flow equations describe the evolution of the partially dressed vertex functions to the fully dressed ones in the IR.

Note that these flow equations are similar to the Dyson-Schwinger equations, see e.g. [107] for a more detailed discussion.

Retaining Momentum Dependence

While the derivative expansion allows to calculate universal as well as non-universal quantities defined at vanishing momentum, see e.g. [105], it does not provide access to the full momentum dependence of vertex functions. An alternative expansion aims at retaining the full momentum dependence in the s-point function $\Gamma_k^{(s)}$ while approximating the one in the higher n-point functions $\Gamma_k^{(s+1)}$ and $\Gamma_k^{(s+2)}$. This procedure is known as Blaizot–Méndez-Galain–Wschebor (BMW) approximation of order s and was proposed in [152,153], see [154] for a recent account. Note that the BMW approximation with $s = 0$ corresponds to the local potential approximation.

B. Boson Anomalous Dimension

In this appendix we briefly describe the technique to compute the RG running of the bosonic wave-function renormalisation. In particular, we compute the fermionic loop explicitly. The other contributions shown in, e.g., Chap. 5 are derived in a similar fashion. More details of these calculations can be found for example in [93, 155, 156].

Recall that the wave-function renormalization Z_ϕ appears as the prefactor of the boson kinetic term. Hence, to derive its RG flow we have to allow for a configuration that fluctuates around the constant value.

$$\phi_i(x) = \bar{\phi}_i + \delta\phi_i(x)\,. \tag{B.1}$$

To be precise, we choose the field configuration to point in the σ direction, i.e. $\bar{\phi}_i = \sigma\delta_{i1}$ is constant and $\delta\phi_i(x) = \delta\sigma(x)\delta_{i1}$ denotes the small fluctuation in the σ-direction in bosonic field space. In particular, we allow only for a spatially varying field $\phi(x) \to \phi(\vec{x})$. For the space dependence of the fluctuating field we make an ansatz in plane waves

$$\delta\sigma(\vec{x}) = \delta\sigma e^{i\vec{Q}\vec{x}} + \delta\sigma^* e^{-i\vec{Q}\vec{x}}\,. \tag{B.2}$$

As can be derived easily from our ansatz of the effective action Eq. (2.10), the flow of the wave-function renormalisation can then be calculated via

$$\partial_t Z_\phi = \frac{1}{\Omega}\lim_{Q\to 0}\frac{\partial}{\partial\vec{Q}^2}\frac{\delta^2}{\delta\sigma^*\delta\sigma}\,\partial_t\Gamma_k \tag{B.3}$$

with the three-volume abbreviated by $\Omega = (2\pi)^3\delta^{(3)}(0)$. We consider a momentum-independent wave-function renormalisation here, hence the limit $Q \to 0$.

A rather comfortable way to derive the flow equation of a given coupling proceeds by rewriting the Wetterich equation in terms of the matrices $\mathcal{P}_k$, containing the propagators and regulators, and $\mathcal{F}_k$ involving the field dependences. Furthermore, the flow equation is expanded in a Taylor series:

$$\begin{aligned}
\partial_k\Gamma_k &= \frac{1}{2}\mathrm{STr}\left[\left(\Gamma_k^{(2)} + R_k\right)^{-1}\partial_k R_k\right] && \text{(B.4)}\\
&= \frac{1}{2}\mathrm{STr}\left[\tilde{\partial}_k \log\left(\Gamma_k^{(2)} + R_k\right)\right] && \text{(B.5)}\\
&= \frac{1}{2}\mathrm{STr}\left[\tilde{\partial}_k \log\left(\mathcal{P}_k + \mathcal{F}_k\right)\right] && \text{(B.6)}\\
&= \frac{1}{2}\mathrm{STr}\left[\tilde{\partial}_k \log\left(\mathcal{P}_k\right)\right]\\
&+ \frac{1}{2}\mathrm{STr}\left[\tilde{\partial}_k\left(\mathcal{P}_k^{-1}\mathcal{F}_k\right)\right] - \frac{1}{4}\mathrm{STr}\left[\tilde{\partial}_k\left(\mathcal{P}_k^{-1}\mathcal{F}_k\right)^2\right] \pm \dots\,. && \text{(B.7)}
\end{aligned}$$

It is important to note that in the above equations the operator $\tilde{\partial}_t$ is defined to act on the scale dependence of the regulator R_k only.

The propagator and fluctuation matrix can be easily determined from the definitions in Eq. (B.5) and Eq. (B.6). The first term in Eq. (B.7) does not contribute to the flow of Z_ϕ, since we have to project onto the field dependence corresponding to the desired coupling in order to derive its flow. The field dependence, however, is stored in $\mathcal{F}_k$. All higher terms then include powers of $\mathcal{P}_k^{-1}\mathcal{F}_k$, which can be calculated by simple matrix multiplication.

Note also that the expansion in Eq. (B.7) does not constitute an additional truncation of the system. For a given coupling one can uniquely identify *all terms* that contribute to its flow - and there are finitely many of them - just by considering the field content.

For the present case, since we are interested in the fermionic loop contribution to the boson anomalous dimension, it suffices to compute the $(\psi, \bar{\psi})$ contributions to the fluctuation and propagator matrices, i.e. leave out the contribution from the mesonic potential. In detail, the reduced propagator and fluctuation matrix read

$$\mathcal{P}_k = \begin{pmatrix} 0 & -\Delta_F^T \\ \Delta_F & 0 \end{pmatrix} (2\pi)^3 \delta(\vec{p} - \vec{p}\,') \,,$$

$$\mathcal{F}_k = \begin{pmatrix} 0 & -C^T(\vec{p} - \vec{p}\,') \\ C(\vec{p}\,' - \vec{p}) & 0 \end{pmatrix} ,$$

with $C(\vec{p}\,' - \vec{p}) = \delta\sigma\delta(\vec{p}\,' - \vec{p} + \vec{Q}) + \delta\sigma^*\delta(\vec{p}\,' - \vec{p} - \vec{Q})$. The definition of Δ_F will be given below.

Considering the first graph in Fig. 5.2 we conclude that we have to compute contributions $\sim \bar{h}^2$ to derive the desired flow $\partial_t Z_\phi$. To this end, the quadratic term $(\mathcal{P}_k^{-1}\mathcal{F}_k)^2$ has to be calculated. This operator is subsequently plugged into Eq. (B.3) and we have to perform the colour, flavour, Dirac and momentum traces as well as the derivatives. Calculating the fermion trace and derivative w.r.t. $\delta\sigma$, $\delta\sigma^*$ we find

$$\partial_t Z_\phi \;=\; -\frac{\bar{h}^2}{2} \lim_{Q\to 0} \frac{\partial}{\partial \vec{Q}^2} \mathrm{Tr}_{F,C,D} \sum_n \int_p \tilde{\partial}_t \left[\Delta_F^{-1}(\vec{p}) \Delta_F^{-1}(\overrightarrow{p-Q}) + \Delta_F^{-1}(\vec{p}) \Delta_F^{-1}(\overrightarrow{p+Q}) \right] . \tag{B.8}$$

The inverse propagator reads

$$\begin{aligned} \Delta_F^{-1}(\vec{p}) &= \left[-\not{p}(1 + r_F(\vec{p}^{\,2})) - \gamma_0(\omega_{n,F} - \bar{g}A_0 - i\mu) + im_q \right]^{-1} \\ &= \frac{-\not{p}(1 + r_F(\vec{p}^{\,2})) - \gamma_0(\omega_{n,F} - \bar{g}A_0 - i\mu) - im_q}{\vec{p}^{\,2}(1 + r_F(\vec{p}^{\,2}))^2 + (\omega_{n,F} - \bar{g}A_0 - i\mu)^2 + m_q^2} \\ &= \left[-\not{p}(1 + r_F(\vec{p}^{\,2})) - \gamma_0(\omega_{n,F} - \bar{g}A_0 - i\mu) - im_q \right] G_F(\vec{p}^{\,2}) \,. \end{aligned} \tag{B.9}$$

$G_F(\vec{p}^{\,2})$ actually depends on the fermionic Matsubara frequencies $\omega_{n,F}$ and the eigenvalues of the gauge field ν_l as well. For simplicity, we do not show these dependencies explicitly.

Using this expression and taking into account, that the gluon field is diagonal in colour

space, we can easily compute also the flavour, colour and Dirac traces

$$\begin{aligned}\partial_t Z_\phi &= -\frac{4N_f\bar{h}^2}{2}\sum_{l=1}^{d_R}\lim_{Q\to 0}\frac{\partial}{\partial\vec{Q}^2}\sum_n\int_p\tilde{\partial}_t\Big\{\Big[\vec{p}\overrightarrow{(p+Q)}(1+r_F(\vec{p}^{\,2}))(1+r_F(\overrightarrow{(p+Q)}^{\,2}))\\ &\qquad+(\omega_{n,F}-\nu_l-i\mu)^2-m_q^2\Big]\cdot G_F(\vec{p}^{\,2})G_F(\overrightarrow{p+Q}^{\,2})\\ &\qquad+(Q\to -Q)\Big\}\,. \end{aligned}\tag{B.10}$$

Next, we need to perform the derivative w.r.t $\vec{Q}^{\,2}$. To this end we define

$$R(y) = (1+r_F(y))G_F(y)\,.\tag{B.11}$$

This function is then expanded around $y=\vec{p}^2$ and we find for the first expression in the braces in Eq. (B.10)

$$\begin{aligned}&\vec{p}\cdot\overrightarrow{(p+Q)}\;R(\vec{p}^{\,2})R(\overrightarrow{(p+Q)}^{\,2})+\vec{p}\cdot\overrightarrow{(p-Q)}\;R(\vec{p}^{\,2})R(\overrightarrow{(p-Q)}^{\,2}) \quad = \\ &2R\left\{\vec{p}^{\,2}R+\vec{p}^{\,2}\vec{Q}^{\,2}R'+2\vec{p}^{\,2}(\vec{p}\cdot\vec{Q})^2R''+\frac{1}{2}\vec{p}^{\,2}(\vec{Q}^{\,2})^2R''+2(\vec{p}\cdot\vec{Q})^2R'+4(\vec{p}\cdot\vec{Q})^2\vec{Q}^{\,2}R''\right\}\end{aligned}\tag{B.12}$$

where the arguments of R have been omitted in the second line and primes denote the derivative w.r.t. the argument, evaluated at $\vec{p}^{\,2}$. The same thing can be done for the second contribution involving G_F only.

Now we can take the derivative w.r.t. $\vec{Q}^2$ and perform the limit

$$\begin{aligned}\partial_t Z_\phi &= -2N_f\bar{h}^2\sum_{l=1}^{d_R}\sum_n\int_p\tilde{\partial}_t\left\{R\left[\vec{p}^{\,2}R'\left(1+\frac{2}{3}\right)+\frac{2}{3}(\vec{p}^{\,2})^2R''\right]\right.\\ &\qquad\left.+\left[(\omega_{n,F}-\nu_l-i\mu)^2-m_q^2\right]G_F\left[G_F'+\frac{2}{3}\vec{p}^{\,2}G_F''\right]\right\}\,.\end{aligned}\tag{B.13}$$

The integral can be simplified by a suitable transformation of variables as well as integration by parts and we finally find the result

$$\begin{aligned}\partial_t Z_\phi &= \frac{2\bar{h}^2N_fT}{3\pi^2}\sum_{l=1}^{d_R}\sum_n\int_0^\infty dx\tilde{\partial}_t x^{3/2}\left\{x\left(\frac{d}{dx}\left[(1+r_F(x))G_F(x)\right]\right)^2\right.\\ &\qquad\left.+((\omega_{n,F}-\nu_l-i\mu)^2-m_q^2)\left(\frac{d}{dx}G_F(x)\right)^2\right\}\,.\end{aligned}\tag{B.14}$$

C. Threshold Functions

In the FRG flow equations presented in this thesis, several dimensionless threshold functions, which describe the decoupling of thermal and massive modes are used. Furthermore these functions encode the regulator dependence of the results and are collected in the present appendix.

For all calculations in this work, the three-dimensional optimised regulator functions for bosons and fermions [82]

$$R_B(p_0,\vec{p}) = Z_\phi \vec{p}^{\,2} r_B(\vec{p}^{\,2}/k^2)\,, \tag{C.1}$$

$$R_F(p_0,\vec{p}) = Z_\psi \not{p}\, r_F(\vec{p}^{\,2}/k^2) \tag{C.2}$$

with the regulator shape functions

$$r_B(\vec{p}^{\,2}/k^2) = \left(\frac{k^2}{\vec{p}^{\,2}} - 1\right)\Theta(1-\vec{p}^{\,2}/k^2)\,, \tag{C.3}$$

$$r_F(\vec{p}^{\,2}/k^2) = \left(\sqrt{\frac{k^2}{\vec{p}^{\,2}}} - 1\right)\Theta(1-\vec{p}^{\,2}/k^2)\,, \tag{C.4}$$

have been used. The optimised regulator functions maximise the gap in the RG equation and in this manner stabilise the flow. Furthermore, it was shown that a convex effective action is smoothly approached in the IR with optimised flows [157]. As can be seen from, e.g., Eq. (3.2), the thermal fluctuations factorise in the bosonic and fermionic threshold functions using the optimised regulator, which need not be the case for a generic regulator.

In the following, the shorthand notation $x = \vec{p}^{\,2}$ is used and furthermore the zeroth component of the fermionic momentum squared, which includes the chemical potential as well as the four-component of the gauge field, represented by the corresponding eigenvalues ν_l, is denoted by $x_0^F = (\omega_{n,F} - \nu_l|\phi| - i\mu)^2$. A similar abbreviation is used for bosons: $x_0^B = \omega_{n,B}^2$. The Matsubara frequencies for fermions and bosons are given by $\omega_{n,F} = (2n+1)\pi T$ and $\omega_{n,B} = (2n\pi T)^2$, respectively.

Usually, the threshold functions can be defined in an arbitrary dimension d. Since we consider the case of three spatial dimensions exclusively in this work, only the results relevant for this dimensionality are shown.

In this notation, the dimensionfull fermion and boson propagators are given by

$$G_F(x) = \frac{1}{x(1+r_F(x))^2 + x_0^F + m_q^2}\,, \tag{C.5}$$

$$G_B(x) = \frac{1}{x(1+r_B(x)) + \omega_{n,B}^2 + m_B^2}\,, \tag{C.6}$$

where we allowed for massive fermions as well as massive bosons. The dependence of these

propagators on $\omega_{n,B}, \nu_l$ and μ is not written explicitly. For later convenience we define the reduced propagators

$$\bar{G}_F(x_0^F, m_q) = \frac{1}{k^2 + x_0^F + m_q^2}, \tag{C.7}$$

$$\bar{G}_B(x_0^B, m_B) = \frac{1}{k^2 + x_0^B + m_B^2}. \tag{C.8}$$

First, we give the expressions for the purely bosonic threshold functions appearing in Chap. 4. The bosonic loop is given by

$$\begin{aligned} l_0^{(\mathrm{B})}(T, m_B; \eta_\phi) &= \frac{T}{2\,k^4} \sum_{n=-\infty}^{\infty} \int_0^\infty dx\, x^{\frac{3}{2}} (\partial_t r_B - \eta_\phi r_B) G_B(x_0^B, m_B) \\ &= \frac{2}{3} \frac{k}{\sqrt{k^2 + m_B^2}} \left(1 - \frac{\eta_\phi}{5}\right) \left(\frac{1}{2} + \bar{n}_B(T, m_B)\right), \end{aligned} \tag{C.9}$$

with the Bose-Einstein distribution

$$\bar{n}_B(T, \omega) = \frac{1}{e^{\sqrt{k^2+\omega}/T} - 1}. \tag{C.10}$$

Note that this threshold function depends explicitly on the bosonic anomalous dimension η_ϕ. In the rest of this thesis, the argument η_ϕ is sometimes suppressed. The threshold functions with higher index n can be computed from $l_0^{(\mathrm{B})}$ by differentiation

$$\frac{\partial}{\partial \omega} l_n^{(\mathrm{B})}(T, \omega; \eta_\phi) = -(n + \delta_{n,0}) l_{n+1}^{(\mathrm{B})}(T, \omega; \eta_\phi). \tag{C.11}$$

For the fermionic loop diagram, a similar relation holds

$$\frac{\partial}{\partial \omega} l_n^{(\mathrm{F})}(T, \tilde{\mu}, \omega; \eta_\psi) = -(n + \delta_{n,0}) l_{n+1}^{(\mathrm{F})}(T, \tilde{\mu}, \omega, ; \eta_\psi), \tag{C.12}$$

with

$$\begin{aligned} l_0^{(\mathrm{F})}(T, \tilde{\mu}, m_q; \eta_\psi) &= \frac{T}{k^4} \sum_{n=-\infty}^{\infty} \int_0^\infty dx\, x^{\frac{3}{2}} (\partial_t r_F - \eta_\psi r_F)(1 + r_F) G_F(x_0^F, m_q) \\ &= \frac{1}{3} \frac{k}{\sqrt{k^2 + m_q^2}} \left(1 - \frac{\eta_\psi}{4}\right) \left(1 - \bar{n}_q(T, \tilde{\mu}, m_q) - \bar{n}_q(T, -\tilde{\mu}, m_q)\right). \end{aligned} \tag{C.13}$$

In the above equation, n_q denotes the Fermi-Dirac distribution function

$$\bar{n}_q(T, \tilde{\mu}, m_q) = \frac{1}{e^{(\sqrt{k^2+m_q^2} - \tilde{\mu})/T} + 1} \tag{C.14}$$

and $\tilde{\mu} = \mu + \nu_l$. For the calculation of the flow of the Yukawa coupling, the following threshold function, that corresponds to the fermion-boson triangle diagram shown in Fig. 5.1, is

needed

$$\begin{aligned}\ell_{1,1}^{(F,B)}(T,\mu;m_q,m_B) &= \frac{-T}{2}\sum_{n=-\infty}^{\infty}\int_0^\infty dx\; x^{1/2}\;\tilde{\partial}_t\left\{G_B(x)G_F(x)\right\}\\ &= \frac{2Tk^5}{3}\sum_{n=-\infty}^{\infty}\Bigg\{\bar{G}_F^2(x_0^F,m_q)\bar{G}_B(x_0^B,m_B)\\ &\qquad + \bar{G}_F(x_0^F,m_q)\bar{G}_B^2(x_0^B,m_B)\Big\}\;. \end{aligned}\tag{C.15}$$

Furthermore, we need the contributions to the boson anomalous dimension η_ϕ. A sketch of the derivation of the flow equation can be found in App. B. Here, we only give the final expressions of the arising threshold functions. The purely fermionic contribution to η_ϕ reads

$$\begin{aligned}m_4^{(F)}(T,\tilde{\mu},m_q) &= -2T\sum_{n=-\infty}^{\infty}\int_0^\infty dx\; x^{3/2}\;\tilde{\partial}_t\Bigg\{x\left(\frac{d}{dx}\left[(1+r_F(x))G_F(x)\right]\right)^2\\ &\qquad + (x_0^F-m_q^2)\left(\frac{d}{dx}G_F(x)\right)^2\Bigg\}\\ &= 4Tk^3\sum_{n=-\infty}^{\infty}\Bigg\{(k^2+x_0^F-m_q^2)k^2\bar{G}_F^4(x_0^F,m_q)+k^2\bar{G}_F^3(x_0^F,m_q)\\ &\qquad -\frac{3}{4}\bar{G}_F^2(x_0^F,m_q)\Bigg\}\;,\end{aligned}\tag{C.16}$$

while the bosonic contribution is given by

$$\begin{aligned}m_{2,2}^{(B)}(T,m_\sigma,m_\pi) &= k^2T\sum_{n=-\infty}^{\infty}\int_0^\infty dx\; x^{3/2}\tilde{\partial}_t\left\{\left(\frac{d}{dx}G_\sigma(x)\right)\left(\frac{d}{dx}G_\pi(x)\right)\right\}\\ &= -2k^7T\sum_{n=-\infty}^{\infty}\bar{G}_B^2(x_0^B,m_\sigma)\bar{G}_B^2(x_0^B,m_\pi)\,.\end{aligned}\tag{C.17}$$

The Matsubara sums can be performed analytically also for these threshold functions. However, we refrain from showing the lengthy expressions here, since the general structure of the threshold functions can already be seen from the definitions.

D. Numerical Implementation: Differential Evolution Algorithm

When solving the flow equation for the effective average potential of the PQM model, as needed in Chap. 3, the main numerical effort goes into the solution of the equations of motion (EoM) Eq. (3.9) with high accuracy. A standard technique to find the global minimum $\chi_0(T,\mu) = \{\sigma_0, \Phi_0, \bar{\Phi}_0\}(T,\mu)$ of this three-dimensional system would be Newton's method. This method is known to converge quadratically, if initialised sufficiently close to the solution. Tests of this and similar methods for the present system, however, showed that in order to get an acceptable solution, at least $\mathcal{O}(10^4)$ Newton steps are needed. Each of these steps involves several RG runs that take from several seconds up to minutes. For the computation of thermodynamic quantities - which involve derivatives - and especially at low temperatures, a method that needs fewer RG runs is hence desired. To this end the differential evolution (DE) algorithm for global optimization as introduced in Ref. [158] was implemented.

In practice, since the effective average potential is discretised on a grid in the mesonic invariant $\rho = \sigma^2$, it is easy to determine the minimum in this direction. This is done directly by our RG solving routine. As a result, the EoM for σ is automatically fulfiled and one is only left with a two-dimensional system for the Polyakov-loop variables $(\Phi, \bar{\Phi})$. For these, a cost function $f(\Phi, \bar{\Phi})$ can be defined as follows[1]

$$f(\Phi,\bar{\Phi}) = \left(\frac{\partial\Omega_{k\to 0}}{\partial\Phi}\right)^2 + \left(\frac{\partial\Omega_{k\to 0}}{\partial\bar{\Phi}}\right)^2 . \tag{D.1}$$

The DE algorithm is subsequently applied to this cost function.

1. In the first step of the algorithm, a *generation* of N 2-dimensional target vectors $x_{i,G}$, containing values $(\Phi_i, \bar{\Phi}_i)$,is chosen randomly in a user-defined interval.

2. Next, the target vectors are *mutated* according to the law

$$v_{i,G+1} = x_{r_1,G} + F(x_{r_2,G} - x_{r_3,G})\,, \tag{D.2}$$

   with $r_1, r_2, r_3 \in \{1, 2, \ldots, N\}$ chosen randomly, but distinct and using a user-defined constant $F \in [0, 2]$.

3. In the following *crossover* step, a trial vector $u_{ij,G+1}$, $j = 1, 2, \ldots, D$ is computed via

$$u_{ji,G+1} = \begin{cases} v_{ji,G+1} & \text{if } (rand(j) \le C) \text{ or } j = rnr(i) \\ x_{ji,G} & \text{if } (rand(j) > C) \text{ and } j \ne rnr(i) \end{cases}$$

[1] The additional external variables T, μ are suppressed throughout this section.

Here, $rand(j)$ denotes the jth evaluation of the uniform number generator, $C \in [0,1]$ and $rnr(i) \in 1, 2, \ldots, D$ is a randomly chosen index. This step is designed to increase the diversity of the perturbed parameter vector.

4. Subsequently, the *selection* step is performed, where the cost function $f(\Phi, \bar{\Phi})$ is evaluated at the trial vector and compared to its value of the current target vector. If the result is smaller, then the corresponding entry in the target vector is replaced by the one from the trial vector. Note that this step is the only one that involves the solution of the RG equations.

Using this algorithm it is possible to reach an accuracy of at least $\mathcal{O}(10^{-3})$ in the PQM EoM after $\mathcal{O}(10^2)$ generations, corresponding to $\mathcal{O}(10^3)$ RG runs. For comparison, the same number of RG steps in a Newton solver typically yields EoM results of the order of only $\mathcal{O}(10^2)$. Especially for the computation of thermodynamic quantities this hence represents a huge improvement in accuracy and runtime.

Bibliography

[1] M. Gell-Mann, Synchroton Laboratory Report **CTSL-20** (1961).

[2] Y. Ne'eman, Nucl. Phys. **26**, 222 (1961).

[3] R. Alkofer, D. Diakonov, J. Pawlowski, H. Reinhardt, V. Zakharov, et al., AIP Conf.Proc. **1343**, 17 (2011), 1012.3192.

[4] D. J. Gross and F. Wilczek, Phys. Rev. Lett. **30**, 1343 (1973).

[5] H. D. Politzer, Phys. Rev. Lett. **30**, 1346 (1973).

[6] J. Bell and R. Jackiw, Nuovo Cim. **A60**, 47 (1969).

[7] S. L. Adler, Phys. Rev. **177**, 2426 (1969).

[8] K. Fujikawa, Phys.Rev.Lett **42**, 1195 (1979).

[9] S. Weinberg, *The quantum theory of fields. Vol. 2: Modern applications* (Cambridge University Press, Cambridge, 1996).

[10] H. Fukaya et al. (JLQCD and TWQCD collaborations), Phys.Rev. **D83**, 074501 (2011), 1012.4052.

[11] G. t Hooft, Nucl. Phys. **B138** (1978).

[12] G. 't Hooft, Nucl. Phys. **B153** (1979).

[13] S. Elitzur, Phys. Rev. **D12**, 3978 (1975).

[14] O. Kaczmarek, F. Karsch, P. Petreczky, and F. Zantow, Phys.Lett. **B543**, 41 (2002), hep-lat/0207002.

[15] K. Holland and U.-J. Wiese (2000), hep-ph/0011193.

[16] F. Marhauser and J. M. Pawlowski (2008), 0812.1144.

[17] N. Weiss, Phys.Rev. **D24**, 475 (1981).

[18] D. J. Gross, R. D. Pisarski, and L. G. Yaffe, Rev.Mod.Phys. **53**, 43 (1981).

[19] J. Braun, H. Gies, and J. M. Pawlowski, Phys.Lett. **B684**, 262 (2010), 0708.2413.

[20] J. Braun, A. Eichhorn, H. Gies, and J. M. Pawlowski, Eur.Phys.J. **C70**, 689 (2010), 1007.2619.

[21] K. Huebner, F. Karsch, O. Kaczmarek, and O. Vogt, Phys.Rev. **D77**, 074504 (2008), 0710.5147.

[22] S. Gupta, K. Huebner, and O. Kaczmarek, Phys.Rev. **D77**, 034503 (2008), 0711.2251.

[23] F. Karsch and M. Lutgemeier, Nucl.Phys. **B550**, 449 (1999), hep-lat/9812023.

[24] J. Engels, S. Holtmann, and T. Schulze, Nucl.Phys. **B724**, 357 (2005), hep-lat/0505008.

[25] E. Bilgici, C. Gattringer, E.-M. Ilgenfritz, and A. Maas, JHEP **0911**, 035 (2009), 0904.3450.

[26] J. Braun and A. Janot, Phys.Rev. **D84**, 114022 (2011), 1102.4841.

[27] B. Friman, C. Hohne, J. Knoll, S. Leupold, J. Randrup, et al., Lect.Notes Phys. **814**, 1 (2011).

[28] J. Cleymans, H. Oeschler, K. Redlich, and S. Wheaton, Phys.Rev. **C73**, 034905 (2006), hep-ph/0511094.

[29] P. Braun-Munzinger, J. Stachel, and C. Wetterich, Phys.Lett. **B596**, 61 (2004), nucl-th/0311005.

[30] G. Endrodi, Z. Fodor, S. Katz, and K. Szabo, JHEP **1104**, 001 (2011), 1102.1356.

[31] O. Kaczmarek, F. Karsch, E. Laermann, C. Miao, S. Mukherjee, et al., Phys.Rev. **D83**, 014504 (2011), 1011.3130.

[32] E. Shuryak, Prog. Part. Nucl. Phys. **62**, 48 (2009), 0807.3033.

[33] A. Bazavov, T. Bhattacharya, M. Cheng, C. DeTar, H. Ding, et al., Phys.Rev. **D85**, 054503 (2012), 1111.1710.

[34] S. Borsanyi et al. (Wuppertal-Budapest Collaboration), JHEP **1009**, 073 (2010), 1005.3508.

[35] P. Braun-Munzinger, K. Redlich, and J. Stachel (2003), nucl-th/0304013.

[36] L. McLerran and R. D. Pisarski, Nucl.Phys. **A796**, 83 (2007), 0706.2191.

[37] K. Fukushima, Phys.Rev. **D77**, 114028 (2008), 0803.3318.

[38] A. Andronic, D. Blaschke, P. Braun-Munzinger, J. Cleymans, K. Fukushima, et al., Nucl.Phys. **A837**, 65 (2010), 0911.4806.

[39] L. Y. Glozman, V. Sazonov, and R. Wagenbrunn (2011), 1111.0949.

[40] G. Torrieri, S. Lottini, I. Mishustin, and P. Nicolini (2011), 1110.6219.

[41] K. Fukushima (2012), 1204.0594.

[42] D. Son and M. Stephanov, Phys.Rev. **D70**, 056001 (2004), hep-ph/0401052.

[43] Y. Aoki, Z. Fodor, S. Katz, and K. Szabo, Phys.Lett. **B643**, 46 (2006), hep-lat/0609068.

[44] S. Roessner, C. Ratti, and W. Weise, Phys.Rev. **D75**, 034007 (2007), hep-ph/0609281.

[45] K. Fukushima, Phys.Part.Nucl.Lett. **8**, 838 (2011), 1008.4322.

[46] T. K. Herbst, J. M. Pawlowski, and B.-J. Schaefer, Phys.Lett. **B696**, 58 (2011), 1008.0081.

[47] S. Gupta, X. Luo, B. Mohanty, H. G. Ritter, and N. Xu, Science **332**, 1525 (2011), 1105.3934.

[48] T. K. Herbst, J. M. Pawlowski, and B.-J. Schaefer, Acta Phys. Polon.B **5**, 733 (2012), 1202.0758.

[49] A. Ohnishi, K. Miura, T. Nakano, N. Kawamoto, H. Ueda, et al. (2012), 1201.6206.

[50] B. Berdnikov and K. Rajagopal, Phys.Rev. **D61**, 105017 (2000), hep-ph/9912274.

[51] M. A. Stephanov, K. Rajagopal, and E. V. Shuryak, Phys.Rev. **D60**, 114028 (1999), hep-ph/9903292.

[52] D. T. Son, Physics **2**, 5 (2009).

[53] B. Schaefer and M. Wagner, Phys.Rev. **D85**, 034027 (2012), 1111.6871.

[54] M. Stephanov, J.Phys.G **G38**, 124147 (2011).

[55] M. G. Alford, A. Schmitt, K. Rajagopal, and T. Schafer, Rev.Mod.Phys. **80**, 1455 (2008), 0709.4635.

[56] J. C. Collins and M. Perry, Phys.Rev.Lett. **34**, 1353 (1975).

[57] E. Witten, Phys.Rev. **D30**, 272 (1984).

[58] T. Hatsuda and K. Maeda (2009), 0912.1437.

[59] G. Bali, F. Bruckmann, G. Endrodi, Z. Fodor, S. Katz, et al., JHEP **1202**, 044 (2012), 1111.4956.

[60] V. Skokov (2011), 1112.5137.

[61] K. Fukushima and J. M. Pawlowski (2012), 1203.4330.

[62] C. Gattringer and C. B. Lang, *Quantum Chromodynamics on the Lattice* (Springer, 2010).

[63] P. de Forcrand and O. Philipsen, Nucl.Phys. **B642**, 290 (2002), hep-lat/0205016.

[64] O. Philipsen, PoS **LAT2005**, 016 (2006), hep-lat/0510077.

[65] C. Schmidt, PoS **LAT2006**, 021 (2006), hep-lat/0610116.

[66] O. Philipsen, PoS **CONFINEMENT8**, 011 (2008).

[67] R. Alkofer and L. von Smekal, Phys. Rept. **353**, 281 (2001), hep-ph/0007355.

[68] C. S. Fischer, J.Phys.G **G32**, R253 (2006), hep-ph/0605173.

[69] A. Maas (2011), 1106.3942.

[70] C. D. Roberts (2012), 1203.5341.

[71] J. Luecker and C. S. Fischer, Prog.Part.Nucl.Phys. **67**, 200 (2012), 1111.0180.

[72] C. S. Fischer, J. Luecker, and J. A. Mueller, Phys.Lett. **B702**, 438 (2011), 1104.1564.

[73] C. S. Fischer and J. Luecker (2012), 1206.5191.

[74] M. Mitter and B. J. Schaefer, in preparation (2012).

[75] J. M. Pawlowski, AIP Conf.Proc. **1343**, 75 (2011), 1012.5075.

[76] L. Kadanoff, Physics **2**, 263 (1966).

[77] K. G. Wilson, Adv. Math. (1974).

[78] www.wikipedia.org (2012).

[79] J. Polchinski, Nucl.Phys. **B231**, 269 (1984).

[80] C. Wetterich, Phys.Lett. **B301**, 90 (1993).

[81] S.-B. Liao, Phys.Rev. **D53**, 2020 (1996), hep-th/9501124.

[82] D. F. Litim, Phys.Lett. **B486**, 92 (2000), hep-th/0005245.

[83] G. J.-L. Y. Nambu, Phys. Rev. **122**, 345.358 (1961).

[84] M. Fierz, Z. Physik **104**, 553 (1937).

[85] H. Gies and C. Wetterich, Phys.Rev. **D69**, 025001 (2004), hep-th/0209183.

[86] J. Braun and H. Gies, Phys. Lett. **B645**, 53 (2007), hep-ph/0512085.

[87] J. Braun and H. Gies, JHEP **0606**, 024 (2006), hep-ph/0602226.

[88] J. Braun, Eur. Phys. J. **C64**, 459 (2009), 0810.1727.

[89] D. J. Gross and A. Neveu, Phys. Rev. D **10**, 3235 (1974).

[90] J. Hubbard, Phys.Rev.Lett **3**, 77 (1959).

[91] R. Stratonovic, Dokkl. Akad. Nauk. **115**, 1097 (1957).

[92] J. Braun, J.Phys.G **G39**, 033001 (2012), 1108.4449.

[93] N. Tetradis and C. Wetterich, Nucl.Phys. **B422**, 541 (1994), hep-ph/9308214.

[94] D. Jungnickel and C. Wetterich, Phys.Rev. **D53**, 5142 (1996), hep-ph/9505267.

[95] B.-J. Schaefer and J. Wambach, Nucl.Phys. **A757**, 479 (2005), nucl-th/0403039.

[96] J. Braun, B. Klein, and H.-J. Pirner, Phys.Rev. **D71**, 014032 (2005), hep-ph/0408116.

[97] B.-J. Schaefer and J. Wambach, Phys.Rev. **D75**, 085015 (2007), hep-ph/0603256.

[98] K. Fukushima, Phys.Lett. **B591**, 277 (2004), hep-ph/0310121.

[99] B.-J. Schaefer, J. M. Pawlowski, and J. Wambach, Phys.Rev. **D76**, 074023 (2007), 0704.3234.

[100] T. K. Herbst, Master's thesis, Karl-Franzens-University Graz (2009).

[101] C. Ratti and W. Weise, Phys.Rev. **D70**, 054013 (2004), hep-ph/0406159.

[102] V. Skokov, B. Friman, E. Nakano, K. Redlich, and B.-J. Schaefer, Phys.Rev. **D82**, 034029 (2010), 1005.3166.

[103] R. D. Pisarski and F. Wilczek, Phys.Rev. **D29**, 338 (1984).

[104] D. F. Litim and J. M. Pawlowski, World Sci. pp. 168–185 (1999), hep-th/9901063.

[105] J. Berges, N. Tetradis, and C. Wetterich, Phys.Rept. **363**, 223 (2002), hep-ph/0005122.

[106] J. M. Pawlowski, Annals Phys. **322**, 2831 (2007), hep-th/0512261.

[107] H. Gies (2006), hep-ph/0611146.

[108] B.-J. Schaefer and J. Wambach, Phys.Part.Nucl. **39**, 1025 (2008), hep-ph/0611191.

[109] V. Skokov, B. Stokic, B. Friman, and K. Redlich, Phys. Rev. **C82**, 015206 (2010), 1004.2665.

[110] B.-J. Schaefer and H.-J. Pirner, Nucl.Phys. **A627**, 481 (1997), hep-ph/9706258.

[111] N. Strodthoff, B.-J. Schaefer, and L. von Smekal, Phys.Rev. **D85**, 074007 (2012), 1112.5401.

[112] L. von Smekal (2012), 1205.4205.

[113] D. F. Litim, JHEP **0507**, 005 (2005), hep-th/0503096.

[114] J. Braun, K. Schwenzer, and H.-J. Pirner, Phys.Rev. **D70**, 085016 (2004), hep-ph/0312277.

[115] J. Braun, L. M. Haas, F. Marhauser, and J. M. Pawlowski, Phys.Rev.Lett. **106**, 022002 (2011), 0908.0008.

[116] K. Fukushima, Phys. Lett. **B695**, 387 (2011), 1006.2596.

[117] K. Nakamura (Particle Data Group), J. Phys. G **37**, 075021 (2010).

[118] S. Borsanyi, G. Endrodi, Z. Fodor, A. Jakovac, S. D. Katz, et al., JHEP **1011**, 077 (2010), 1007.2580.

[119] A. Bazavov and P. Petreczky (HotQCD collaboration), J.Phys.Conf.Ser. **230**, 012014 (2010), qCD phase transition, 1005.1131.

[120] J. Braun, B. Klein, and B.-J. Schaefer, Phys.Lett. **B713**, 216 (2012), 1110.0849.

[121] B.-J. Schaefer and M. Wagner, Phys.Rev. **D79**, 014018 (2009), 0808.1491.

[122] P. Gerber and H. Leutwyler, Nucl.Phys. **B321**, 387 (1989).

[123] B.-J. Schaefer and H.-J. Pirner, Nucl.Phys. **A660**, 439 (1999), nucl-th/9903003.

[124] A. Bazavov, T. Bhattacharya, M. Cheng, N. Christ, C. DeTar, et al., Phys.Rev. **D80**, 014504 (2009), 0903.4379.

[125] J. Greensite, Prog. Part. Nucl. Phys. **51**, 1 (2003), hep-lat/0301023.

[126] J. Braun and T. K. Herbst (2012), 1205.0779.

[127] J. Kogut and D. Sinclair, Nucl.Phys.Proc.Suppl. **53**, 272 (1997), hep-lat/9607083.

[128] S. Catterall, R. Galvez, J. Hubisz, D. Mehta, and A. Veernala (2011), 1112.1855.

[129] H. S. Fukano and F. Sannino, Phys.Rev. **D82**, 035021 (2010), 1005.3340.

[130] L. Del Debbio, A. Patella, and C. Pica, Phys. Rev. **D81**, 094503 (2010), 0805.2058.

[131] S. Catterall, J. Giedt, F. Sannino, and J. Schneible, JHEP **0811**, 009 (2008), 0807.0792.

[132] L. Del Debbio, B. Lucini, A. Patella, C. Pica, and A. Rago, Phys.Rev. **D80**, 074507 (2009), 0907.3896.

[133] F. Sannino, Acta Phys. Polon. **B40**, 3533 (2009), 0911.0931.

[134] D. D. Dietrich and F. Sannino, Phys.Rev. **D75**, 085018 (2007), hep-ph/0611341.

[135] E. Megias, E. Ruiz Arriola, and L. Salcedo, Phys.Rev. **D74**, 065005 (2006), hep-ph/0412308.

[136] T. Zhang, T. Brauner, and D. H. Rischke, JHEP **1006**, 064 (2010), 1005.2928.

[137] B.-J. Schaefer, M. Wagner, and J. Wambach, Phys.Rev. **D81**, 074013 (2010), 0910.5628.

[138] J. Berges, D. Jungnickel, and C. Wetterich, Phys.Rev. **D59**, 034010 (1999), hep-ph/9705474.

[139] J. Braun, Phys.Rev. **D81**, 016008 (2010), 0908.1543.

[140] H. Gies, J. Jaeckel, and C. Wetterich, Phys.Rev. **D69**, 105008 (2004), hep-ph/0312034.

[141] H. Gies and J. Jäckel, Eur.Phys.J. **C46**, 433 (2006), hep-ph/0507171.

[142] S. R. Coleman and E. Witten, Phys.Rev.Lett. **45**, 100 (1980).

[143] P. N. Meisinger and M. C. Ogilvie, Phys.Lett. **B379**, 163 (1996), hep-lat/9512011.

[144] D. D. Scherer and H. Gies (2012), 1201.3746.

[145] J. Braun, H. Gies, and D. D. Scherer, Phys.Rev. **D83**, 085012 (2011), 1011.1456.

[146] H. Nishimura and M. C. Ogilvie, Phys.Rev. **D81**, 014018 (2010), 0911.2696.

[147] H. Gies, S. Rechenberger, and M. M. Scherer, Eur.Phys.J. **C66**, 403 (2010), 0907.0327.

[148] J. Berges, D.-U. Jungnickel, and C. Wetterich, Eur.Phys.J. **C13**, 323 (2000), hep-ph/9811347.

[149] Y. Aoki, S. Borsanyi, S. Durr, Z. Fodor, S. D. Katz, et al., JHEP **0906**, 088 (2009), 0903.4155.

[150] D. F. Litim, JHEP **0111**, 059 (2001), hep-th/0111159.

[151] O. Bohr, B. Schaefer, and J. Wambach, Int.J.Mod.Phys. **A16**, 3823 (2001), hep-ph/0007098.

[152] J.-P. Blaizot, R. Méndez-Galain, and N. Wschebor, Phys. Rev. E **74**, 051116 (2006).

[153] J.-P. Blaizot, R. Mendez-Galain, and N. Wschebor, Phys.Lett. B **632**, 571 (2006), ISSN 0370-2693.

[154] F. Benitez, J.-P. Blaizot, H. Chate, B. Delamotte, R. Mendez-Galain, et al., Phys.Rev. **E85**, 026707 (2012), 1110.2665.

[155] S. Bornholdt and C. Wetterich, Z.Phys. **C58**, 585 (1993).

[156] C. Wetterich, Z. Phys. **C 57**, 451 (1993).

[157] D. F. Litim, Phys. Rev. **D64**, 105007 (2001), hep-th/0103195.

[158] R. Storn and K. Price, Journal of Global Optimization **11**, 341 (1997).

Acknowledgements

Zu allererst möchte ich mich bei meinem Betreuer, Bernd-Jochen Schaefer für die Möglichkeit an diesem Projekt zu arbeiten und seine Unterstützung seit meiner Diplomarbeit bedanken. Ich fand Arbeit sehr spannend und habe viel gelernt.

Außerdem Danke ich Jan-Martin Pawlowski für die gute Zusammenarbeit und viele interessante Diskussionen.

Besonders möchte ich mich auch bei Holger Gies, Jens Braun und allen anderen am Theoretisch-Physikalischen Institut in Jena für die freundliche Aufnahme während meines Aufenthalts bedanken. Insbesondere Jens gebührt mein Dank für die vielen lehrreichen Diskussionen und Fragestunden.

Meinem 'Langzeit-Bürokollegen' Mario Mitter möchte ich meinen Dank für unzählige Diskussionen und die mathematische/physikalische/moralische Unterstützung in vielen Situationen danken. Danke auch für das Korrekturlesen und die kritischen Kommentare zu Teilen dieser Arbeit.

I would also like to express my gratitude to all the members of the SIC!QFT group. All our meetings, discussions, group lunches etc. have contributed substantially to the broadening of my scientific horizon.

Big thanks also go to the people from Mozartgasse - coffee break is an institution that I always enjoy - no matter if the topic is physics related or not.

Schlussendlich bedanke ich mich bei meiner Familie für ihre Unterstützung während meiner gesamten Ausbildung und dafür, dass sie immer daran glauben, dass ich meine Ziele erreichen kann. Insbesondere will ich meiner Schwester dafür danken, dass sie mich immer mal wieder aus der 'Physik-Welt' rausholt um sicher zu gehen, dass ich nicht allzu spleenig werde.

Financial Support:
This thesis was supported by the FWF Doctoral college "Hadrons in Vacuum, Nuclei and Stars, Grant No. W1203 and the Austrian Academy of Sciences in the form of a DOC-fFORTE scholarship.